

# MONITORING HYDROLOGICAL DYNAMICS AND CONNECTIVITY IN NON-PERENNIAL RIVERS USING REMOTE SENSING



REPORT TO THE



**PREPARED BY:**

SAGWATI EUGENE MASWANGANYE<sup>1</sup>, EISON KAPANGAZIWIRI<sup>2</sup>, TIMOTHY DUBE<sup>1</sup>,  
DOMINIC MAZVIMAVI<sup>1</sup>, & NEBO JOVANOVIĆ<sup>1</sup>

<sup>1</sup>Institute for Water Studies  
University of the Western Cape

<sup>2</sup>The Water Centre  
Council for Scientific and Industrial Research

WRC Report No. 2936/1/23  
ISBN 978-0-6392-0501-4

APRIL 2023



Water Research Commission  
Bloukrans Building, 2<sup>nd</sup> Floor  
Lynnwood Bridge Office Park  
4 Daventry Road  
Lynnwood Manor  
PRETORIA

[orders@wrc.org.za](mailto:orders@wrc.org.za) or download from [www.wrc.org.za](http://www.wrc.org.za)

#### DISCLAIMER

This report has been reviewed by the Water Research Commission (WRC) and approved for publication. Approval does not signify that the contents necessarily reflect the views and policies of the WRC, nor does mention of trade names or commercial products constitute endorsement or recommendation for use.

## ACKNOWLEDGEMENTS

The authors acknowledge the Water Research Commission for funding project No. K5/2936/1 and the project's Reference Group for their invaluable input. The project also appreciates the Agricultural Research Council for providing some weather data to complete this work. The citizen scientist programme provided us with valuable data

This page was intentionally left blank

# CONTENTS

1	INTRODUCTION.....	1
1.1	Rationale: Non-perennial rivers-occurrence & use.....	1
1.2	Aim and objectives of the study.....	2
1.3	Aim of this report.....	3
1.4	Summary of work undertaken.....	3
1.5	Capacity building and dissemination of information.....	5
1.6	Acknowledgements.....	6
2	METHODOLOGY.....	8
2.1	Ground data collection.....	8
2.1.1	Citizens' science program.....	8
2.1.2	Research monitoring program.....	13
2.2	Remote sensing data.....	16
2.2.1	Description of Sentinel-2 Multispectral Instrument (MSI).....	16
2.2.2	Description of Landsat-8 Operational Land Imager (OLI).....	16
2.2.3	Satellite remote-sensed indices.....	17
2.2.4	Rainfall, geology, land cover/use dataset.....	17
2.3	Data analysis.....	17
2.3.1	Detection of pools along the river.....	17
2.3.2	Sentinel-1 Processing.....	19
2.3.3	General classification accuracy.....	19
2.3.4	Accuracy assessment of remotely sensed pool's surface area.....	20
2.3.5	Assessing the difference between the observed and remotely sensed surface area of pools.....	21
2.3.6	Pool Water Balance Analyses.....	21
2.3.7	Water balance description.....	22
2.3.8	Statistical analysis.....	24
2.4	Detection of hydrological phases.....	26
2.4.1	Identification of flow-contribution areas.....	28

2.4.2	Evaluation metrics .....	30
2.5	Methods to determine flow using remote sensing .....	30
2.5.1	Area-discharge curve.....	31
2.5.2	Empirical equations .....	33
3	RESULTS .....	35
3.1	Molototsi River catchment.....	35
3.1.1	Rainfall.....	35
3.1.2	River flow .....	36
3.1.3	Groundwater .....	37
3.2	Touws River catchment.....	40
3.2.1	Rainfall and river flow.....	40
3.2.2	Pools and Groundwater .....	41
3.3	Heuningnes catchment.....	44
3.3.1	Rainfall.....	44
3.3.2	River flow .....	45
3.3.3	Pool.....	46
4	SPATIAL AND TEMPORAL DYNAMICS OF POOLS ALONG NON-PERENNIAL RIVER	48
4.1	Assessment of detection of pools along Touws and Molototsi rivers at catchment scale.....	48
4.2	Accuracy assessment of remotely sensed pool's surface area in the Touws and Molototsi rivers. ....	52
4.3	Assessment of changes in pool sizes and factors that controls the changes in Touws and Molototsi Rivers .....	54
4.4	Discussion and Conclusion .....	56
5	WATER BALANCE OF POOLS .....	59
5.1	Water level assessment.....	59
5.1.1	Assessment of the water losses from the pool .....	59
5.1.2	Probability of the pool drying out .....	60
5.2	Water Balance Model.....	61
5.3	Remote sensing water balance analysis .....	64

Comparison of the remote sensing and observed models' inputs .....	64
5.4 Discussion and Conclusion .....	68
5.4.1 Discussion.....	68
5.4.2 Conclusion .....	71
6 DETECTION OF HYDROLOGICAL PHASES.....	73
6.1 Detection of the hydrological phases in the Touws and Molototsi River.....	73
6.2 Relationship between flow detection and flow event duration and the use of Sentinel-1 to improve flow detection.....	75
6.3 Temporal dynamics of the phases.....	75
6.4 Flow contributing area in the Touws and Molototsi River.....	77
6.5 Discussion and conclusion .....	81
7 DISCHARGE ESTIMATION .....	83
7.1 The comparison of the spectral signature of pools and flowing water in non-perennial rivers.....	83
7.2 Establishing the rating curves.....	87
7.2.1 Heuningnes.....	87
7.2.2 Touws River.....	88
7.2.3 Estimation of flow.....	88
7.3 Evaluation of the remote sensing discharge estimate.....	90
7.4 Discussion and conclusion .....	92
8 DEVELOPMENT OF A PREDICTIVE TOOL.....	94
8.1 INTRODUCTION .....	94
8.2 Methodology.....	94
8.2.1 Data requirements and data used.....	94
8.2.2 Calculation .....	95
8.3 Website Interface.....	96
8.4 Web Application.....	96
8.5 The administration site.....	99
9 CONCLUSIONS.....	104
10 REFERENCES.....	106

This page was intentionally left blank

# 1 INTRODUCTION

## 1.1 RATIONALE: NON-PERENNIAL RIVERS-OCCURRENCE & USE

Effective and sustainable water resource management, planning and development demand the understanding and full exploitation of all possible and available water resources wherever they occur. With demands on water resources rapidly growing across the globe there is a growing need to find and use any water resources that occur on the earth. One of the interesting and available resources is the surface water in pools that occur in the non-perennial river (NPR) systems. Drylands comprise 41.3% of the earth's surface in hyper-arid, arid, semi-arid and dry sub-humid areas, and they are home to 2.1 billion people (UN, 2017). Ephemeral and torrential rivers are common throughout the world's drylands. Low and variable rainfall, in addition to negligible groundwater contribution, causes these rivers to remain dry with only seasonal or occasional surface water flows and accumulations or pooling. Where the underlying geology is favourable, the sediments deposited by ephemeral rivers can form useful aquifers, especially when few other water resources are accessible for use. Water table depth in these aquifers is generally shallow, less than a few meters, and if water demand is low and recharge is regular, long-term groundwater depletion is not expected, and these aquifers can be considered renewable water resources (Owen, 1989). Water resources obtained from these alluvial aquifers can provide for millions of people and have been utilised for millennia both for water supply to communities and irrigation (Love et al., 2011).

In the context of South Africa, where in most catchments surface water resources are fully allocated, aquifers formed in ephemeral riverbeds are a potentially useful source of water, especially for small, isolated villages in semi-arid and arid regions. Policymakers recognise that rural development has an important role in the reduction of poverty and improving livelihoods. There is therefore a need to improve the availability of water, and ephemeral rivers have the potential to be alternative useful water sources, particularly for poor rural communities and small-scale subsistence agriculture. Ephemeral rivers often take the form of sand rivers, with shallow alluvial aquifers associated with active river courses. The exploitation of sand rivers is described in literature, e.g. Owen (1989), Davies et al., (1998), and Hussey (2007). High yields are frequently achieved as a result of the high conductivity of the sand deposits and the water quality is generally acceptable because of the frequent recharge and filtering effect of the sand (Jovanovic et al., 2018).

Discharge from ephemeral rivers is almost entirely from surface water flow during annual and/or occasional flood events with direct precipitation providing minimal recharge. In sandy riverbeds, surface water flow only occurs when the sand beds are fully saturated. Thus, near real-time knowledge of the frequency of surface water flow events, coupled with groundwater level measurements, is required for effective and sustainable management of abstraction. While flow records would be the most obvious way of determining surface/recharge frequencies and episodes, such records are scarce in South Africa as a priority for streamflow gauging and monitoring is often given to perennial streams. Furthermore, ephemeral river flows often peter out quickly which would require the installation of multiple gauging stations in a small stretch of river to be able to catch the flows and obtain reasonable data that could be useful. During the flow recession, ephemeral rivers often form pools that become disconnected over time. The mechanisms and processes that regulate pool dynamics and connectivity are generally poorly studied and unknown. For practical purposes, if ephemeral river systems are to be exploited as a source of water, it is imperative to understand the pool recharge/discharge processes and dynamics to manage and predict water availability and ensure a certain level of security where these form a huge source of water for improving rural livelihoods. The use of remote sensing technology has the potential to play an important role in detecting surface flow, estimating streamflow, recharge, and frequency, providing valuable insights into the dynamics and connectivity of pools, and ultimately supporting the management of available water in data-scarce regions. This is the basis of this study.

## **1.2 AIM AND OBJECTIVES OF THE STUDY**

The general aim of this project is two-fold. Firstly, gaps in scientific knowledge on the mechanisms of recharge/discharge and pool dynamics and connectivity of ephemeral rivers are investigated using remote sensing technologies. Secondly, the project proposed to develop low-cost methods for monitoring streamflow and water availability in ungauged non-perennial streams in rural areas in support of, and with the participation of the community through a citizens' science program.

The specific objectives of the project are:

1. To develop remote sensing-based methods for observation of non-perennial river flows, and the dynamics (recharge/discharge), connectivity and thresholds of pools occurring along these rivers during recession stages.
2. To use remote sensing-based methods to identify source areas and thresholds for the occurrence of flows, and transmission losses along non-perennial rivers.
3. To establish a citizen science monitoring program for surface and groundwater in specific rural areas (case studies).

4. To develop a predictive tool for the management of water resources in non-perennial rivers and pools by rural communities.

### 1.3 AIM OF THIS REPORT

This document represents the final deliverable of the contract with the Water Research Commission. It reports on the use of remote sensing technology in the collection of hydrological data, and the collection and processing of in situ data during the two hydrological years of the project. It also describes the citizens' science methodology used to collect data both on the ground and the results obtained in the two study catchments (Molototsi in Limpopo and Touws River in the Western Cape) and conclusions drawn from these two years of hydrological data collection.

### 1.4 SUMMARY OF WORK UNDERTAKEN

Table 1.1 and Table 1.2 summarise the work carried out, and deliverables submitted during the tenure of the project.

**Table 1.1.** Work planned and completed during the project.

No.	Task	Summary of work
1	Background Information	The study design has been finalised and necessary monitoring sites in Limpopo (in the Molototsi River Catchment) and the Western Cape (in the Touws River Catchment) for the collection of requisite data established.
2	Citizen Science Program	Stakeholder engagement was undertaken, and the establishment of a citizen science program was completed. The program continues to assist in the collection of water (e.g. rainfall and streamflow) data that are relevant to achieving the set objectives of the project.
3	Remote Sensing and hydrological data collection	Campaigns to collect field data from the monitoring sites are an ongoing exercise to the end of the project. This has been ongoing since the beginning of the project. Data are collected to cover both the wet and dry seasons.

No.	Task	Summary of work
4	Development of remote sensing to estimate streamflow and pool dynamics	The data collected thus far has been used to put into place the initial phases of the development of how remote sensing could be used to estimate streamflow and pool dynamics in non-perennial rivers. Additional data are being collected and analysed to finalise this development by fine-tuning the initial development.
5	Development of a predictive tool	The team has completed the development of this tool which aims to predict volumes of water stored and abstracted from aquifers as well as the sustainable length of use. A report was submitted to the WRC and was accepted.

**Table 1.2.** Deliverables submitted during the study.

No.	Deliverable	Submission date
1	Report on background information and site establishment Report on background data collected, selection and establishment of monitoring sites	30/06/2019
2	Citizens' Science Program Report on stakeholder engagement and the implementation of the citizens' science program	31/01/2020
3	Interim report 1 Report on remote sensing and hydrological data collected on the ground – first hydrological year	31/08/2020
4	Report on remote sensing methodologies Report on the methodologies developed to estimate streamflow and pool dynamics	15/01/2021
5	Interim Report 2 Report on remote sensing and hydrological data collected on the ground	31/08/2021
6	Development of a predictive tool Report on the development and implementation of the predictive tool for water storage, abstraction, and length of use	15/01/2022
7	Interim Report 3	31/08/2022

No.	Deliverable	Submission date
	Report on remote sensing and hydrological data collected on the ground	
8	Final Report	This report

## 1.5 CAPACITY BUILDING AND DISSEMINATION OF INFORMATION

Initially, the project had targeted to recruit one postgraduate student at the MSc level. However, the project then managed to recruit a student at the PhD level. Mr Eugene MASWANGANYE was the PhD student who worked on the majority of the project objectives. Mr Maswanganye was registered at the University of the Western Cape (UWC) and was ably co-supervised by Profs T. Dube, D. Mazvimavi and N. Jovanovic. Dr Kapangaziwiri as the project leader became an unofficial co-supervisor based on his being the principal investigator of the project when he took over from Prof Jovanovic. At the time of writing this report, Mr Maswanganye had prepared a final draft of his PhD thesis in preparation for submission to external examiners for grading. A second PhD student joined the project through the WRC Water Research, Development, and Innovation (RDI) Roadmap programme to March 2021. This student was Ms Nikki FUNKE who was registered with the Institute for Environmental Studies at Vrije Universiteit Amsterdam in The Netherlands. It would be remiss to not mention the capacity building that was transferred to the cohort of citizen scientists that helped with the collection of scientific field data for the project.

Besides the very informative and dynamic interactions with the members of the Reference Group (RG), the project team members were privileged to attend a number of national conferences where different outputs of the project were presented. Ensuing discussions better-informed awareness of issues related to the objectives of the project, especially the hydrological processes and water exchange dynamics in pools formed in non-perennial river systems, and the use of remote sensing technology to derive useful information for the project. The following conferences were attended by the key project team members:

1. 1<sup>st</sup> South African Hydrology Society (SAHS) conference, 10-12 October 2022, 26 Degree South, Muldersdrift, Gauteng, South Africa, attended by E. Kapangaziwiri and S.E. Maswanganye.

2. 23<sup>rd</sup> WaterNet/WARFSA/GWP-SA Symposium, 19-21 October 2022, Sun City Resort, Rustenburg, South Africa, attended by S.E. Maswanganye, D. Mazvimavi, T. Dube and E. Kapangaziwiri.
3. 2020 Green Campus Conference, 10 July 2020, attended by S.E. Maswanganye.

At these conferences the following papers were presented:

1. Maswanganye, SE, Dube, T., Jovanovic, N., Mazvimavi, D & Kapangaziwiri, E., 2022. Using the water balance approach to understand pool dynamics along non-perennial rivers in semi-arid areas of SA
2. Maswanganye, SE, 2020. The impact of COVID-19 on the Environment.

The following publications were made from the outputs of the project:

1. Maswanganye et al., 2021. Remotely sensed applications in monitoring the spatio-temporal dynamics of pools and flows along non-perennial rivers: a review. *South African Geographical Journal*. doi.org/10.1080/03736245.2021.1967774.
2. Maswanganye et al., 2022. Use of multi-source remotely sensed data in monitoring the spatial distribution of pools and pool dynamics along non-perennial rivers in semi-arid environments, *South Africa. Geocarta International*. doi.org/10.1080/10106049.2022.2043453
3. Maswanganye et al., 2022., Using the water balance approach to understand pool dynamics along non-perennial rivers in the semi-arid areas of South Africa. *Journal of Hydrology: Regional Studies*

## 1.6 ACKNOWLEDGEMENTS

The project team is very grateful for the financial and administrative support provided by the Water Research Commission (Project No. K5/2936/01). A very important part of this project was the participation of various individuals in the Reference Group (RG) meetings which were ably chaired by Mr Yazeed van Wyk of the Water Research Commission (WRC). The following table lists the names and organisations of the individuals who attended the RG meetings and, therefore, contributed to the successful completion of this project:

Name	Organisation
Mr Yazeed VAN WYK (Chairperson)	Water Research Commission (WRC)
Ms Danita HOHNE	DWS, Northern Cape

Dr Elhadi ADAM	University of Witwatersrand
Mr Fanus FOURIE	DWS, Pretoria
Mr Kobus STREUDERS	DWS, Northern Cape
Mr Stephan PRETORIUS	AGES Group
Prof Onesimo MUTANGA	UKZN
Dr Tendai SAWUNYAMA	IUCMA
Mr Jan VAN STADEN	BGCMA
Prof Abel RAMOELO	University of Pretoria

During the course of the project, several discussions with other organisations involved in non-perennial river systems, hydrological science, and remote sensing research were held. The contributions of different institutions and individuals (too many to mention) are acknowledged.

Lastly, the project team is grateful and would like to acknowledge the data that were received from Agricultural Research Council (ARC) to augment field data collection. Without these data, it would have been nearly impossible to have undertaken the research reported herein.

## 2 METHODOLOGY

### 2.1 GROUND DATA COLLECTION

#### 2.1.1 Citizens' science program

A citizens' science program was initiated at each study catchment. The local community and government representatives were briefed on the project and its data requirements. Advice was sought and discussions were held to identify community members and monitoring sites to conduct the citizens' science program. The citizens' science program is aimed at co-designing and training local communities, landowners, government officials and practitioners in the collection of hydrological data. The monitoring program involves the following measurements at river cross-sections (monitoring sites):

- Detection of river flow and measurement of channel flow dimensions with tape measures.
- Detection of pools and measurement of pool dimensions (length, width, depth) with tape measures.
- Groundwater level measurements with manual dip-meters.

There are three levels of commitment to the program:

- i) participants that were already collecting rainfall data (agreed to share the data),
- ii) participants collecting rainfall data, and have agreed to notify the researcher if there is flow in the river,
- iii) participants that collect rainfall data and river flow measurements (fully committed).

The role of community leader(s) and/or government officials in the program is to liaise between the researchers and the participants and share the records in case the participant(s) do not have the means to share the records. The researchers are responsible for capturing the data from pictures and other formats to digital formats. The citizens' science programme was established in the Touws and Molototsi catchments; it was not established in the Heuningnes catchment as it is well covered with monitoring instruments (Figure 2.3). Tables 2.1 and 2.2 summarize the measurements taken by citizen scientists in the Molototsi and Touws River catchments. Figure 2.1 shows Google Earth maps of the farms and features monitored in the Molototsi catchment. Detailed information on boreholes is provided in Tables 2.3 and 2.4.

**Table 2.1** Summary of citizens' science measurements done at the case study site in the Molototsi River catchment.

Farm	Lat/Long	Rainfall	River	Pools	Groundwater
Nhlambeto	-23.564; 30.700	Manual rain gauge	Flow events: width and depth	Size and depth as they occur	No
Duvadzi	-23.567; 30.820	Manual rain gauge	Flow events: width and depth	Size and depth as they occur	3 boreholes with manual readings
A hi tirheni Mqekwa	-23.570; 30.660	Manual rain gauge	No	No	7 boreholes with manual readings

**Table 2.2** Summary of citizens' science measurements done at the case study site in the Touws River catchment.

Farm	Lat/Long	Rainfall	River	Pools	Groundwater
Wolverfontein Guest House	-30.820; 23.567	Manual rain gauge	Flow events: width and depth	Size and depth as they occur	Boreholes with manual readings
Sean's place	-30.660; 23.570	Estimated from rain harvested from the roof+ rain gauge	Occurrence of flow	No	Water quality samples

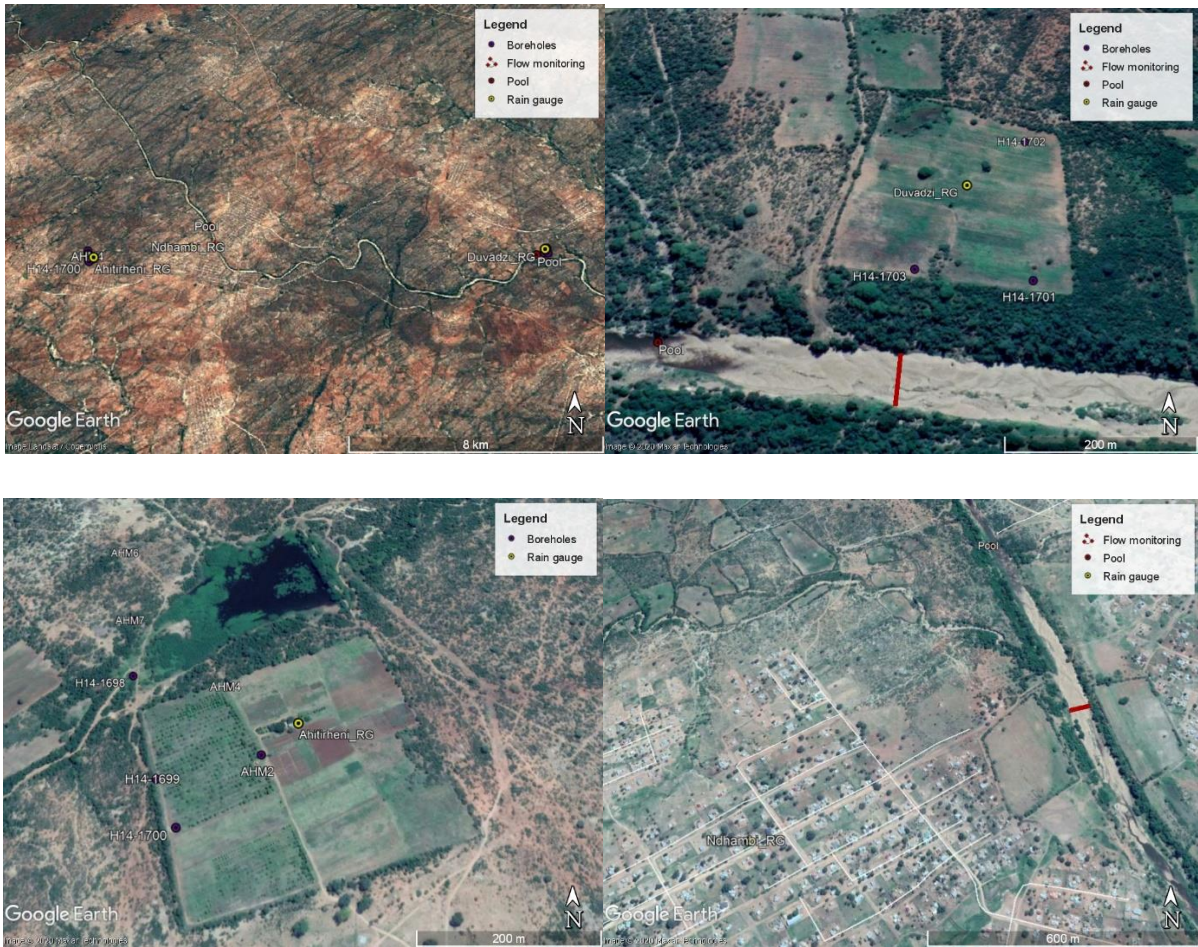


**Figure 2.1** Citizens' science monitoring sites in the Molototsi River on Google Earth images: *Top left*: Location of farms in the mid-reaches of the Molototsi River. *Top right*: A hi tirheni Mqekwa Farm; monitoring of groundwater levels and rainfall. *Bottom left*: Nhlambeto Multipurpose Agricultural Primary Cooperative Ltd.; monitoring of rainfall and river pools and flow (the red bar indicates the monitored river cross-section). *Bottom right*: Duvadzi farm; monitoring of groundwater level, rainfall and river pools and flow (the red bar indicates the monitored river cross-section).

TABLE 2.3: Boreholes in the Molototsi River Catchment

Borehole	Depth of borehole	Latitude Y	Longitude X	Altitude (m)	Depth of Water Strike	Purpose
AHM2	20.1	-23.57	30.65966	464	--	Crop irrigation
AHM4	29.17	-23.569	30.65921	467	--	Crop irrigation
AHM5	46.6	-23.5692	30.6583	461	--	Crop irrigation
AHM6	-	-23.5669	30.6576	459	--	Crop irrigation
AHM7	>95	-23.568	30.65783	457	--	Crop irrigation
H14-1698	120	-23.5689	30.65794	467	16; 25; 93	Crop irrigation
H14-1699	120	-23.5703	30.65841	471	25	Crop irrigation
H14-1700	120	-23.5709	30.65878	473	18; 25; 27; 70	Crop irrigation
H14-1701	120	-23.5673	30.82098	397	22	Crop irrigation
H14-1703	102	-23.5671	30.81966	400	27	Crop irrigation
H14-1702	120	-23.5654	30.82118	397	31; 47; 77	Crop irrigation

TABLE 2.4: Boreholes in the Touws River Catchment

Borehole name	Depth of Borehole	Latitude (Y)	Longitude (X)	Altitude (m)	Depth of Water Strike	Purpose
TW_BH1	25	-33.637833	20.973403	338	--	Research: Groundwater and surface water interaction
TW_BH2	60	-33.637812	20.973372	338	--	Research: Groundwater and surface water interaction



Figure 2.2 Citizens' science monitoring sites in the Touws River on Google Earth images, (red bars are flow sites and yellow dots are rain monitoring sites).

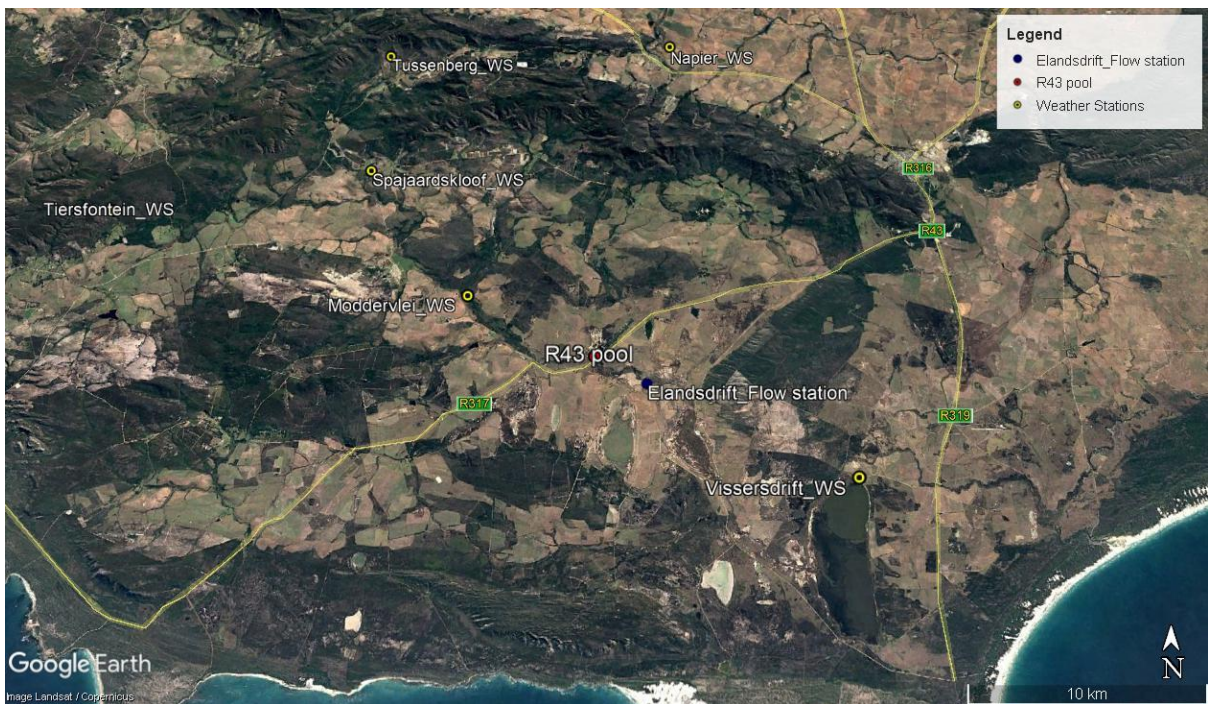


Figure 2.3 Monitoring sites in the Heuningnes Catchment on Google Earth images, (the red dot is the pool, the blue dot is the flow monitoring site, and the yellow dots are weather monitoring sites).

## 2.1.2 Research monitoring program

The hydrometeorological monitoring program conducted by the research team, in addition to the citizens' science program, is summarized below:

### *Molototsi River Catchment*

- Three groundwater levels at Dzuvadzi farm are equipped with data loggers
- One weather station (Agricultural Research Council) in Gravelotte

### *Touws River Catchment*

- Automated hydrometeorological dynamics measurements
  - Water levels at boreholes of different depths in one site, equipped with data loggers
  - Water levels at two adjacent pools with data loggers
- One rain gauge
- One game camera captures the river flow hourly
- One weather station (Agricultural Research Council)

### *Heuningnes Catchment*

- 6 Weather stations and one rain gauge
- 4 flow monitoring stations
- Water level was monitored in 27 boreholes, 14 manually, 13 equipped with data loggers

### *Other parameters*

#### *Water Quality*

Water samples collected from the pools and boreholes are sent to the lab to analyse potassium, sodium, calcium, sulphate, chloride, alkalinity, nitrate, phosphate, electrical conductivity (EC), pH and total dissolved solids (TDS) to further determine if there is an interaction between the pools and groundwater. pH, EC, and temperature were measured during the field visits.

#### *Pool location*

During the field visits, Garmin GPS 60 was used to mark the location of pools within the study areas. The accuracy was within 5 m for all points collected. Four field surveys were done in the Touws River Catchment (winter rainfall region) on 29 July to 02 August 2019,

30 September to 02 October 2019, 20 to 21 November 2019, 24 to 26 February 2020, and 16 to 20 November 2020 (Table 2.3). For the Molototsi catchment, which is a summer rainfall region, the field survey occurred between 7 and 10 January 2020 and 27 May 2020 (Table 2.3).

Table 2.3 Field survey in Touws and the Molototsi River catchments

Touws River			Molototsi River		
Year	Date	No. of pools	Year	Date	No. of pools
2019	29/07-02/08	11	2019	12/12-17/12	Flow
	30/09-02/10	Flow D/S	2020	07/01-10/01	8
	20/11-21/11	6			
2020	24/02-26/02	7			
	16/11-20/11	4			
2021	30/03-31/03	4	2021	29/06-02/07	6
2022	25/04-27/04	4	2022	02/03	4

### *Sizes of pools*

The length and the width of the pools were measured using a measuring tape. Where feasible, points around the pools were also collected using handheld GPS (e.g. Figure 2.4). These points were connected using mapping software (ArcGIS or Google Earth). Table 2.4 provides a consolidated summary of all ground data collected.



Figure 2.4 An example of the field-collected points using a GPS

Table 2.4 Consolidated summary of ground data collected

	Touws	Molototsi	Heuningnes
Pool location	5 Surveys, 11 pools	2 Surveys, 8 pools	1 pool
Pool sizes	6 Surveys	4 Survey	X
Pool levels	2 Pools monitored	X	X
Pool Water Quality	2 Trips	1 Trip	*
Weather Data	1 WS (ARC), 2 RG (1 CS)	1 WS (ARC), 3 RG data (CS)	6 WS, 1 RG
GW level	2 BHs	7 BHs	27 BHs
GW quality	1 Trip	X	X
Flow sites	1 DWS	X	4 Sites

N.B: CS (Citizen Science), DWS (Department of Water and Sanitation), ARC (Agricultural Research Council) WS (Weather Station), BH (Borehole), RG (Rain gauge) \* data will be obtained from another project that is assessing hydrochemistry in the catchment.

## 2.2 REMOTE SENSING DATA

Two methods were used to derive the spatial distribution of pools along non-perennial rivers. The first method was field surveys of the location and sizes of pools. The second method was to attempt to use satellite images to detect the location and sizes of these pools. Many satellites provide images (varying in spatial, spectral, and temporal characteristics) that can be used for the extraction of water bodies. However, this study will use Sentinel-2 MSI and Landsat 8 OLI, in addition, Sentinel-1 was used in the absence of Sentinel-2 and Landsat 8 due to cloud cover. Both Sentinel 2 and Landsat 8 images are freely accessible, respectively. Li *et al.* (2013) and Avisse *et al.* (2017) have shown that Sentinel 2 and Landsat 8 data have the potential to extract surface water information reliably at small scales. Landsat platform data are the most used in water research as they are suitable for application and user-friendly (accessibility and processability) (Guo *et al.*, 2017). These relatively new sensors have not been fully exploited to derive surface water information in African settings. The accuracy of satellite remote sensing methods had to be assessed. The data that were used are described below.

### 2.2.1 Description of Sentinel-2 Multispectral Instrument (MSI)

Sentinel-2 comprises twin polar-orbiting satellites in the same orbit, phased at 180° to each other. The first satellite was launched in 2015, and the second one was launched in 2017. The combination of these satellites reduces the revisit time from 10 days for each satellite to 5 days at the equator and 2-3 days at mid-latitudes. The purpose of the mission was to provide data for operations such as land cover maps, land change detection and geophysical variables. Sentinel-2 has 13 spectral bands in total, four bands at 10, six bands at 20 m and three bands at 60 m spatial resolution. Sentinel-2 data is provided at different pre-processed level products for users (i.e. 1B, 1C and 2A). The data are available on the USGS earth explorer (<http://earthexplorer.usgs.gov/> accessed on 8 August 2020) and Copernicus (<https://scihub.copernicus.eu/> accessed on 8 August 2020) website. For this study, the level 1C data was downloaded from the USGS website throughout the study duration.

### 2.2.2 Description of Landsat-8 Operational Land Imager (OLI)

Landsat 8 is the satellite launched in February 2013 and built to continue the work of the previous Landsat satellites that operated since 1972. Landsat 8 has a revisit time of 16 days. Landsat 8 has 11 bands in total, with nine bands with 30 m resolution except for the panchromatic band with 15 m spatial resolution. The two thermal infrared bands are with 100 m resolution. Data is available for level-1 data products. Landsat data is freely accessible and available from USGS Earth Explorer, GloVis, and Landsat lookout viewer platforms. For this study, the Earth explorer was used to acquire the images.

## *Sentinel-1 SAR*

Sentinel-1 mission is a European RADAR observatory for Copernicus by European Commission and the European space agency (ESA) launched in 2014 and 2016. The mission's objective was to provide an independent operational capability for continuous RADAR mapping of the Earth. SAR is the main instrument carried by the Sentinel-1 spacecraft. The mission has C-band imaging operating in 4 modes (Stripmap, Interferometric-wide swath, extra wide swath, and wave modes). This band can reach down to 5 m and coverage swath of up to 400 km. It has a revisit time of 6 days, each satellite has a 12-day revisit time at the equator, and the revisit time is bettered by sentinel-1 two satellites (Sentinel-1A and Sentinel-1B) orbiting in the same plane (~700 km above the earth). For the Sentinel-1 SAR data under interferometric wide-swath (IW) mode were downloaded from the National Aeronautics and Space Administration Alaska Satellite Facility (NASA/ASF) (<https://search.asf.alaska.edu/#/>).

### 2.2.3 Satellite remote-sensed indices

Sentinel-2 images were downloaded from USGS for the two catchments and analysed. Normalized Difference Water Index (NDWI) and Modified Normalized Difference Water Index (MNDWI) were applied to these images. For time-series analyses of the pools, monthly images were obtained from 2016 to 2020; images closest to mid-month (15<sup>th</sup>) were used. For assessing the accuracy of the methods, images that were captured on the same day as the field surveys were used, when these images were not available closest day was used.

### 2.2.4 Rainfall, geology, land cover/use dataset

A combination of remotely sensed rainfall estimates using CHIRPS (Climate Hazards Group InfraRed Precipitation with Station data) and a few data sets obtained from the local community were used. Both soil and geology data were obtained from WR2012 (Water Resources of South Africa, 2012). Land cover data were obtained from the National Geographic Institute (NGI) of South Africa.

## 2.3 DATA ANALYSIS

### 2.3.1 Detection of pools along the river

This study proposed to use both *in situ* data and satellite remote sensing data. For remote sensing data, the best methods to detect water bodies/features ad to be established. Seaton *et al.*, (2020) compared atmospheric correction methods (Sen2Cor, DOS1, TOA), and concluded that the Top of the Atmosphere (TOA) reflectance images are the most suitable methods for both Sentinel-2 and Landsat 8. A similar conclusion was made by Rumora *et al.*, (2019). Seaton *et al.* (2020) further indicated that the incorporation of atmospheric

correction eliminates some of the significant water surfaces. Therefore, the TOA images were used for this study.

The downloaded Sentinel-2 images were first resampled to 10 m using Sentinel Application Platform (SNAP) using Band 3 as the reference band. Water indices were used to extract water areas from the images because the method is reliable, it is user-friendly, efficient and has a low computational cost (Du *et al.*, 2016). The processing was done using SNAP and ESRI ArcGIS 10.3 software. The indices that were used are described below.

Water Indices are used to distinguish between water and non-water features. Studies evaluated the accuracy of different indices, and they obtained varied results based on the area of study, therefore this study will assess the indices that are described below. Normalized Difference Water Index (NDWI) (McFeeters, 1996) is one of the most commonly used methods to extract water bodies from the rest of the land surface features (Equation 1). In this index, any pixel with a value of more than 0 is classified as water and any pixel with a value below 0 is classified as anything else.

$$NDWI = (Green - NIR) / (Green + NIR) \dots\dots\dots (1)$$

where Green is the green band and NIR is the near-infra-red band. Pixels of water have positive values. In addition, thresholds of 0.2 and 0.3 were tested in this study to determine whether there is an improvement.

Modified Normalized Difference Water Index (MNDWI) was proposed by Xu (2006) where short wave infrared (SWIR2) is used instead of NIR (Equation 2). However, some researchers (Elsahabi *et al.*, 2016) have shown that NDWI is more accurate than MNDWI in areas with less noise (shadows, residential features).

$$MNDWI = (Green - SWIR2) / (Green + SWIR2) \dots\dots\dots (2)$$

Normalized Difference Vegetation Index was proposed by Tucker (1979) to identify vegetation; however, research has shown that the approach/index is capable of extracting water-surface areas with acceptable accuracy (Equation 5)

$$NDVI = (NIR - Red) / (NIR + Red) \dots\dots\dots (3)$$

where NIR is the Near-infrared band, and Red is the red band. Pixels of the water body have negative values.

To improve the classification, random forest classification as proposed by Breiman (2001) was also used to classify water and non-water features. Random forest classification is an ensemble classification that produces multiple decision trees using a randomly selected

subset of training images. In this case, the pools that were assessed were excluded from the training set.

### 2.3.2 Sentinel-1 Processing

SNAP was used for pre-processing the Sentinel-1 images. Firstly, the images were calibrated to convert raw digital numbers to the RADAR backscatter coefficient. To reduce speckle noise, a lee filter was used with 3X3 kernel width and height. The images were aligned and corrected for elevation interference using the STRM 3sec DEM which is auto-downloaded by the SNAP tool. Water surfaces act as mirrors and reflect almost all incoming radiation, they cause exceptionally low backscatter. Therefore, surface water detection using SAR datasets is often based on applying a threshold of the SAR backscatter coefficient, with low backscatter values attributed to surface water (Pham-Duc *et al.*, 2017).

Therefore, the thresholding method was used for Sentinel-1 separation between water and non-water features. The threshold was determined for each scene, as the accuracy of sentinel-1 in distinguishing water from other features is affected by wind-induced roughing effects, poor image quality (speckle noise) and incidence angle variance (Guishain *et al.*, 2020). However, based on trial and error, the threshold used for this study was  $\sim -22$  dB on the VH polarisation. This is similar to many studies.

To assess whether remote sensing was able to detect pools along the river, the surface area of pools was calculated as the product of length and the average width. The field-collected points were also plotted in ArcGIS, the points were connected, and the surface area was determined.

### 2.3.3 General classification accuracy

Accuracy assessment was done in two folds, one to focus on the location of the pools in the landscape, and the other on the pool size. To assess the accuracy of remote sensing methods in detecting pools at a sub-catchment level, reference data points were obtained by creating random points and labelled based on expert knowledge of the area (field observation) and high-resolution images from Google Earth Pro and points that could be of water removed. The location of the field observed pools were also added to the random points as water areas. Pixel values at a point were then extracted for the created points. The extracted values were then compared to the field observed. The number of corrected identified pixels(points) was counted and classified as per table 2.5. Thereafter, the accuracy was assessed using the user's accuracy (equation 4), the producer's accuracy (equation 5) and overall accuracy (equation 6). User's accuracy is the proportion of correctly classified water pixels compared to all pixels classified as water. Producer's accuracy is the proportion of correctly classified pixels on an image compared to the number of pixels that are water.

Overall accuracy is the proportion of correctly classified pixels compared to the total number of pixels.

**Table 2.5:** Confusion matrix

		Reference Data	
		Water	Non-water
Classified Data	Water	<i>True positive</i>	<i>False Positive</i>
	Non-water	<i>False Negative</i>	<i>True Negative</i>

$$User's\ accuracy = \frac{True\ Positive}{True\ Positive + False\ Positive} \dots\dots\dots (4)$$

$$Producer's\ accuracy = \frac{True\ Positive}{True\ Positive + False\ Negative} \dots\dots\dots (5)$$

$$Overall\ accuracy = \frac{True\ Positive + True\ Negative}{Total} \dots\dots\dots (6)$$

where true positive is the number of correctly extracted water pixels; false negative is the number of undetected water pixels; false positive is the number of incorrectly extracted water pixels, and true negative is the number of correctly rejected non-water pixels.

#### 2.3.4 Accuracy assessment of remotely sensed pool's surface area

The accuracy of the detection of pools was examined to determine the method to be used for pool dynamics (time series). Two representative pools were selected at each of the study catchments. The pools were selected based on the feasibility to monitor using satellite images, determined by pre-inspection. The variation in the riverbed material (bedrock, sand, gravel) was considered to determine how the underlying material affects the pool's storage. Proximity to hydrometeorological monitoring stations was also taken into consideration in the selection of pools. Accessibility, in terms of roads and permission, was considered. The digitised field boundary of the pools was used as reference data. The buffer technique proposed by Brovelli *et al.*, (2015) was applied to develop a confusion matrix (Table 2) for the accuracy assessments. All pixels within the boundaries of the surface water

bodies digitised were known to be water pixels. All pixels within the area of the buffer were known to be non-water pixels.

### 2.3.5 Assessing the difference between the observed and remotely sensed surface area of pools

The surface water area of the selected pools was measured during the field visits, these were then compared to the sizes that were obtained from the remote sensing using the Differential Area Index (DAI) also referred to as the deviation. DAI is a dimensionless index used to compare true area estimates (Acharya *et al.*, 2018.; Sawunyama *et al.*, 2006) In this study, DAI is used to get standardised differences between the observed area and the estimated area of pools by remote sensing approaches. The DAI values range from -1 to 1, with 0 being the perfect score, indicating total agreement and -1 and 1 being the worse score. Negative indicates underestimation and positive indicates overestimation (Acharya *et al.* 2018). In this study we multiply the DAI by 100 to obtain the Percentage DAI, which allows for easy comparison.

$$DAI = (A_o - A_e)/A_o \dots\dots\dots (7)$$

where  $A_o$  is the observed area and  $A_e$  is the estimated area.

### 2.3.6 Pool Water Balance Analyses

The study first examined the water levels of the focal pool about the water fluxes to gain insight into water gains and losses. The time to empty and the probability of the pool drying out were then determined. *In-situ* data were used to construct the water balance model (explained in the next section). To assess the transferability of the model, the model was used to simulate the water levels of two neighbouring pools. Satellite-derived rainfall and evaporation estimates were incorporated into the model by substituting observed rainfall and evaporation, resulting in an in-situ and remote sensing hybrid water balance, this model does not consider groundwater in and out-flows (Figure 2.5). The fully remote sensing-based model uses changes from surface area obtained from Sentinel-2 images and satellite-derived rainfall and evaporation. The performance of all the models was evaluated using actual water levels measured from the pools. Figure 2.5 illustrates the methodological flow of the analyses.

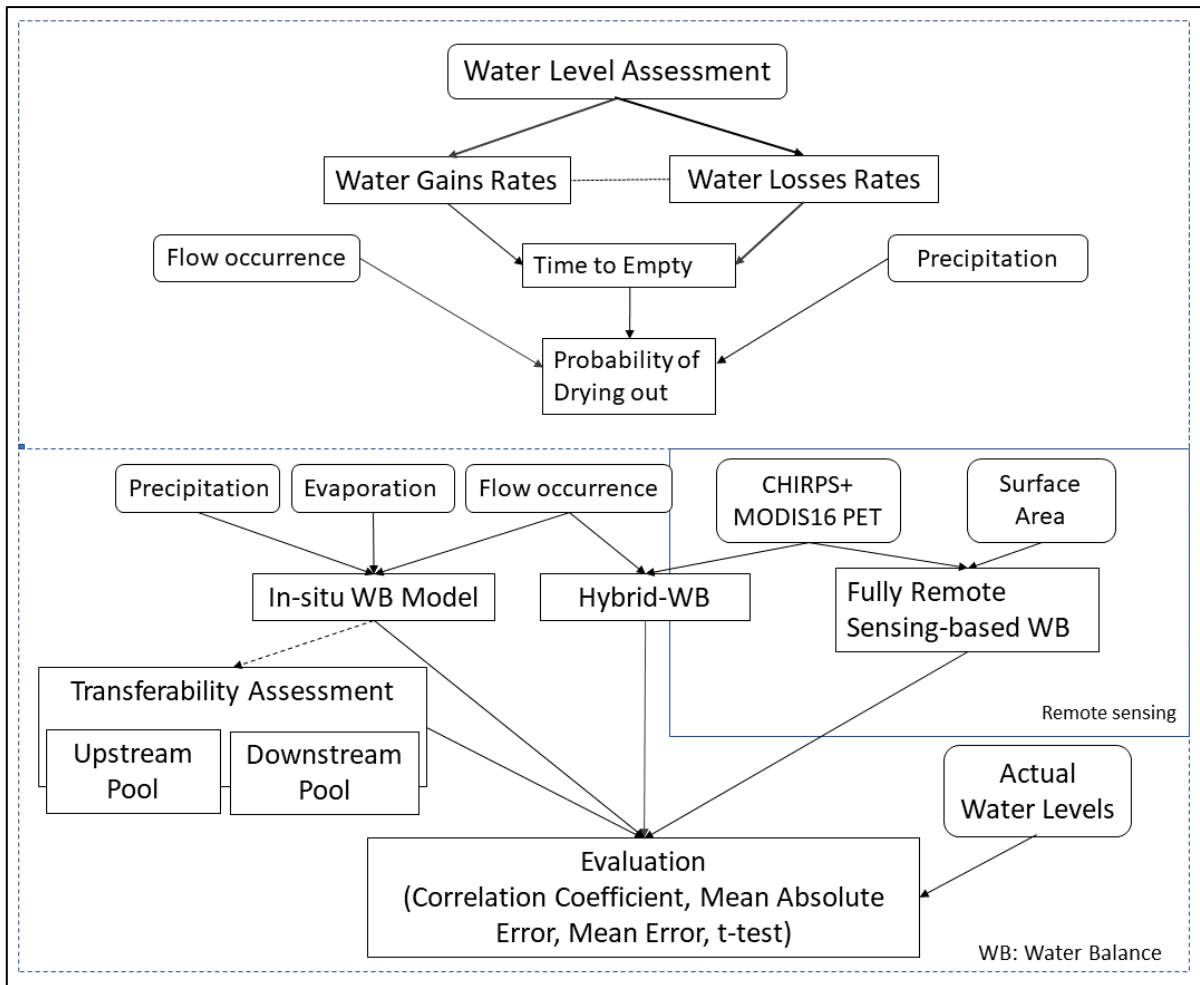


Figure 2.5 A flow chart illustrating the methodological procedure followed in this study.

In this study, time to empty (TE) was defined as the time it takes a pool to completely drain out the water from being full. This is based on the pool’s rate of water loss and assumes that there are no surface water inflows in the pool.

$$TE = \frac{S_{max}}{L_{wl}} \dots\dots\dots (8)$$

where  $S_{max}$  is the maximum water level in meters and  $L_{wl}$  is the average water loss per day in meters. The probability of the pool drying out is the chance of finding the pool dry calculated based on the dry period (no-flow duration) exceeding the time to empty while considering that rainfall over the pool can reduce the number of dry days. In this study, this was calculated using 30 years of flow occurrence and rainfall data, because there is no long-term data on the other water balance components to derive this using water balance.

### 2.3.7 Water balance description

To assess and understand the pool dynamics, a water balance approach was used. The water balance is based on the changes that are observed in the pool (Equation 9).

$$\Delta S = S_{t-1} - S_t \dots\dots\dots (9)$$

Where  $S_t$  is storage,  $S_{t-1}$  is the storage of the previous day/month and  $S_t$  is the present-day/month. Any change in the pool water level can be explained by the water balance (Equation 10) as illustrated in Figure 2.6.

$$\Delta S = P - E + Q_{in} - Q_{out} + GWin - GWout \dots\dots\dots (10)$$

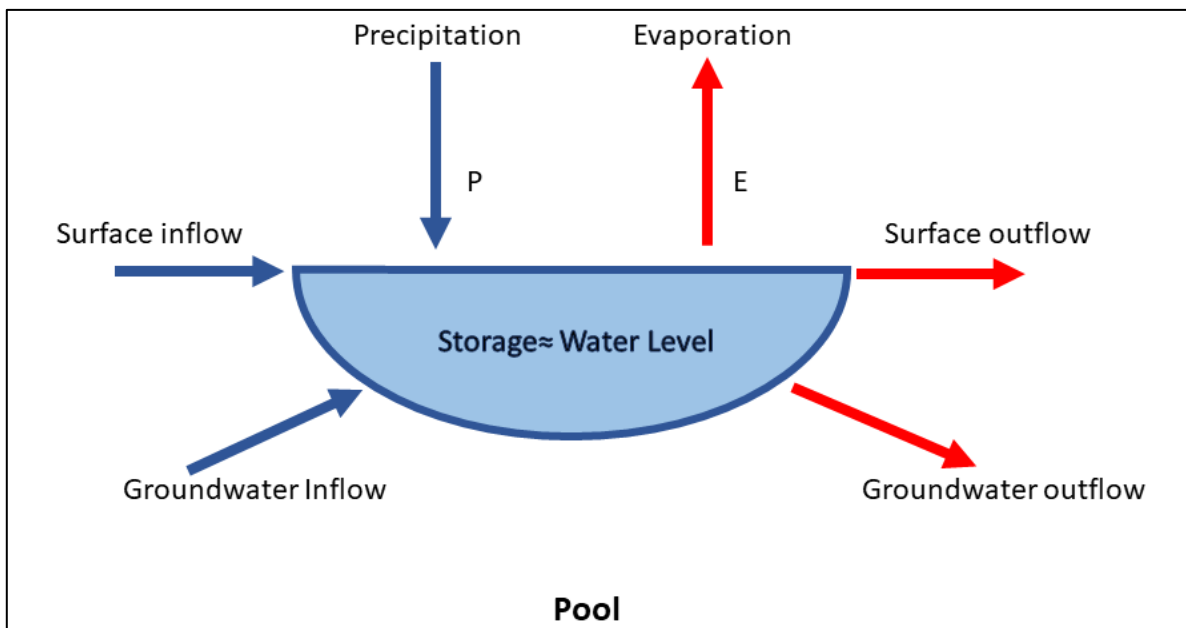


Figure 2.6 Concept of water balance model with blue arrows showing water gains (precipitation, surface, and groundwater inflows) and red arrows showing water losses (evaporation, surface, and groundwater outflows) from the pool.

Rainfall (P) was monitored on-site and in other parts of the catchment that may supply water to Touws River. However, for direct rainfall into the pool, the closest rainfall station which was monitored on a nearby farm (600 m from the WW2 pool) was considered.

Evaporation (E) from the pool was estimated using the Penman, (1948) method based on weather station data as it is one of the commonly used methods to estimate open water evaporation (Mbanguka *et al.*, 2016; Yihdego and Webb, 2018). Losses into the subsurface area ( $GW_{out}$ ) were estimated using the residual losses of water from the pool, defined as (Equation 11).

$$Subsurface\ losses = TL - E \dots\dots\dots (11)$$

where TL is total losses and E is evaporation.

Groundwater into the pool ( $GW_{in}$ ) was also estimated as residual, assuming that positive change in water level can be explained using rainfall and surface water inflow (Equation 12). Therefore, this means that a positive change in storage without surface water inflow or rainfall may indicate groundwater feeding the pool (Equation 13).

$$+\Delta S = GWin + P + Qin \dots\dots\dots (12)$$

$$+\Delta S = GWin, \text{ when } P + Qin = 0 \dots\dots\dots (13)$$

Surface inflow ( $Q_{in}$ ) and outflow ( $Q_{out}$ ): the only discharge information used in this study was flow occurrence observations. The study assumed that when flow occurs, the pool is filled to capacity since the pools are small and will fill up to capacity within minutes if not seconds. The rate of losses at this point is insignificant to change the water levels of the pool. At this point, the pool will continue to spill at an equal rate as the inflow until the flow ceases. Therefore.

$$Qout = Qin \text{ (at } S_{max}) \dots\dots\dots (14)$$

where  $S_{max}$  is the maximum water level of the pool

The model was built specifically for the WW2 pool and was transferred to WW1 and TWB pools. Only two adjustments were made; the initial water level (starting point) and the maximum water level as these pools are not equal in size. These pools are close to the WW2 pool, therefore, we assumed they have the same hydroclimatic conditions.

### 2.3.8 Statistical analysis

In evaluating the performance of the simulations, the mean error, mean absolute error, correlation coefficient and paired T-test methods were used. Mean error ( $ME$ ) also called bias measures the average of estimation error; this considers the direction of the errors (Equation 15).  $ME$  ranges from negative infinity to positive infinity and has a perfect score of 0. A positive score indicates that the model is overestimating, while a negative score indicates that the model is underestimating on average. However, with the  $ME$ , a perfect score can be achieved when overestimation and underestimation compensate for each other. Hence, the mean absolute error ( $MAE$ ) was used to provide a true estimation error (Equation 16) and  $ME$  to derive the direction of the error.

$$ME = \frac{1}{n} \sum_{i=1}^n (E_i - O_i) \dots\dots\dots (15)$$

$$MAE = \frac{1}{n} \sum_{i=1}^n |E_i - O_i| \dots\dots\dots (16)$$

where  $E_i$  is the simulated water level,  $O_i$  is the observed water level, and  $n$  is the total number of data points.

A t-test (Equation 17) was used to determine whether there is a significant difference between the estimated and observed water level mean at a 5% significance level.

$$t = \frac{\sum x-y}{\sqrt{\frac{n(\sum x^2-y^2)-(\sum x-y)^2}{n-1}}} \dots\dots\dots (17)$$

where  $t$  is the t-statistic,  $x$  is the observed water level mean,  $y$  is the modelled water level, and  $n$  is the total number of data points. A paired t-test assumes that the data sets are continuous, follow a normal distribution, that the mean is a good measure of central tendency and that the two samples are paired (Helsel *et al.*, 2020).

To assess the relationship between the simulated and observed water level, a correlation coefficient (Equation 18) was used. Correlation ranges from -1 to +1, and  $\pm 1$  is a perfect relationship, and 0 means that there is no relationship between the observed and the simulated values.

$$r = \frac{n(\sum OE)-(\sum O)(\sum E)}{\sqrt{[n\sum O^2-\sum O]^2-[n\sum E^2-\sum E]^2}} \dots\dots\dots (18)$$

where  $O$  is the observed water level measured by a logger,  $E$  is the simulated water level and  $n$  is the number of pairs of scores.

Mean error, mean absolute error, t-test, and correlation coefficient were also used to assess the transferability of the model to a pool upstream and downstream of WW2.

The relationship (rating curves) between surface area, depth and volume were determined to be able to convert the surface area to depth or even volume. The pool's volume estimation was based on the following equations derived using a 3D analyst on ArcGIS using the DGPS points and continuous water level measurements (Equations 19 and 20). These relationships were specifically derived using the WW2 pool.

$$\text{Water level} = 0.00009*\text{Area}; \quad R = 0.99 \quad \dots\dots\dots (19)$$

$$\text{Volume} = 0.00005*\text{Area}^2 + 0.1415*\text{Area} + 18.83; \quad R=0.99 \quad \dots\dots\dots (20)$$

## 2.4 DETECTION OF HYDROLOGICAL PHASES

Sentinel-2 images were used to determine the hydrological state of the river. In some parts of the river, the flow can occur for 32 months, ~100 images per site (July 2019 to March 2022), depending on cloud cover. Sentinel-1 was used to determine if it will be able to detect some of the flow events that could be missed by Sentinel-2. Sentinel-1 is a SAR satellite, capable of penetrating through clouds. MNDWI was used to extract water areas from Sentinel-2 images as Maswanganye *et al.* (2022a) showed that it was superior compared to other methods, for Sentinel-1 the thresholding methods were used.

Selection of the monitoring reach had to have them as representatives of the river. Hence, located in mid catchments. The selected sites are within the dominant geology, and soil types of the catchment, these sites are also located within the average slope of the catchment. The phases were monitored in a selected 5 km of river. Connected surface water meant that the river was flowing. However, because the rivers meander and can tend to be flowing in a small part of the channel, this worsens by the availability of cloud-free images during peak flow, a threshold of 50% or 2.5 km of the 5 km reach was used, meaning that if reach had 2.5 km water, it was assumed that there was flow. Surface water presence of less than 2.5 km was labelled as pool and dry riverbed when no water pixel was detected. Figure 2.7 and 2.8 illustrates the different phases of the Touws River and Molototsi river, respectively.

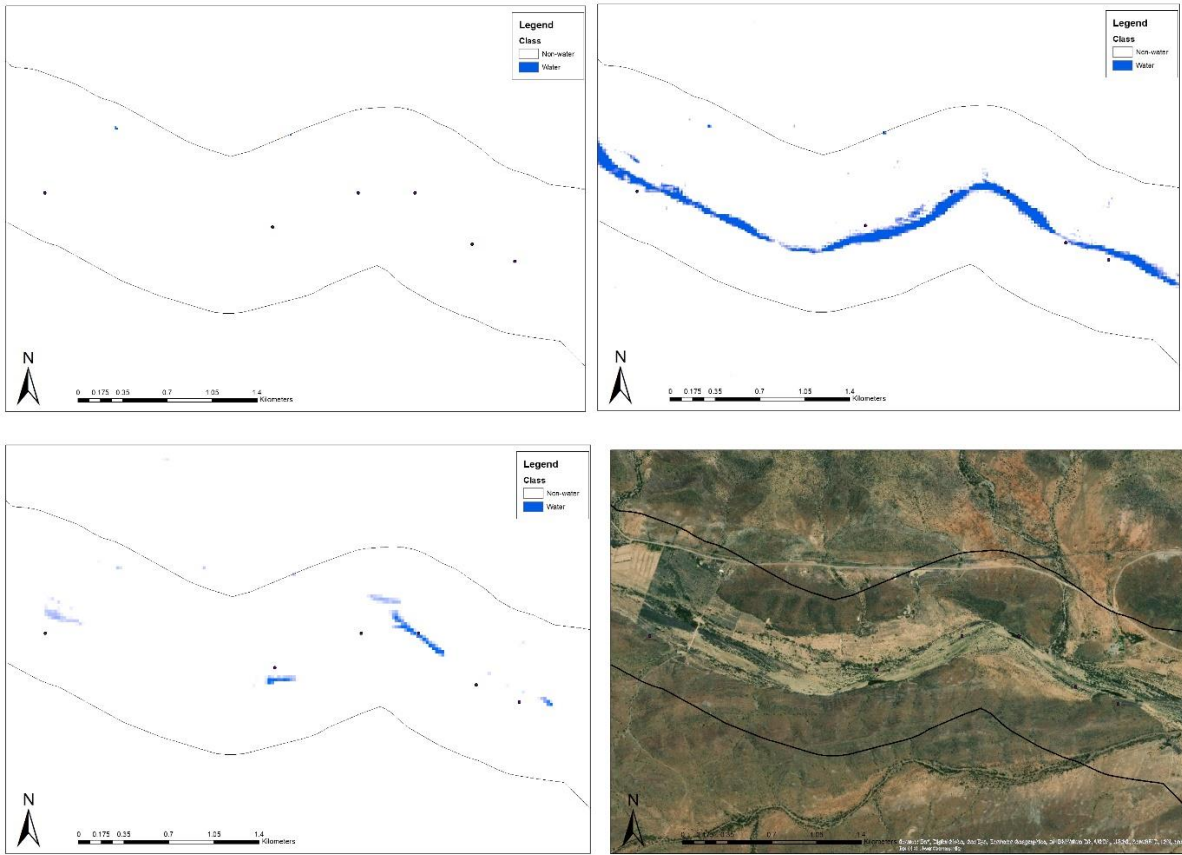
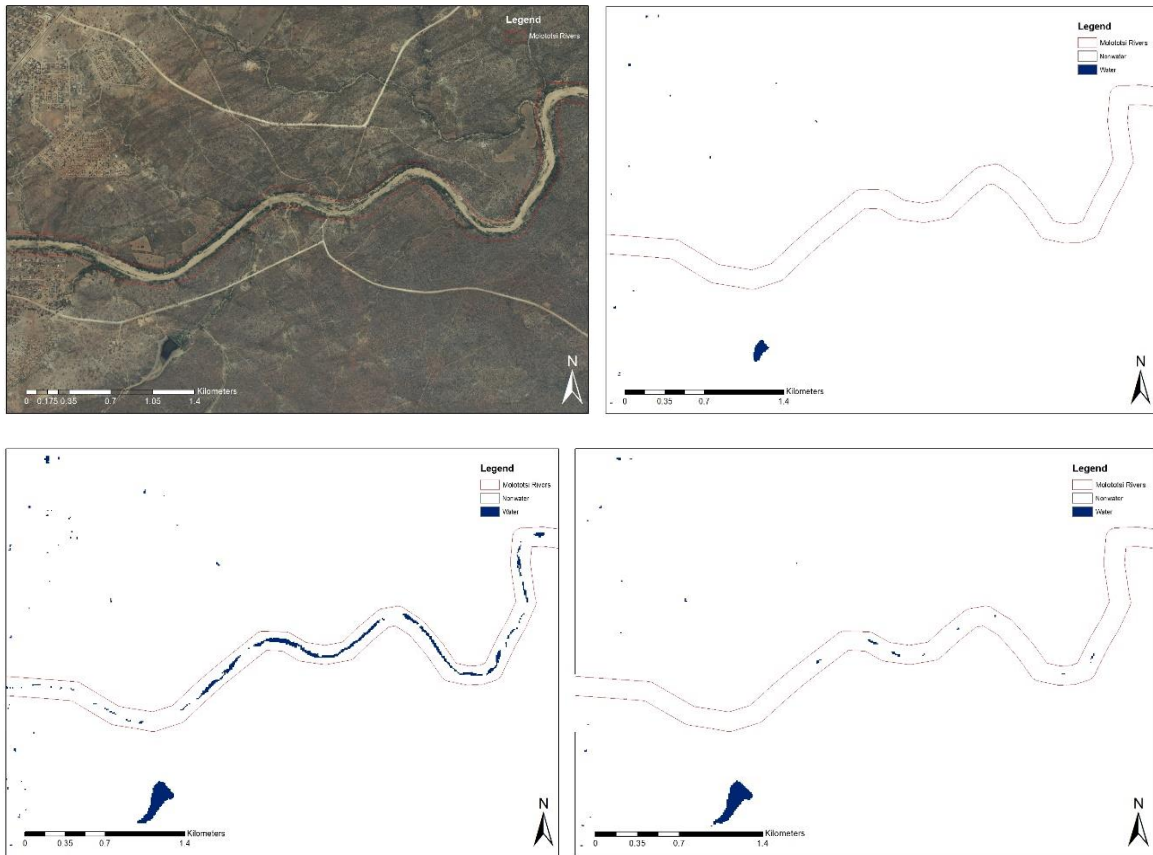


Figure 2.7 Three hydrological phases dry (top left), connected flow (top right) and isolated pools (bottom left) after the flow event in a 5 km reach of the Touws River.



**Figure 2.8** Three hydrological phases dry (top left), connected flow (top right) and isolated pools (bottom left) after the flow event in a 5 km reach of the Touws River.

#### 2.4.1 Identification of flow-contribution areas

Usually, the identification of contributing areas is done using observed data from the tributaries outlet (Tena et al., 2021), however, rainfall and physical characteristics (soil type, slope and land use and cover) can be used in the absence of the flow data. Several methods can be used to determine the contributing area, mainly proxies such as the Soil Conservation Service (SCS) Curve Number method and the Runoff coefficients. This study used remote sensing-derived rainfall to determine where rainfall occurred to produce observed flows (antecedent rainfall). The SCS curve number method was used to determine which parts of the catchment are likely to generate runoff based on the physical characteristics. USDA (1986) describes the curve number method. This is the most popular method for estimating direct runoff (Gajbhiye, 2015) and uses data that can easily be obtained even in data-scarce areas. Soil types were obtained from the WRC website (<https://waterresourceswr2012.co.za/>) (Figure 4). The 2020 South African National Land Cover (SANLC) (<https://egis.environment.gov.za/>) was used for land cover and land use. For topography, Shuttle Radar Topography Mission (SRTM) 1 Arc-Second Global Digital

Elevation Model (DEM) was used, available at the USGS website (<https://earthexplorer.usgs.gov/>).

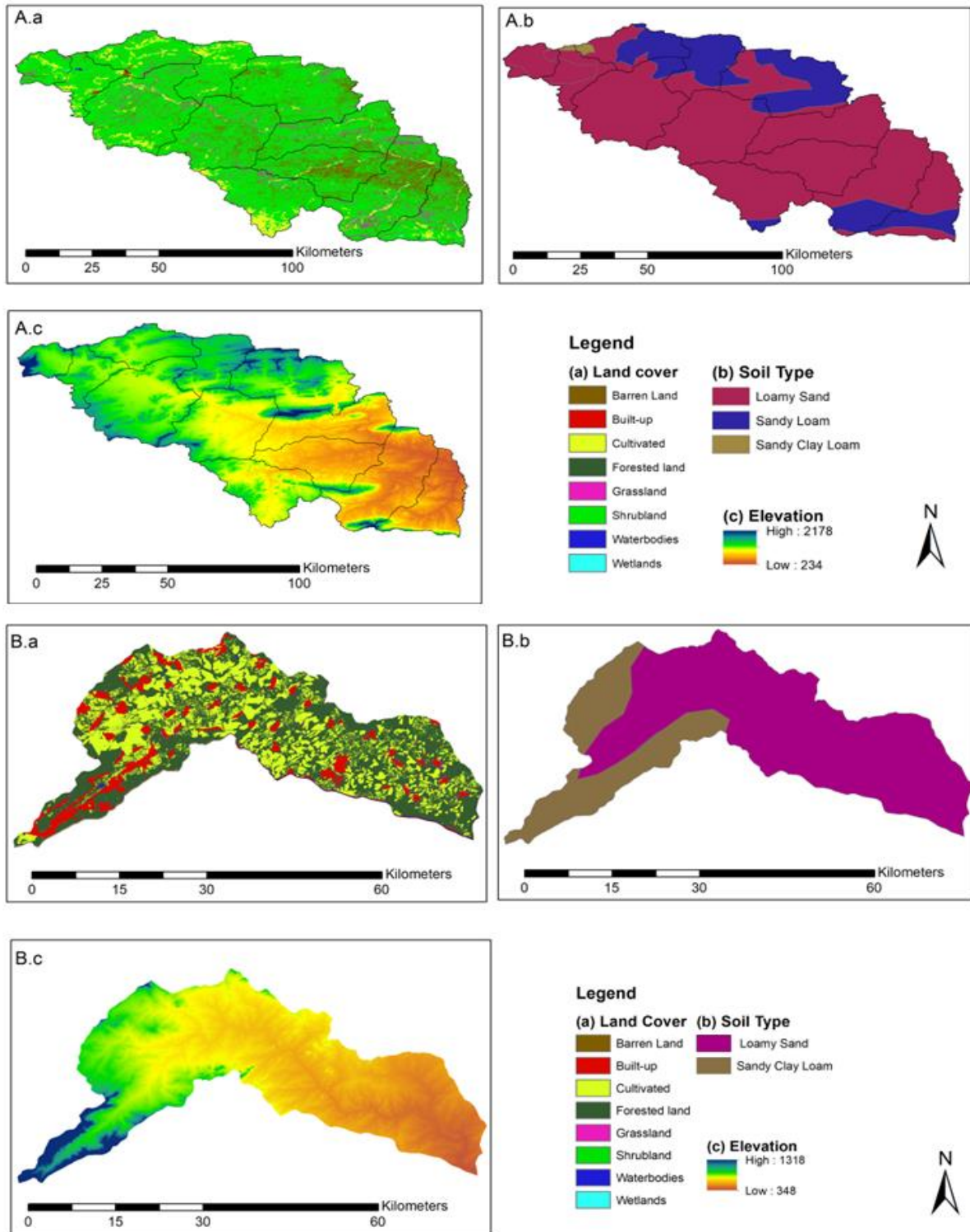


Figure 4 Data that were used to derive curve numbers in the Touws (A) and Molototsi Catchment (B).

### 2.4.2 Evaluation metrics

Overall Accuracy, Producer's accuracy and User's accuracy were used to determine the ability of remote sensing to distinguish between the dry, pools and the flowing state of the rivers (Maswanganye, 2018). To determine the magnitude of the error, percentage error was used. Flow occurrence is of importance for NPRs, for instance, it is important to know how many flow events are likely to be missed by the satellite (Sentinel-2) observation. Hence this study calculates this chance:

$$Fdp = \left( \frac{\text{no. of detected flow events}}{\text{Total no of events}} \right) * 100 \quad (21)$$

Fdp is the flow occurrence detection power

The study investigates whether this flow event detection will be improved by using Sentinel-1. Furthermore, the effect of the duration of flow events on the ability of remote sensing to detect is determined.

## 2.5 METHODS TO DETERMINE FLOW USING REMOTE SENSING

To estimate flow using remote sensing, various methods will be tested to establish the one that works for non-perennial rivers. Sichangi *et al.*, (2016) summarised methods of estimating discharge from remote sensing into four categories. The first category is the water level derived from satellite data (altimetry) which is converted to river discharge based on the water level-discharge rating curve used by Hirpa *et al.*, (2013). However, the availability and access to this kind of data in developing regions is minimal (Cai *et al.*, 2016), and the altimetry mission has a low probability of extracting information about the small water bodies, thus it is used for rivers with a width greater than 100 m (Busker *et al.*, 2018). The technique is still constrained by several factors (corrections, re-tracking, geographical effects) in terms of monitoring inland water bodies as compared to ocean water levels (Pipitone *et al.*, 2018).

The second category uses satellite-derived hydraulic variables such as slope, maximum channel width, water-surface width, and inferred velocity to estimate discharge from hydraulic equations. For instance, Bjerkile *et al.* (2005) used this method to estimate the bank river discharge of 17 rivers, where maximum channel width was obtained from aerial and digital orthophotos. Topographical maps were used to derive slopes. Water-surface width and velocity were derived from SAR data. This was applied to the derivatives of the manning equation to obtain river discharge. Calibration was done using observed discharge, and a calibration function was defined that related to the channel type; this improved the estimates (+72% accuracy).

The third category estimates discharge solely from remotely sensed data including the channel geometry such as width and depth. This is done through the use of characteristics scaling law referred to as At-Many station Hydraulic Geometry (AMHG), which eliminates half of the parameters required by traditional hydraulic geometry, and it can estimate from only several surface widths measurements (Gleason and Smith, 2014; Gleason and Wang, 2015) However, the uncertainty of this method is high and it still requires prior knowledge about the river and was applied to large rivers, and also performed poorly in a river with temporal flows (Sichangi *et al.*, 2018).

The last category correlates satellite-derived surface area with in-situ measured discharge based on the water area-discharge curve. Smith and Pavelsky, (2008) demonstrated that this approach can yield acceptable results ( $r=0.8$ ) when compared to in-situ measurements, even when using moderately poor spatial resolution images (250 m) in Lena River, Siberia which is the 8th largest river in the world in terms of runoff. These methods are rarely applied to a non-perennial river or temporary river. Therefore, in this report, the water surface area-discharge curve approach will be used for non-perennial rivers.

#### 2.5.1 Area-discharge curve

The selection criteria for the water surface width/area should be in proximity of the *in situ* flow station, assuming there are no significant water losses within the reach used to estimate flow from remote sensing and the *in situ* flow station, ii) free of vegetation and the channel should be well defined iii) should not be an area with a pool, iv) wide enough to be cover by at two-pixel of satellite product used (10 m for sentinel-2, 15 m for Landsat 8).

The length of width covered by water on each of the eight cross sections was measured, and this was averaged to obtain averaged water-surface width. Other than using an average width, a reach was used to determine the number of pixels which will be inferred as the amount of water passing through a reach represented by the red box in Figure 2.6. In Touws River Catchment, the site is a few meters away from the DWS gauging station (J1H018) (Figure 2.9) which was used to derive the rating curve.

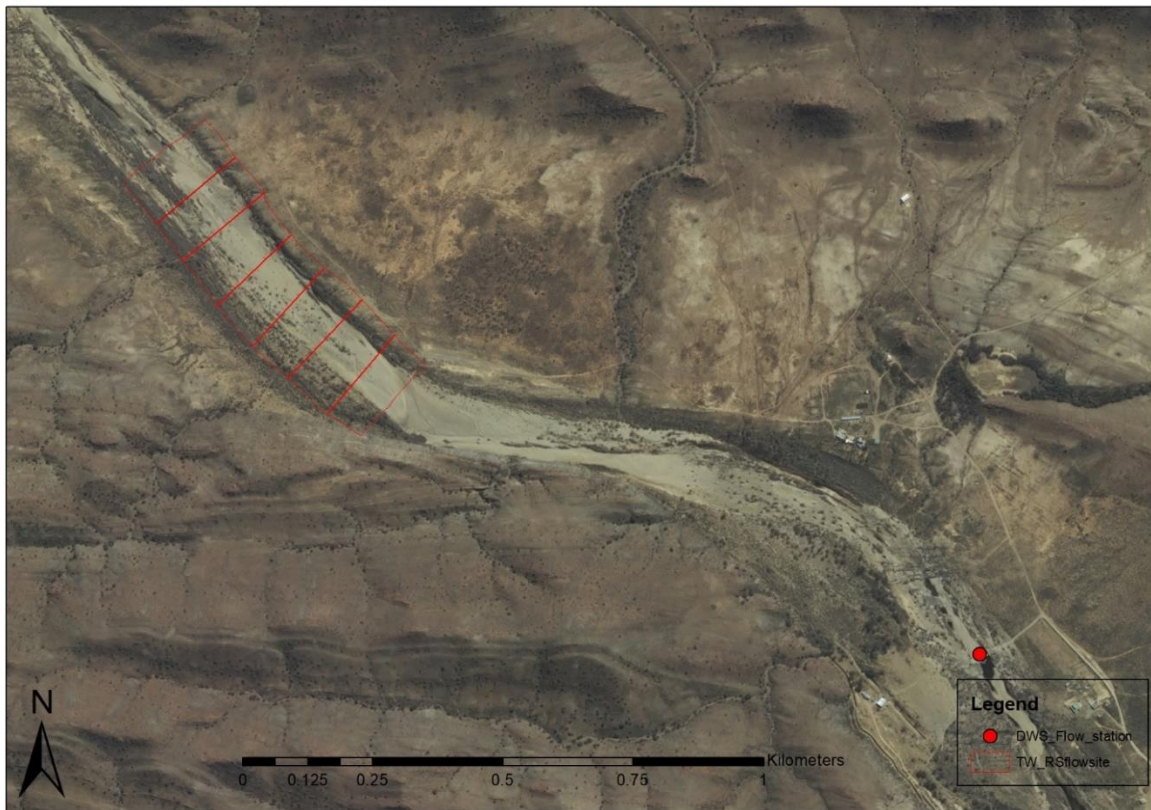


**Figure 2.9** The site that was used to estimate discharge in the Touws River with the Department of Water and Sanitation flow gauging station.

The study uses the below flowchart as guidelines (Figure 2.10), this was determined through the exploration of the available data and detection abilities. Flow usually occurs during days with clouds in non-perennial rivers, as a result, cloud-free optical remote sensing images are often available as flows do not last long after rain, hence the option to use RADAR data that can penetrate the clouds and extract the required information (Figure 2.10) When cloud-free optical remote sensing images are available the selection of method was based on the surrounding characteristics of the river, in this case, NDVI was ideal for the vegetated Heuningnes and Molototsi catchments. Thresholding MNDWI was used for the Mountains Touws River where shadows from the hills are often misclassified by NDVI, NDWI and the original MNDWI. Sentinel-2 and Landsat 8 were used. However, Sentinel-2 was given preference due to its better spatial resolution. For the Touws River flow estimation, Landsat 8 images were included as Sentinel-2 only covered four flow events.

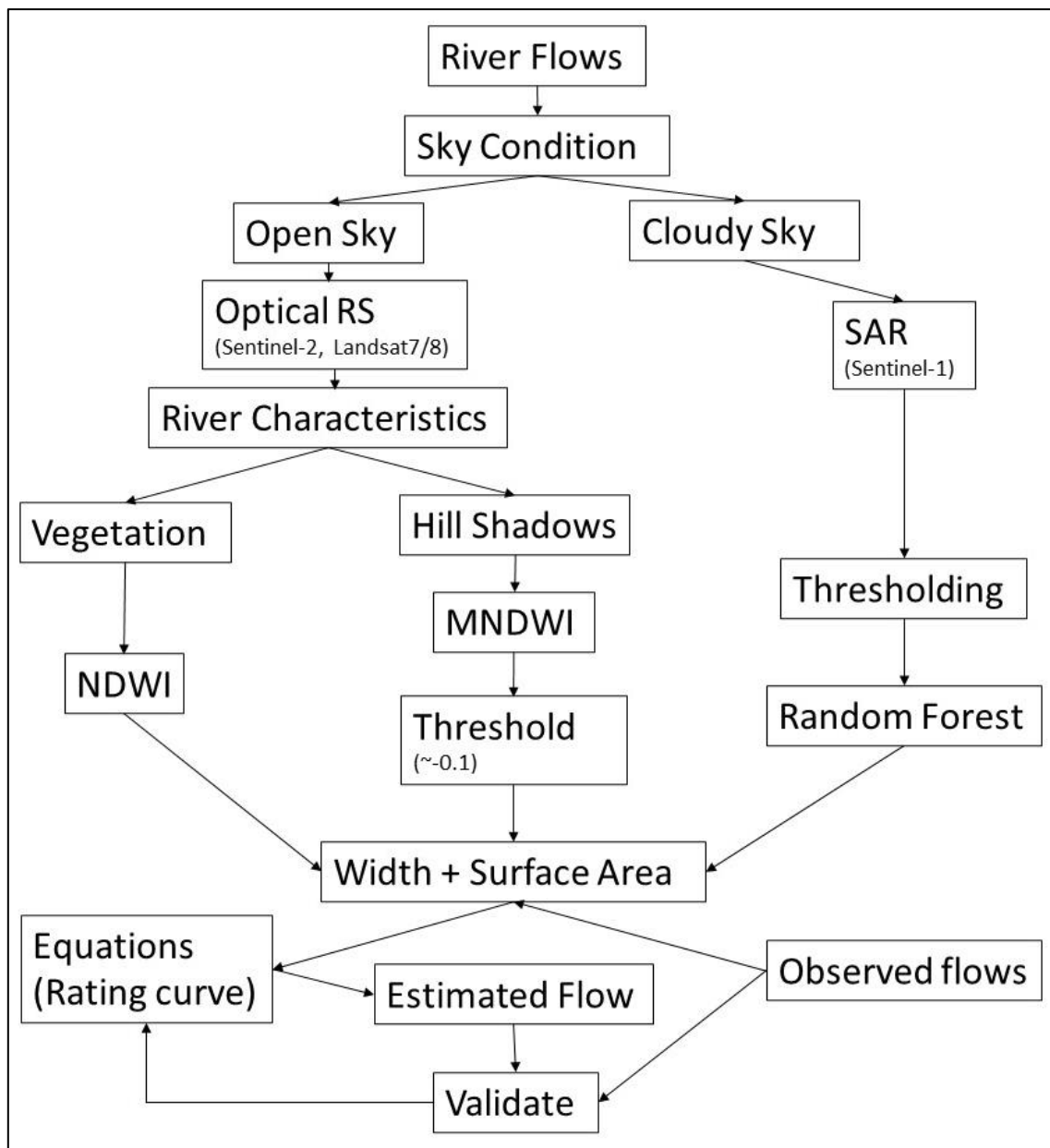


Figure 2.10 Flowchart showing the rating curve method used in estimating discharge using remote sensing.

### 2.5.2 Empirical equations

Many non-perennial rivers do not have flow gauging stations to derive the rating curve. Therefore, this study also tested the use of empirical equations that requires no field measurements to estimate discharge, one of the equations used by Kebede et al. (2020) (Equation 22 to 24).

$$Q = 7.22W^{1.02} D^{1.74} S^{0.35} \dots\dots\dots (22)$$

where Q is the discharge/flow, W is the width, D is the depth, and S is the slope. Width is obtained from satellite images; D is estimated as follows:

$$V = 1.48W^{0.8} S^{0.6} \dots\dots\dots (23)$$

$$D = (V/S^{0.5})^{1.5} \dots\dots\dots (24)$$

*Modification for non-perennial rivers*

$$Q = A * v; Q = W * D * V \dots\dots\dots (25)$$

where Q is discharge, A is the cross-sectional area, V is the velocity, W is width, and D is depth and was defined using width-to-depth area ratio, velocity was estimated using equation 24.

$$\text{Width to depth ratio} = \frac{\text{Max Width}}{\text{Max Depth}} \dots\dots\dots (26)$$

In this study, Google Earth was used to estimate width to depth ratio (Figure 2.11), and it was found to be 1:41. Therefore:

$$D = W/41 \dots\dots\dots (27)$$

where D is the depth and W is estimated from the satellite images.



Figure 2.11 Example of the cross-sections of the river used to estimate the Width-Depth ratio extracted from Google Earth.

### 3 RESULTS

This section presents data that will be used for this study. These include rainfall, river flows, pool, and groundwater levels. The section also provides an interpretation of the data. The data will contribute to assessing the spatial and temporal dynamics of flow and pools along non-perennial rivers. The subsections are subdivided by catchment, the data collected in Molototsi river is presented first, followed by Heuningnes, and then Touws River Catchment.

#### 3.1 MOLOTOTSI RIVER CATCHMENT

##### 3.1.1 Rainfall

During the 2017 to 2022 period, rainfall mostly occurred during the summer season between December and March. The 2018/19 wet season was drier compared to the 2017/18 and 2019/20 wet seasons. 14 days received more than 40 mm/day of rainfall (Figure 3.1). The highest rainy day received was 105 mm/day; however, this might have been received over 2-3 days but recorded into one day, which is a challenge associated with non-recording manual rain gauges. The data show that the catchment has a rainy summer period, usually starting in October and ending in March, which is the case in most parts of South Africa.

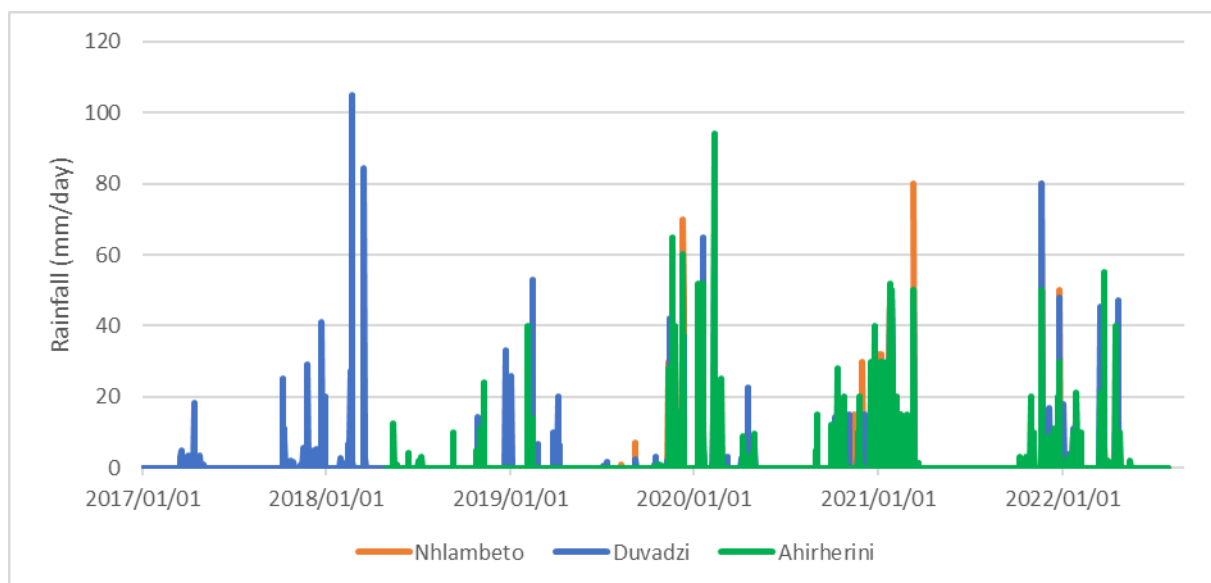


Figure 3.1 Rainfall data collected by three citizen scientists at farms in the Molototsi River catchment

### 3.1.2 River flow

There were three major flow events in the Molototsi River during the 2019/20 summer (December to February). The December 2019 flow occurred for 12 days and received 207 mm of rainfall over six days. In January and February, the flow occurred for 13 and 16 days respectively, after 200 mm over two days in both months. There was a connected flow between January to March (20 days) during the 2020/21 wet season. The 2021/22 wet seasons had fewer days with connected flows compared to the other wet seasons (Figure 3.2). The width and depth of these flow events were recorded through the citizen science monitoring programme (Figure 3.3). There was a good correlation between flow depth and width.

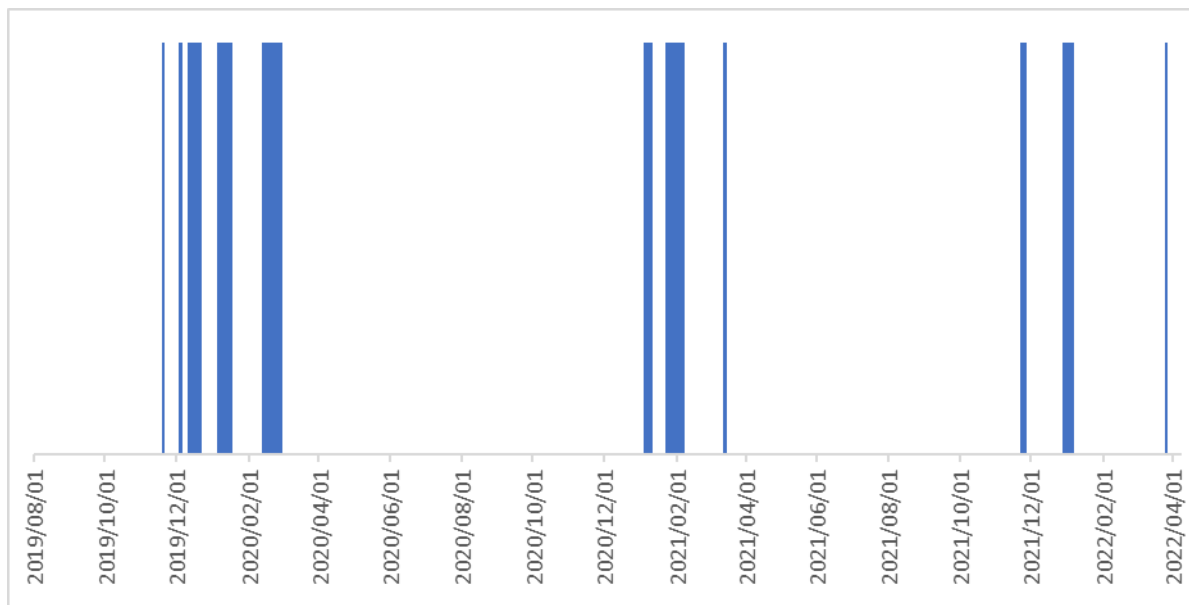
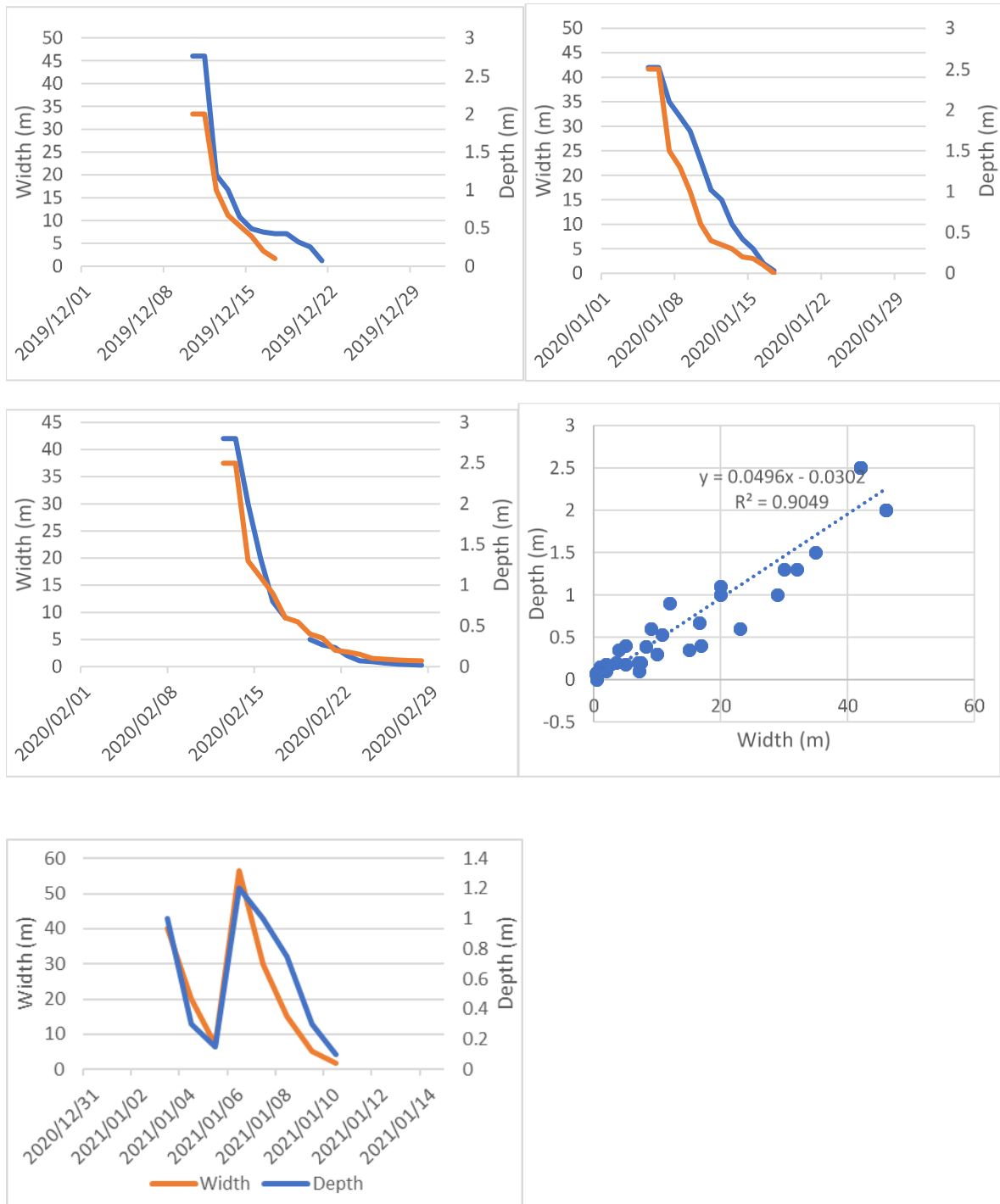


Figure 3.2 Flow occurrence in the Molototsi as per Citizen Science data

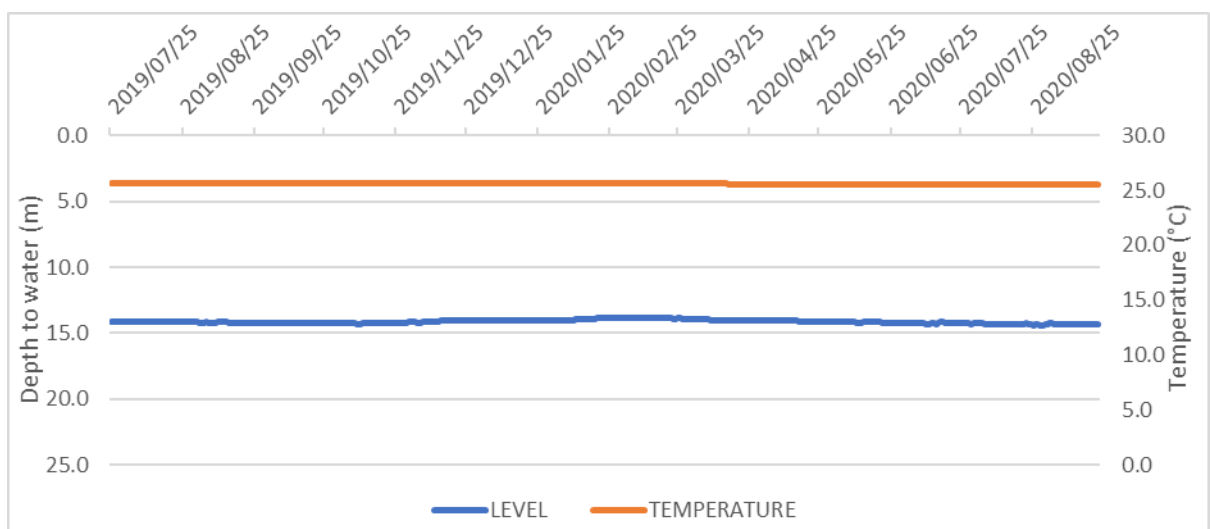
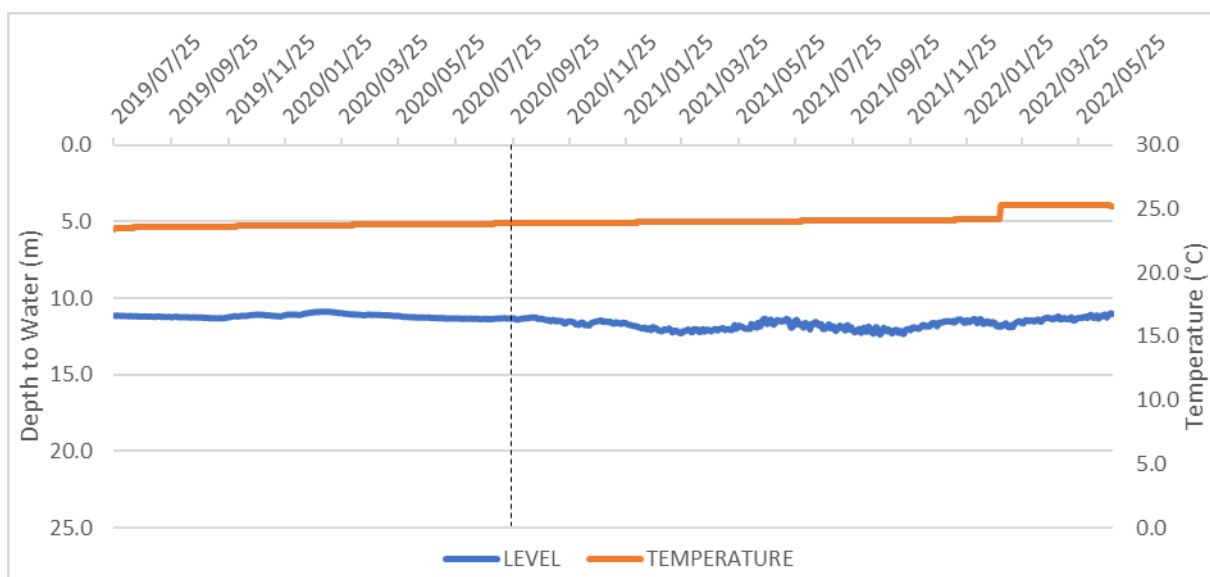


**Figure 3.3** Maximum depth (blue) and width (orange) of the river flow observed by citizen scientists in the Molototsi River, and the overall relationship between flow depth and width (bottom right).

### 3.1.3 Groundwater

Three boreholes were logged on the Duvadzi farm. One of them was equipped and used for irrigation from 20 September 2020. Before that, there was no notable response in

groundwater level to the rain received and flow that occurred from the 10<sup>th</sup> to 21 December 2019, 5<sup>th</sup> to 17 January 2020 and 12<sup>th</sup> to 28 February 2020. All three boreholes at Duvadzi farm showed no response (Figure 3.4). This might indicate that there is no interaction between surface water and groundwater, or this may be delayed. It further suggests that the pools and sand wells in the river are not groundwater-fed, or groundwater driven, and there might be no water coming from groundwater. These observations are consistent with the ones made by Walker *et al.* (2018) over two wet events of the 2015/2016 periods. After the borehole water was used for irrigation, the other boreholes responded to the pumping as the water depth fluctuated, suggesting that the boreholes are within the same aquifer.



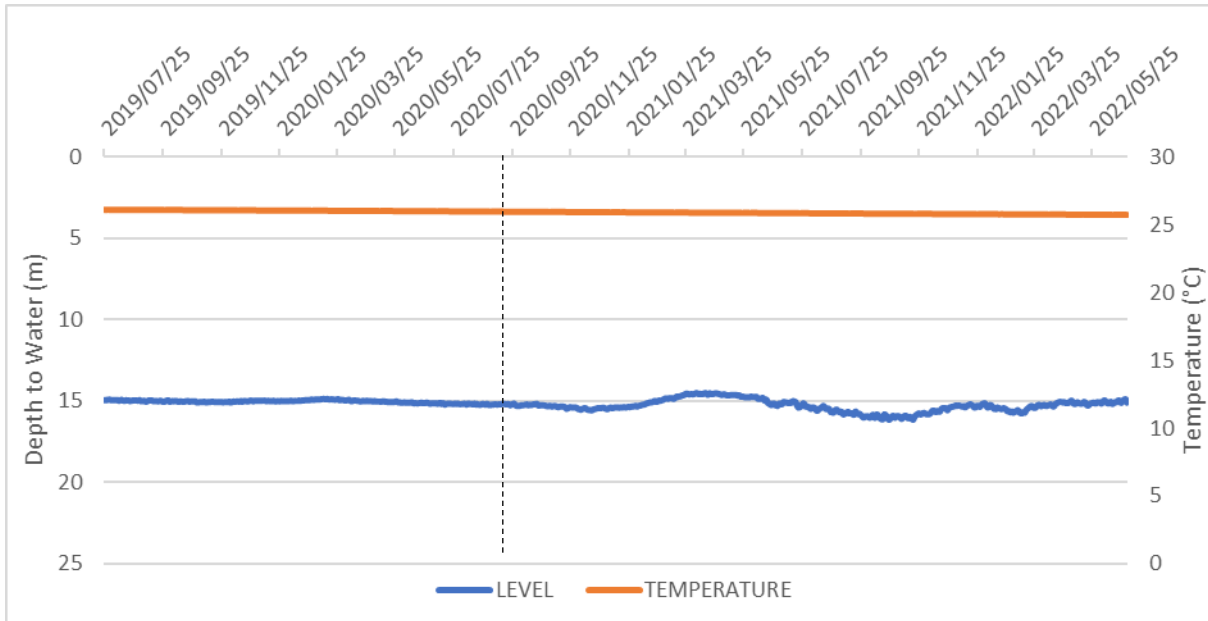


**Figure 3.4** Groundwater levels and temperature measured with data loggers in boreholes at Duvadzi Farm, H14\_1701(Top), H14\_1702 (Middle) and H14\_1703 (bottom).

Another essential factor that influences the dynamics of pools and flow is evaporation. Penman Equation was used to estimate evaporation using Gravelotte weather station data. Evaporation rates were highest in January or December of each year (~180 mm/month), whereas the lowest evaporation rate occurred in June (~75 mm/month). The total annual evaporation was 1540, and 1472 mm for the years 2019 and 2020, respectively.

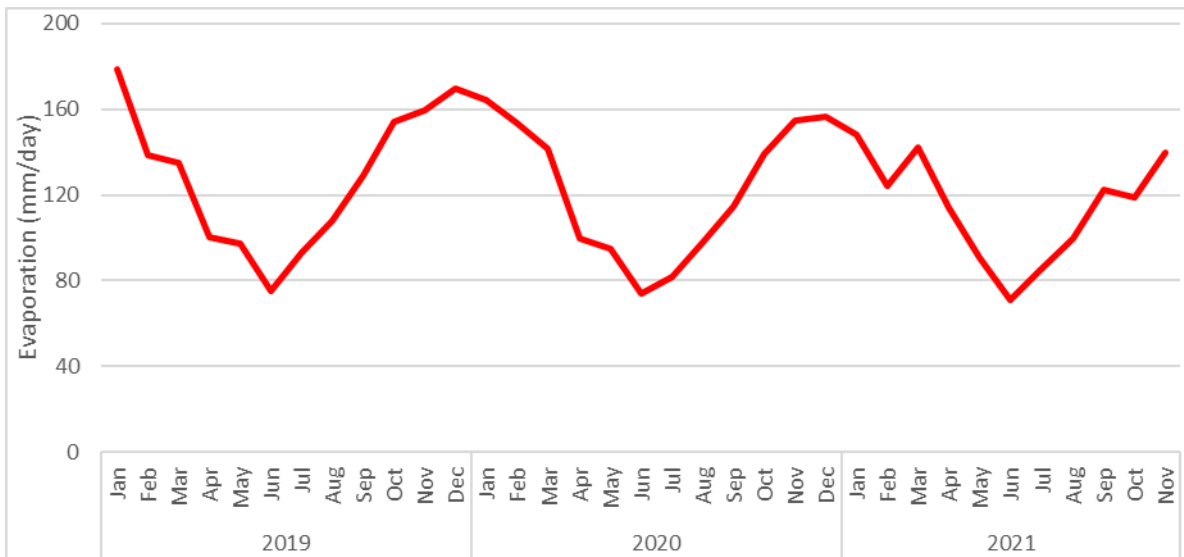


**Figure 3.5** Monthly rate of evaporation of water in mm per month for Molototsi Catchment estimated using the Penman method.

## 3.2 TOUWS RIVER CATCHMENT

### 3.2.1 Rainfall and river flow

From 2018 to 2021, rainfall in the Touws River catchment showed no seasonality. The catchment has a mean annual rainfall of 186.7 mm/year (1979-2018). The catchment received 112, 91, 200 and 230 mm/year in 2018, 2019, 2020, and 2021 respectively. Most rainy days received less than 5 mm/d of rainfall. There were only four events that exceeded 30 mm/d. These major rainfall events produced localised flow that did not reach the flow station (Figures 3.6 and 3.7). Citizen scientists observed these flow events. These events were also observed using the water levels of the pools. Figure 3.5 shows that the catchment might have experienced drought between 2015 and 2018 after the flood that occurred in 2014.

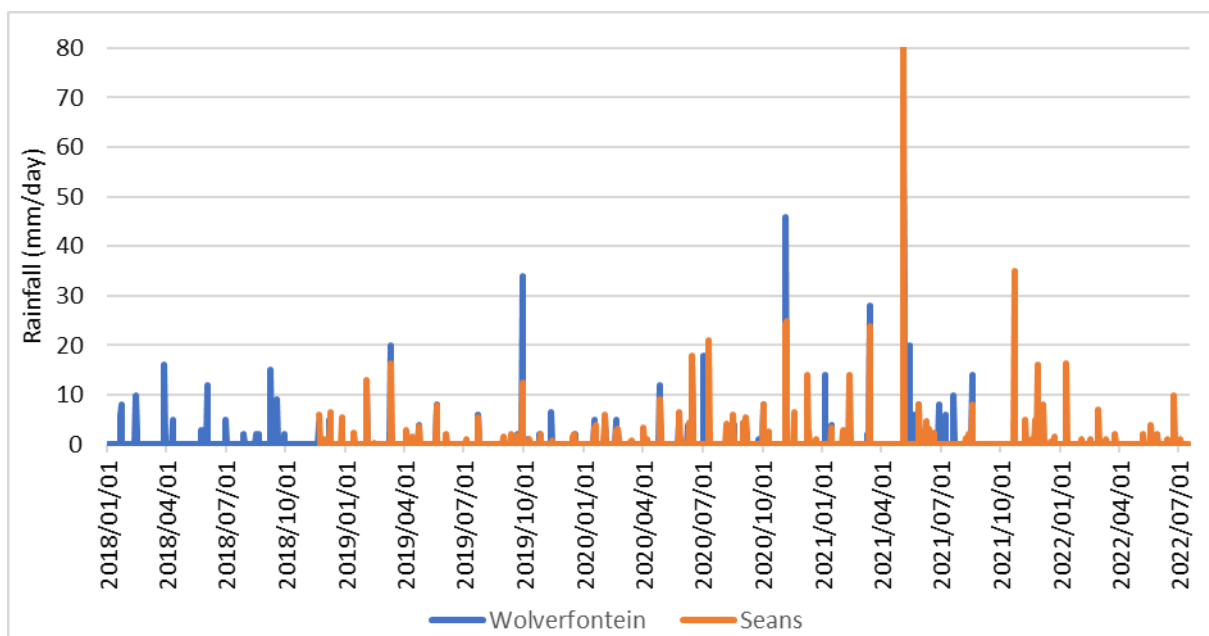


Figure 3.6 Rainfall recorded through the citizen science program in the Touws River catchment

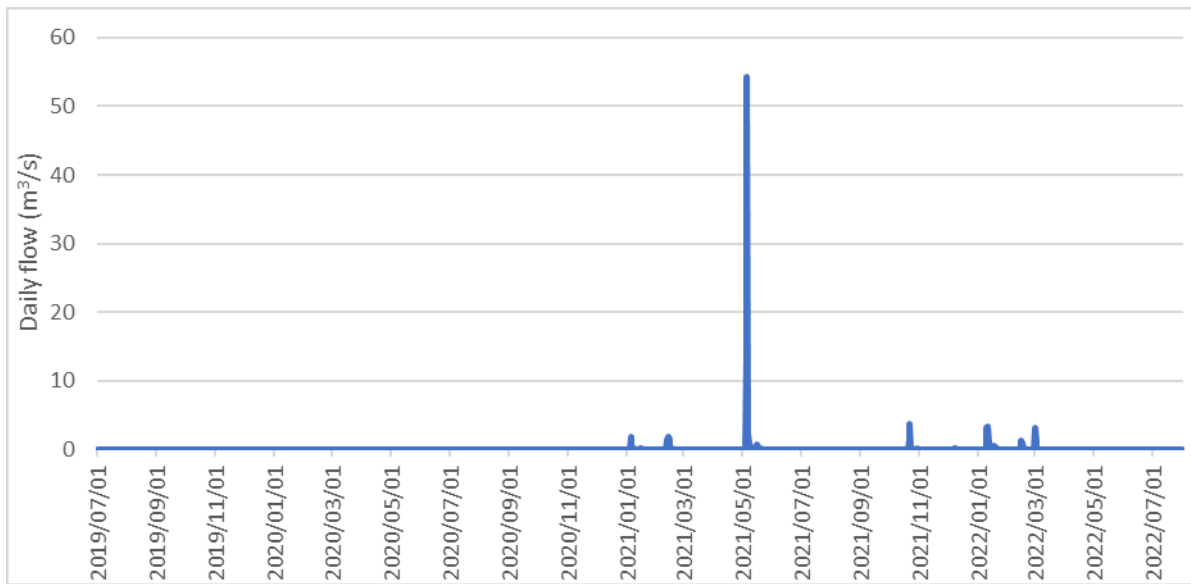


Figure 3.7 Observed diurnal flow time series at the Department of Water and Sanitation station J1H018 near the outlet of the Touws River catchment.

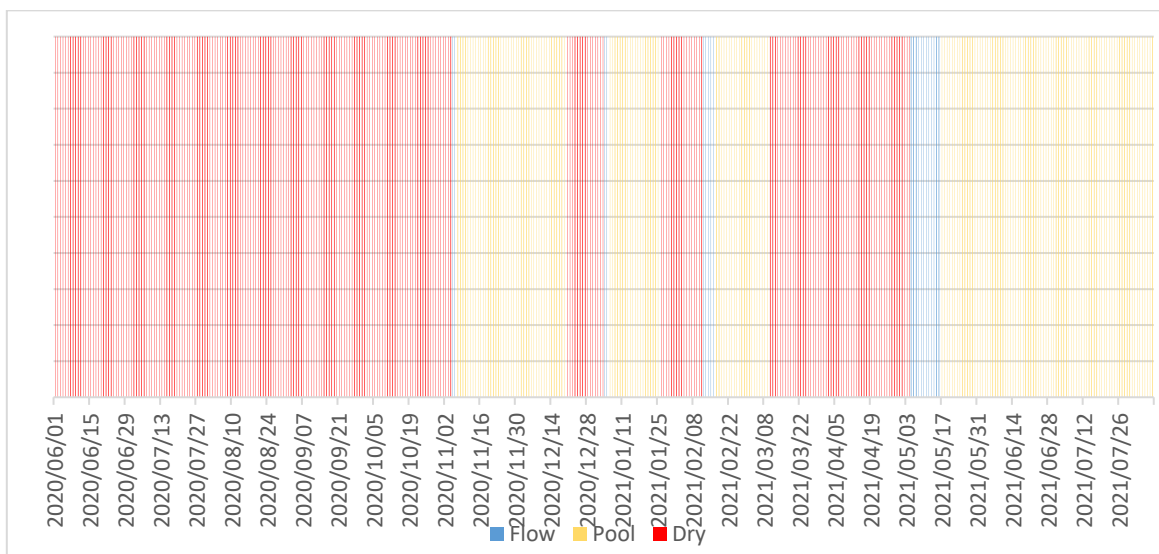


Figure 3.8 Observation of the hydrological state from a trap camera in the Touws River.

### 3.2.2 Pools and Groundwater

The pools show that there were six significant increases in water levels during the monitoring period. These major increases in water levels were followed by significant declines thereafter and followed by constant decreases in water levels (Figures 3.9 and 3.10). The major losses can be either water lost to groundwater or lateral downstream outflow. The two pools

generally had similar trends but with some differences, which is supported by the literature, which states that two neighbouring pools can behave differently (Seaman *et al.* 2016). However, the cause of these differences still needs to be explored. In general, Wolverfontein pool 2 tends to lose 0.01 m/day in winter and 0.02 m/day in summer. The gap is due to the logger going missing during the COVID-19 lockdown (February to July 2020). The water levels will be used to obtain the volume of the pools and used in the water balance analysis that will provide more information about the dynamics of the pools, including whether the water is lost to groundwater or lateral outflow. However, up to this point, there were no notable responses of groundwater levels (Figure 3.10) to flow events, which suggests that the water does not reach both shallow and deep aquifers. Still, it does not indicate that water is not lost to the unsaturated zone.

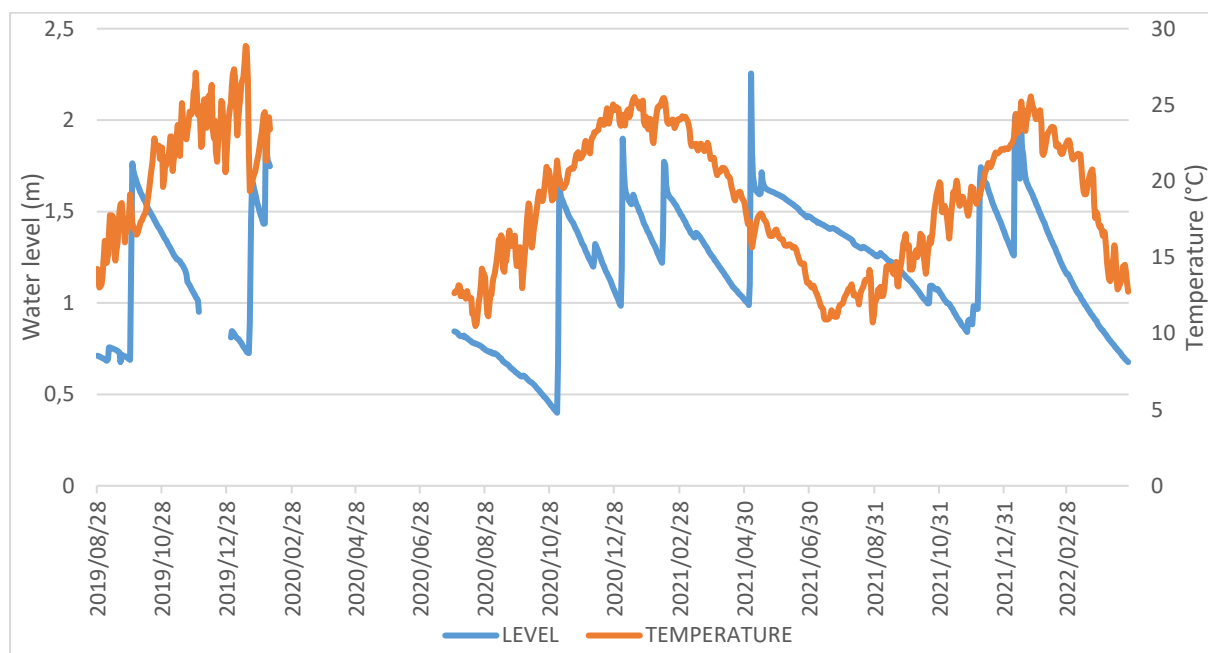


Figure 3.9 Daily water level and temperature of the Wolverfontein pool 2

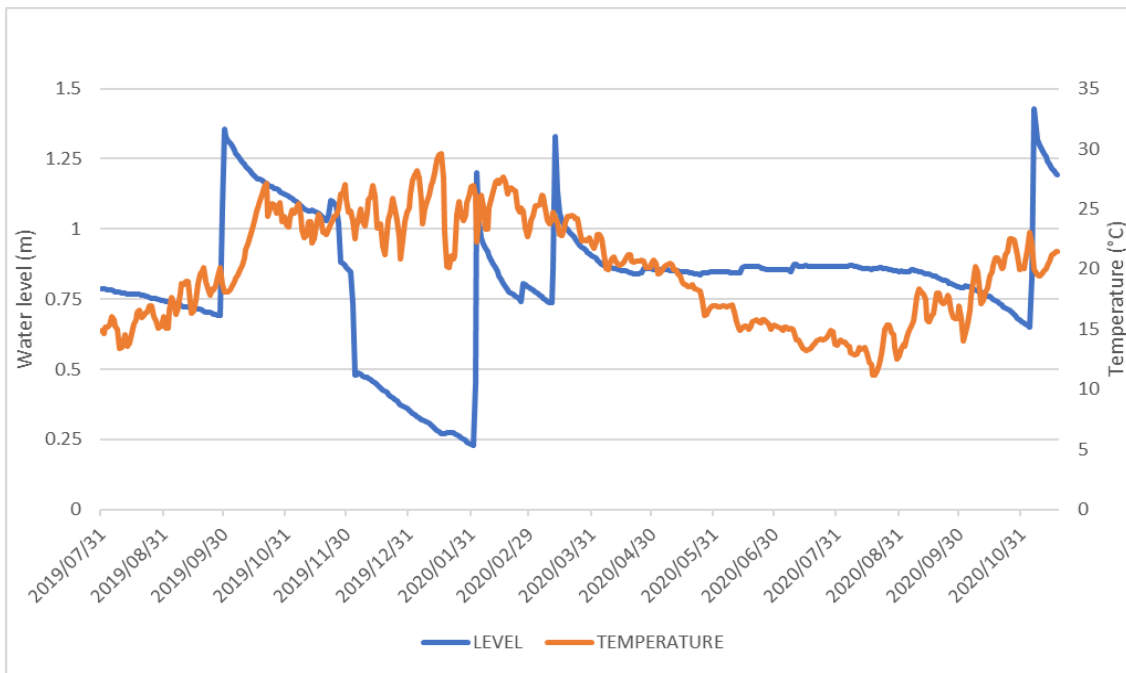


Figure 3.10 Daily water level and temperature of the Touwsberg home pool

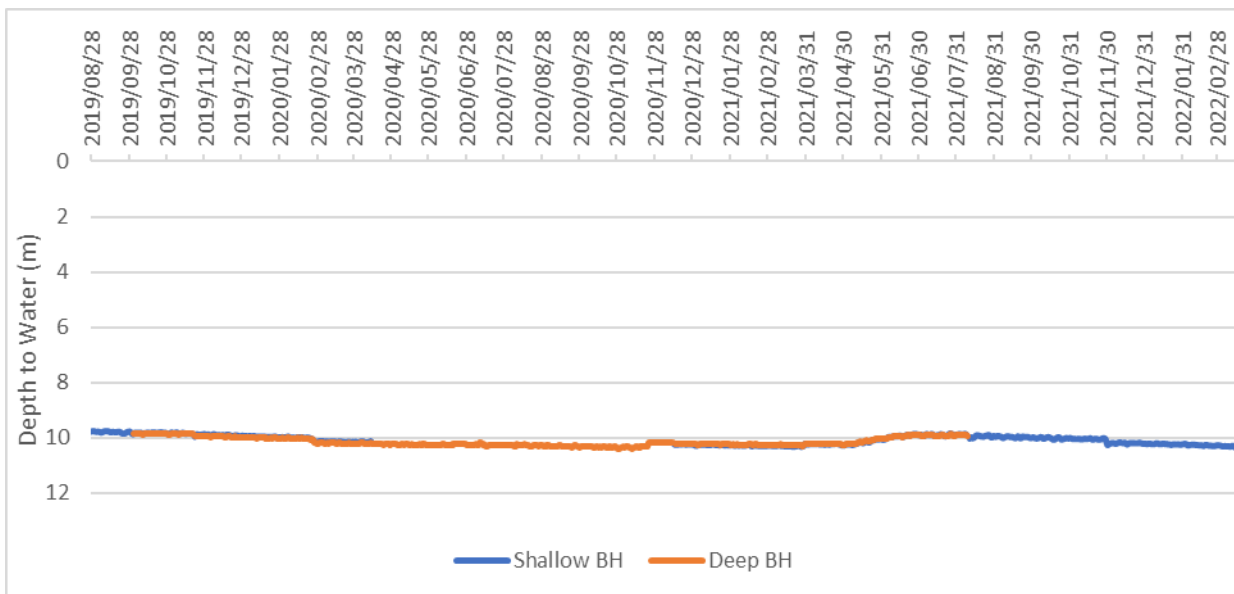


Figure 3.11 Changes in water levels in the shallow borehole (25 m: blue line) and the deep borehole (60 m: orange line) near the monitored pools.

Another important factor that influences the dynamics of pools and flow is evaporation. Penman Equation was used to estimate evaporation using close-by weather station data. Evaporation rates are highest in January or December of each year (~240 mm/month),

whereas the lowest evaporations rate occurs in June (~46 mm/month). The total annual evaporation was 1632 and 1603 mm/year for 2019 and 2020, respectively.

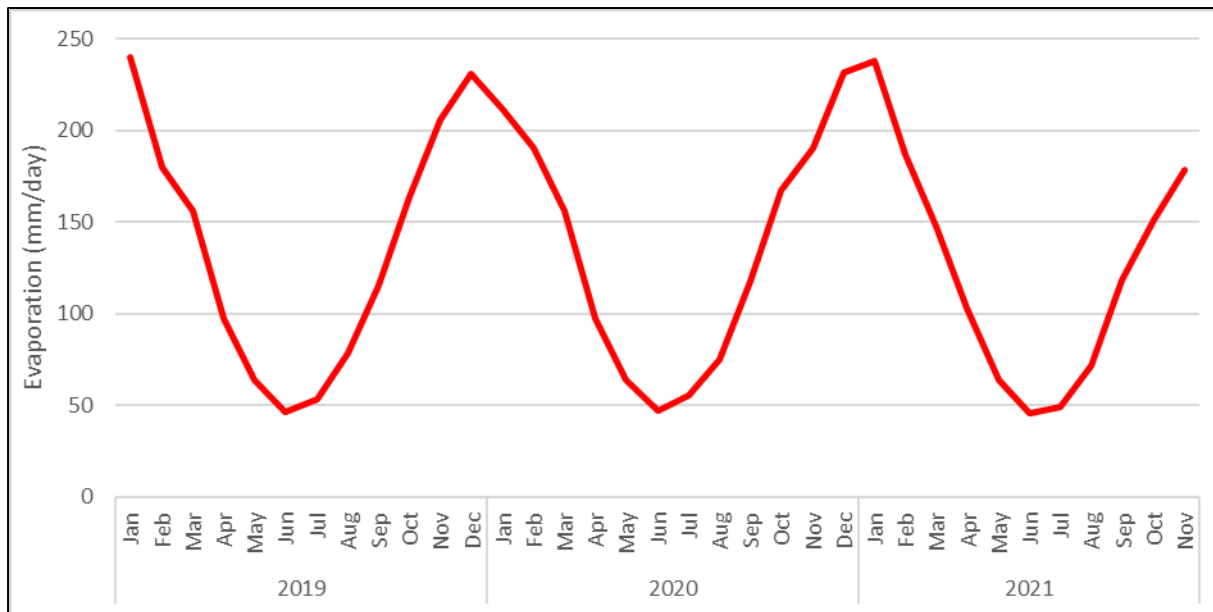


Figure 3.12 Monthly rate of evaporation of water in mm per month in Touws Catchment estimated using the Penman method.

### 3.3 HEUNINGNES CATCHMENT

#### 3.3.1 Rainfall

Long-term data (1917 to 2019) show the catchment has an annual average of ~452 mm/year. The annual rainfall (average of 6 stations) shows that the catchment experienced a drought between 2016 to 2018 (Figure 3.13). There were a few days that received more than 30 mm/d, and only ten days received more than 40 mm/d in the last five years. The highest rainfall was 71 mm/d in Moddervlei station (Figure 3.14).

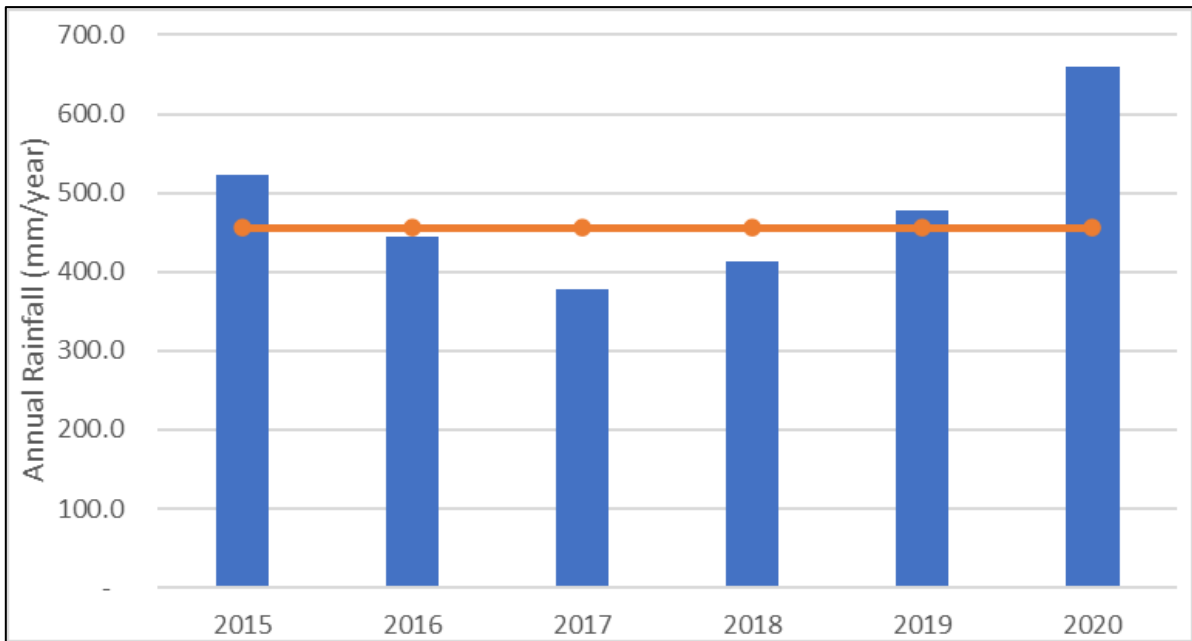


Figure 3.13 Annual rainfall with mean annual rainfall (orange line)

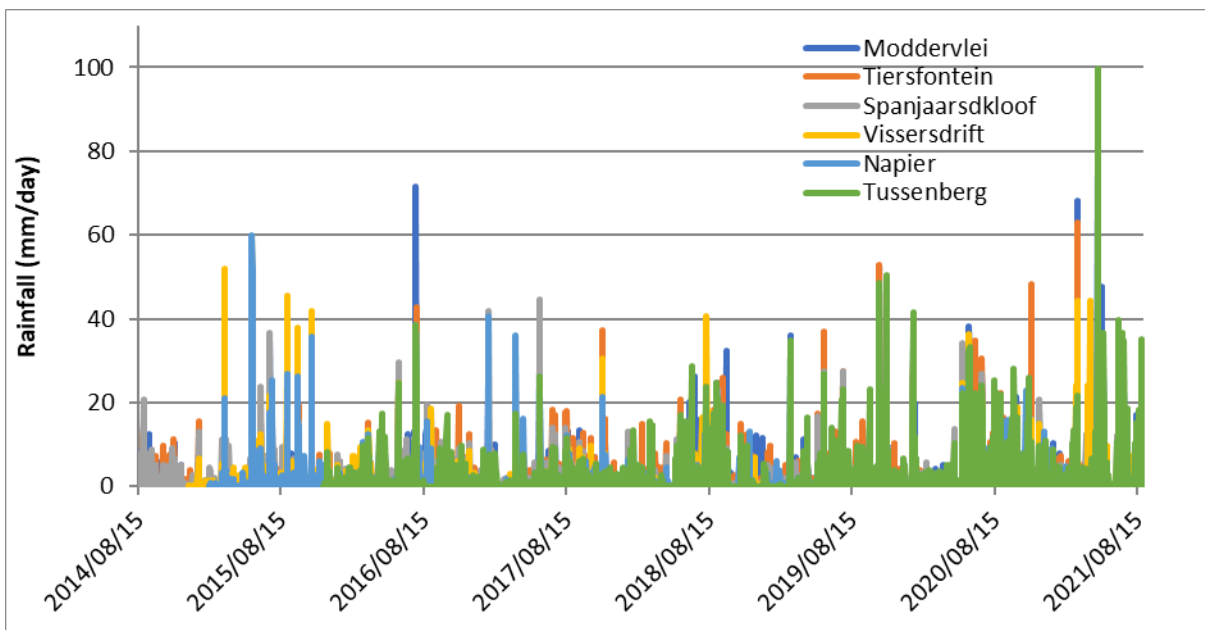


Figure 3.14 Daily rainfall in six stations within the Heuningnes catchment

### 3.3.2 River flow

The catchment experienced drought from 2016 to 2017, and it did not recover yet; even though it has been receiving above-average rainfall in 2018 and 2019 (Figure 3.15), an insignificant runoff was generated. Nevertheless, 2020 seems to have generated a flow that was more than 10 m<sup>3</sup>/d; the last time that the station had a flow of more than 10 m<sup>3</sup>/s per

day, was in 2015. Due to the drought, the logger was removed during the year 2016, hence the gap. The flow at this station will be compared to remote sensing flow estimates.

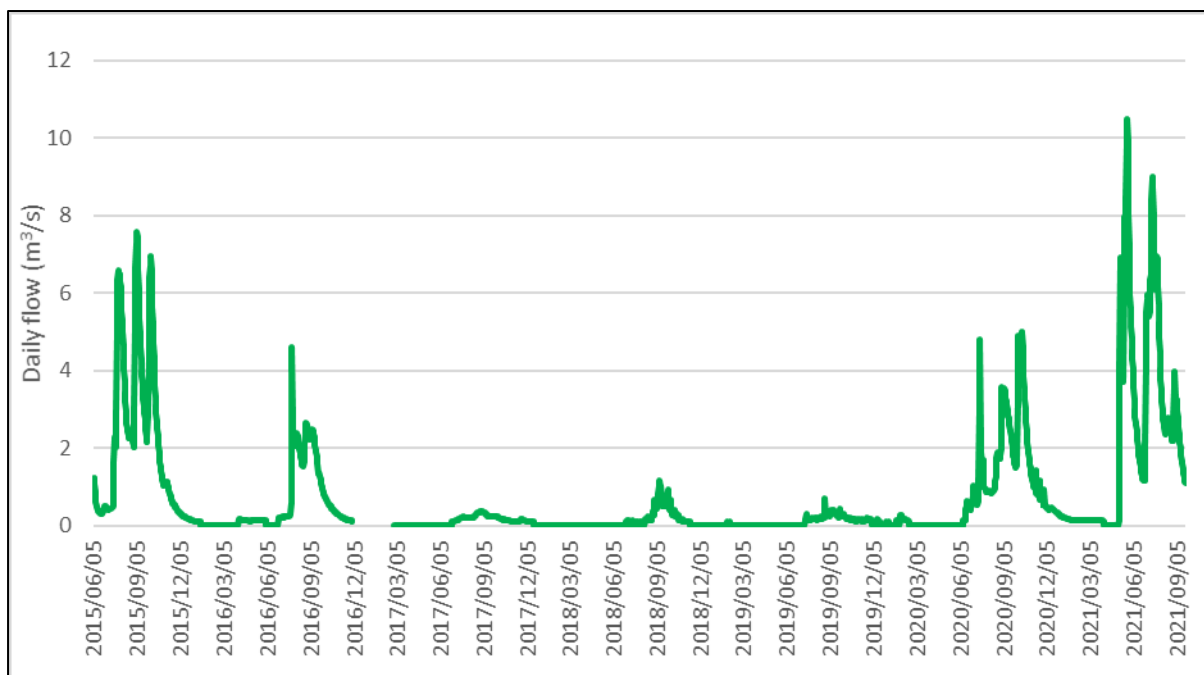


Figure 3.15 Daily flow at Elandsdrift station in the Heuningnes catchment

### 3.3.3 Pool

The pool had water for most of the year but dried up in early January 2020. This is the nature of this pool that dries up in January, hence the name Nuwejaars River meaning “New year” in Afrikaans, indicating that the river dries up at the beginning of the year. The pool also recorded the highest water level in January (Figure 3.16). The conductivity suggests that the pool is fresher when there is no significant inflow. There is a higher conductivity when there is inflow suggesting that stagnant water is fresher than the water coming from upstream. If groundwater does contribute to the water in the pool (which requires further investigation), this could also indicate that the groundwater is fresher than the surface flow.

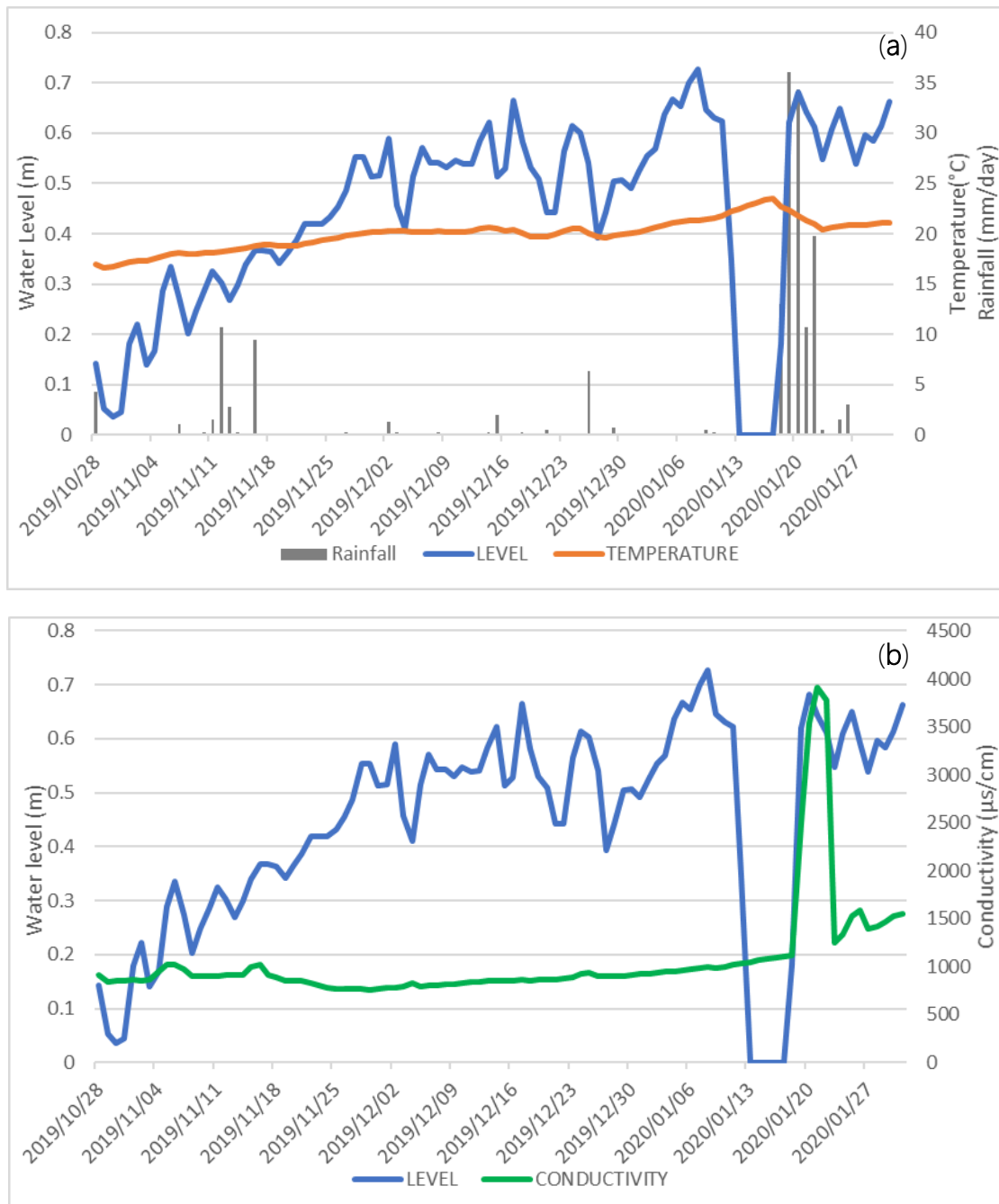


Figure 3.16 (a) changes in water level, temperature, and rainfall from the closest station (Moddervlei), (b) changes in water level and conductivity in an R43-road pool.

## 4 SPATIAL AND TEMPORAL DYNAMICS OF POOLS ALONG NON-PERENNIAL RIVER

This section contributes to determining the nature of the spatial and temporal distribution of pools along non-perennial rivers. Thereafter, the ability of remote sensing to detect the pools is presented.

### 4.1 ASSESSMENT OF DETECTION OF POOLS ALONG TOUWS AND MOLOTOTSI RIVERS AT CATCHMENT SCALE.

In general, remote sensing methods were able to detect the pools along NPRs with limitations, the results varied with methods and site (Table 4.1). In the Touws River, MNDWI was applied on the Sentinel-2 image, and seven out of 11 pools were detected. All pools that were not detected were relatively small ( $>400\text{ m}^2$ ) in size. NDWI detected 10 of the 11 pools, and classified water as almost the entire river (Figure 4.1), this is evident from the high producer's accuracy and the poor user's accuracy (Figure 4.2). NDVI was able to detect the five larger pools. Random Forest classification and the Sentinel-1 thresholding correctly detected four pools of the largest pools. Along the Molototsi river, the eight surveyed pools had an average size of  $1033\text{ m}^2$  and an average depth of  $0.3\text{ m}$  (Table 4.1B). NDWI detected three of eight pools, and MNDWI, NDVI and supervised classification (RF) detected two of the eight pools, whereas the Sentinel-1 that had a threshold did not detect any of the pools. The poor detection of pools in this study site can be attributed to the size of the pools which majority were small. The methods struggled to detect the smaller pools as was the case for the Touws River Catchment. The estimates in the Molototsi study area did not show an overestimation (noise) of water surface areas (Figure 4.1).

Table 4.1: Detection of pools along the Touws and Molototsi River

Touws River (A)							
Pool name	Surface Area	Depth	MNDWI	NDWI	NDVI	RF	S1
Touwsberg Farm 1	237.8	0.41	UD	UD	UD	UD	UD
Touwsberg Farm 2	9694.5	0.94	D	D	D	D	D
Sean	697.2	0.3	D	D	UD	UD	UD
Wolverfontein 1 (WW1)	4403.5	0.76	D	D	D	D	D
Wolverfontein 2 (WW2)	7198	1.3	D	D as one	D	D	D
Touwsberg Office 1	158.4	0.4	UD		UD	UD	UD
Touwsberg Office 2	27500	0.9	D		D	D	D
R62Bridge	413	0.46	UD	D	D	UD	UD
JJ1	680	1.4	D	D	UD	UD	UD
JJ2	1640	0.75	D	D	UD	UD	UD
Die sand	166.4	0.17	UD	D	UD	UD	UD
Molototsi River (B)							
Mol_pool 1	127	0.28	UD	UD	UD	UD	UD
Mol_pool 2	578	0.3	UD	UD	UD	UD	UD
Mol_pool 3	3448	0.46	D	D	D	D	UD
Mol_pool 4	2880	0.43	D	D	D	D	UD
Mol_pool 5	337	0.35	UD	UD	UD	UD	UD
Mol_pool 6	590	0.52	UD	D	UD	UD	UD
Mol_pool 7	111	0.29	UD	UD	UD	UD	UD
Mol_pool 8	190	0.28	UD	UD	UD	UD	UD

N.B: UD= undetected; D =Detected

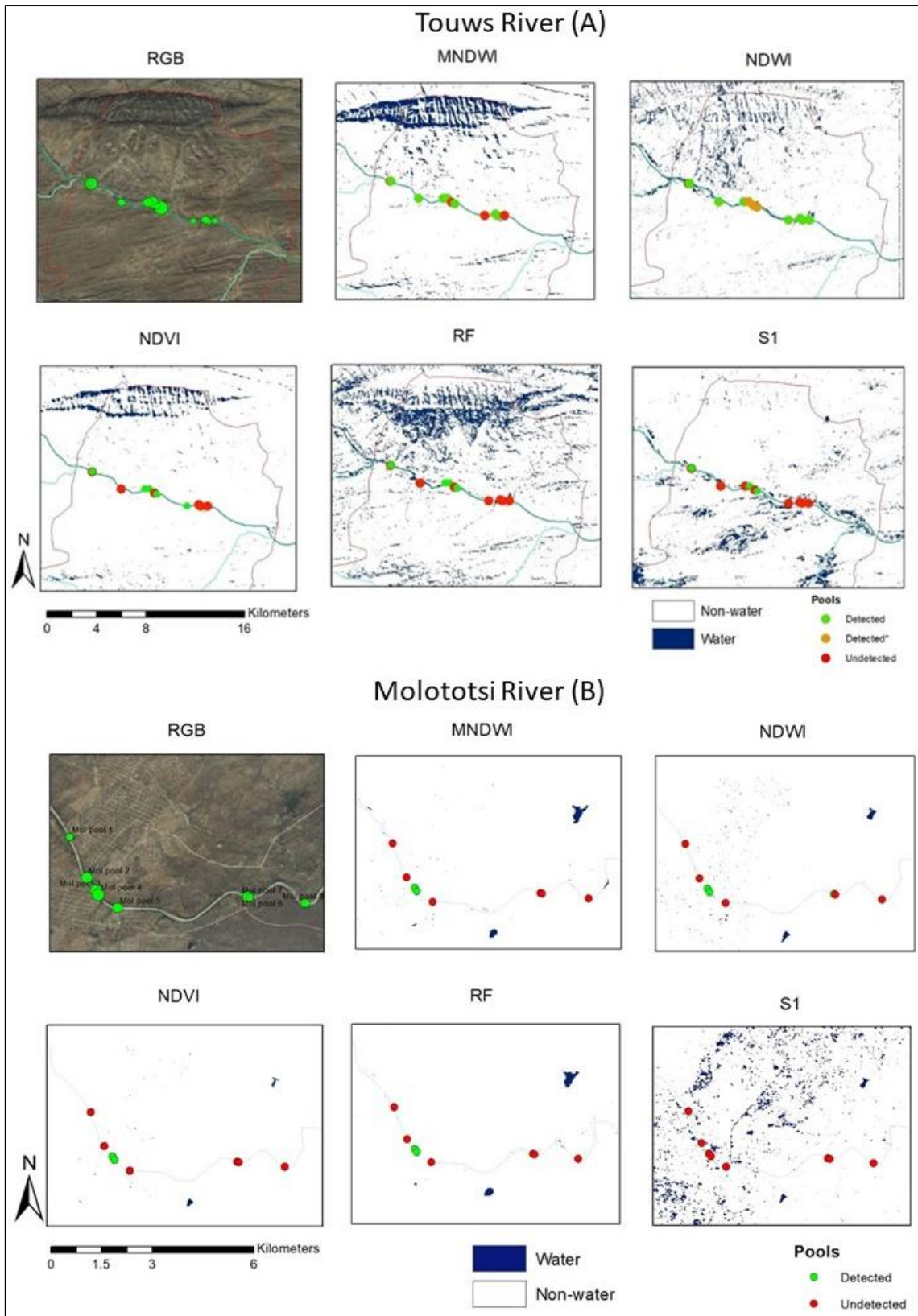
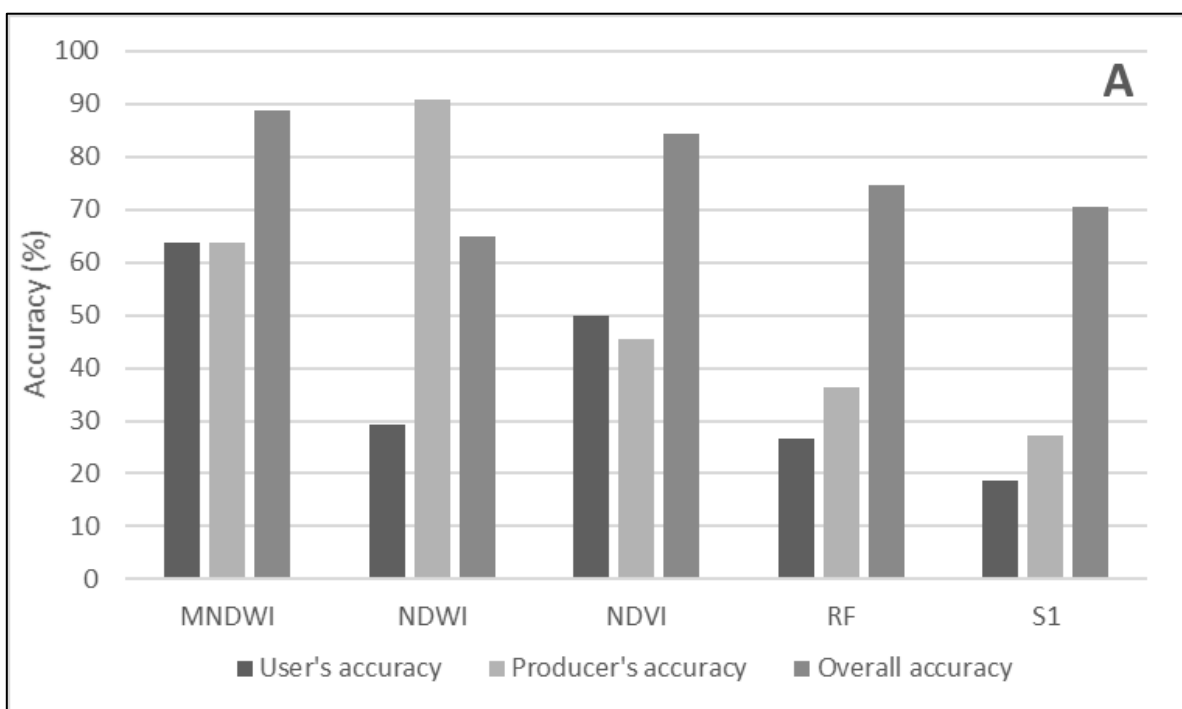
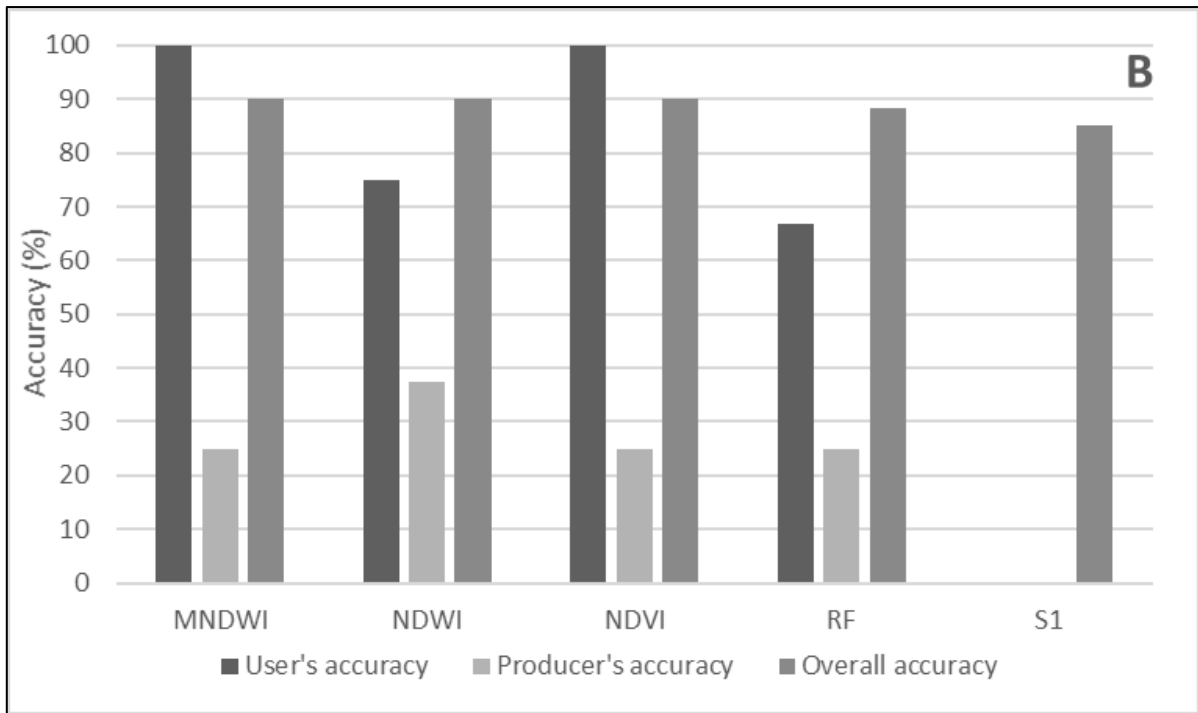


Figure 4.1 Performance of the methods in detection of water surface area along the Touws (A) and Molototsi river (B).

In general, remote sensing methods were able to distinguish between water (pools) and non-water pixels (roads, buildings, mountainous shadows, vegetation, and bare land) in the two study sites. MNDWI outperformed other methods (Overall Accuracy= 89%) whereas NDWI had a high score for user accuracy (Figure 6). NDVI could distinguish between water and non-water pixels. Sentinel-1 (S1) data with a threshold had the worst performance with user's and producer's accuracy of less than 30%. In the Molototsi study site, high user and overall accuracy were obtained, this shows that water and non-water pixels were distinguished with acceptable accuracy (Figure 4.2). Producer's accuracy scores were low for all methods due to failure to detect the smaller pools which were in majority in this study area. MNDWI and NDVI performed better than the other methods and the use of Sentinel-1 was the worst.





**Figure 4.2** Accuracy of the methods in distinguishing water and non-water features at catchment scale in the Touws (A) and Molototsi river (B)

#### 4.2 ACCURACY ASSESSMENT OF REMOTELY SENSED POOL'S SURFACE AREA IN THE TOUWS AND MOLOTOTSI RIVERS.

MNDWI, NDWI, NDVI and random forest classification (RF) applied to Sentinel-2 image and Sentinel-1 threshold (S1) were compared to the field obtained surface areas. Random forest classification and thresholding of Sentinel-1 had the highest user accuracy (92%) for the WW1 and WW2 pools, respectively. Overall, MNDWI outperformed the other methods as it had acceptable accuracies for all three accuracy measures for both pools ranging from 74% to 80% (Figure 4.3). When comparing the scores from the two pools, the WW1 pool was better estimated. A field survey was done from 30 June to 01 July 2021 along the Molototsi river. MNDWI slightly outperformed the other methods for Pool 3 (Figure 10). NDWI outperformed MNDWI in classifying Pool 6, which MNDWI and the other methods did not even detect it. S1 had a worse performance as it did not detect both pools. Comparing the classification of the two pools, Pool 3 was better classified when all methods are considered.

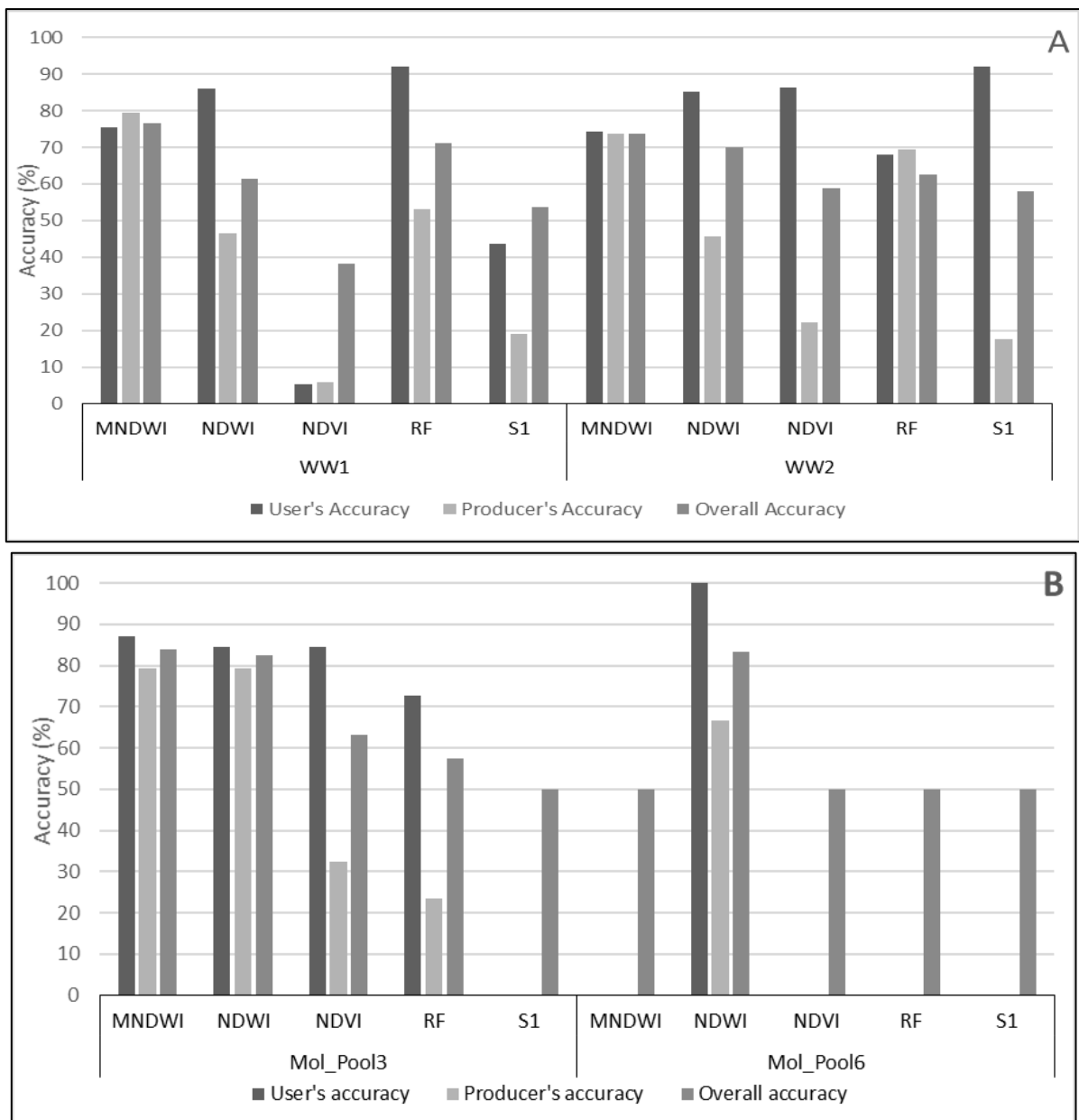


**Figure 4.3** Performance by MNDWI, NDWI, NDVI, RF and Sentinel 1 in the classification of pools in Touws (A) and Molototsi River (B).

### The difference in observed and estimated surface area of pools

In terms of comparing the estimated area and observed area using DAI, remote sensing tends to overestimate the surface area of both pools (Table 4.2). Comparing the methods, MNDWI showed fewer differences when estimating the surface water area of pools, as it outperformed all other methods, in one instance the difference was 2%. Whereas the Sentinel-1 data with a threshold and NDVI showed high differences/errors ranging from 43% to 100%, NDVI had the best estimate for the WW1 pool on one occasion (PDAI= 8.6%).

When comparing the estimate for the two pools, the WW1 pool was better estimated. For the Molototsi pools, NDWI showed to have fewer differences when estimating the surface water area of pools, as it outperformed all other methods, with PDAI of 5.6 and 33.3% for Pool 3 and Pool 6, respectively. Whereas the Sentinel-1 data with a threshold showed to have the highest errors of 100% for both pools, indicating that pools were not detected. When comparing the estimate for the two pools, Pool 3 was better estimated.

Table 4.2: Percent Differential Area Index for three surveys in Touws (A) and Molototsi (B)

*Touws River (A)*

MNDWI	NDWI	NDVI	RF	S1
WW1 pool				
-25.7	-71.4	-8.6	-31.4	85.7
6.1	78.8	100.0	53.0	43.4
1.5	81.8	100.0	87.9	77.5
WW2 pool				
-28.9	58.5	65.5	-31.7	96.2
26.2	74.6	93.1	50.0	71.0
-11.3	27.4	68.9	22.6	70.2

*Molototsi River (B)*

Mol_Pool 3				
8.8	5.9	61.8	67.6	100.0
Mol_Pool 6				
100.0	-33.3	100.0	100.0	100.0

### 4.3 ASSESSMENT OF CHANGES IN POOL SIZES AND FACTORS THAT CONTROLS THE CHANGES IN TOUWS AND MOLOTOTSI RIVERS

There were four noted major flow events in Touws River from 2019 to May 2021. The maximum surface water area estimated was 12000 m<sup>2</sup> and 20800 m<sup>2</sup> in WW1 and WW2 pools, respectively. The maximum surface area is stable for WW1 but fluctuates for the WW2 pool, this can be attributed to the errors at which WW2 is detected (Figure 4.4). From 2019 to 2021, the pools were at their driest with surface water areas of 3700 and 5200 m<sup>2</sup> for WW1 and WW2 respectively, this was after six months without significant inflows. Compared

to Touws, Molototsi had two major flow events during the summer season of each year. The pools were present at the end of flow events in February/March and dried out in June/July of each year (Figure 4.5). The maximum surface water area estimated was 2900 m<sup>2</sup> and 1300 m<sup>2</sup> in Pools 3 and 6, respectively. Pool 3 was completely dry in 2020 and did not exist in 2019. Pool 6 dried up in June 2020, and it was almost completely dry in June 2021 with a surface water area of 100 m<sup>2</sup>.

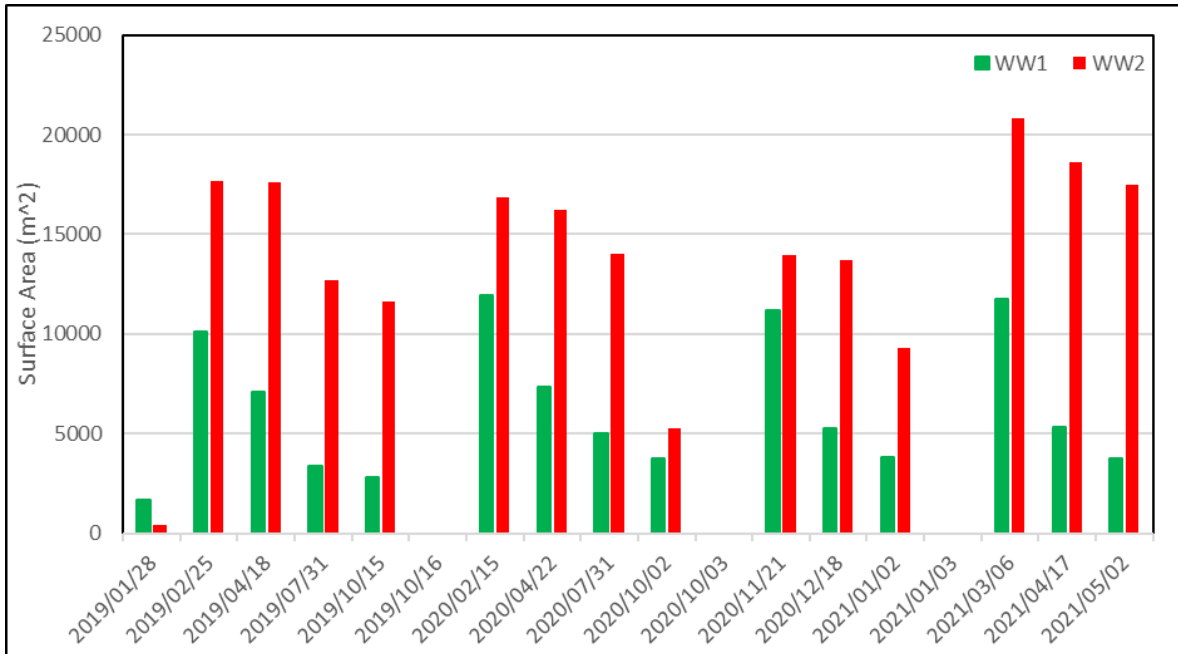


**Figure 4.4** Changes in the surface water area of WW1(green bars) and WW2 (red bars) in the Touws River when full, at the intermediate and dry stage.

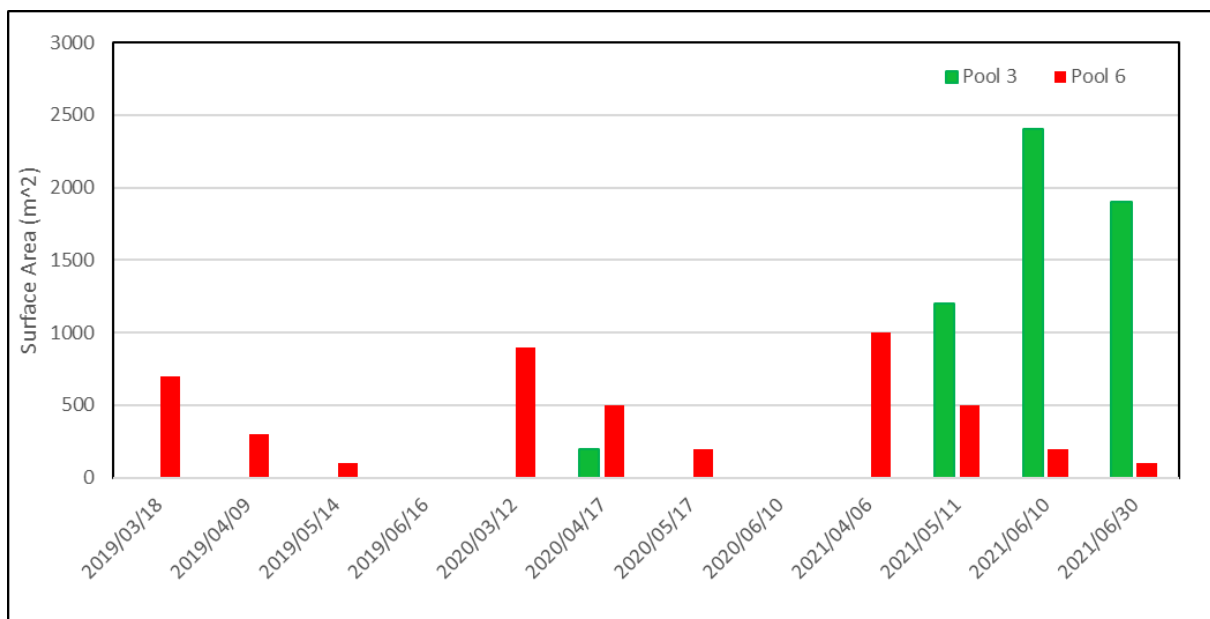


**Figure 4.5** Changes in the surface water area of Pool 3(green bars) and Pool 6 (red bars) in the Touws River when full, at the intermediate and dry stage.

## 4.4 DISCUSSION AND CONCLUSION

This study explored the use of remote sensing in monitoring the spatial distribution of pools and pool dynamics along non-perennial rivers in two distinct areas. The results show that the pools in the Touws River were bigger than the pools in the Molototsi river. This might be due to the Molototsi river having sandy bed material that drains the water after flash floods (Walker *et al.*, 2018). In contrast, the Touws river has bedrock that is not far from the river's surface, hence also classified as a mixed alluvial and bedrock river (Grenfell *et al.*, 2021). Furthermore, Molototsi has a clear dry and wet season, whereas the Touws River site receives rainfall and flows at any time of year. However, the use of remotely sensed data demonstrated the capability to detect pools at both catchment and pool scales.

At both catchments, pools with shallow water (depth of approx. 0.3 m) were detected but those that were smaller in surface area were not detected. The failure to detect pools with a small surface area may be due to these pools being made up of mixed pixels which are then detected as non-water. The MNDWI and NDWI detected pools better than other methods in both Touws and Molototsi catchments, respectively. However, the MNDWI did not detect pools that were smaller than 400 m<sup>2</sup>, this is because the short-wave infrared band of Sentinel-2 has a slightly coarser spatial resolution (20 m) and resampling it to 10 m did not make a difference, whereas the NDWI uses bands that have a 10 m spatial resolution and was able to detect some pools that are less than 400 m<sup>2</sup>. Li *et al.* (2021) made the same observation when mapping a small river. The NDWI is known to have challenges in separating shallows and built-up areas (Bangira *et al.*, 2019) this might explain why the index did not outperform MNDWI on the mountainous Touws river site as compared to the relatively flat Molototsi site.

The random forest classification detected the pools with acceptable accuracy, however, did not meet the expectation at both the catchment and pool scales. This might be because pools tend to have different characteristics that affect the training of the classifier, such as the presence of algae, vegetation, sediments in the pools, and the size and shape of the pool. Even parts of pools can have different spectral signatures. All these might have limited the detection of pools by the random forest classifier as there are usually few water bodies that can be used to train the classifier in these dry areas. As a result, the training might not be diverse enough to capture the differences found in pools. Bangaram *et al.*, (2019) state that this is the disadvantage of machine learning classifiers. Sentinel-1 did not perform well compared to results obtained from Sentinel-2, this is like results obtained by Bangira *et al.*, (2019). Although Sentinel-1 had been applied to mapping floods over a large area, it was not suitable for detecting pools at both study sites. For the index that was produced to detect vegetation, NDVI performed well in both catchments.

When comparing the accuracy at the pools' size scale in Touws River, the WW1 pool was estimated better than the WW2 pool. All methods had difficulty in classifying the pixels around the WW2 pool due to the shadow in the morning, which is the same time that Sentinel-2 captures an image. To reduce this misclassification, a random forest classifier was trained for the hill shadows, thereafter, some misclassified pixels were removed. Pool 3 which was the larger pool in the Molototsi river, was also detected better than Pool 6. However, only the NDWI was able to detect Pool 6.

In both catchments, the surface area of the pools generally correlated well with the occurrence of flows and rainfall. However, in the Touws River catchment, there is one inflow event that did not correlate with a change in the surface area of the WW2 pool. This, therefore, indicate that remote sensing can have inconsistencies associated with the error shown in the results. The results showed no notable responses of groundwater levels to the surface water area of the pools, nor to rainfall and river flows. This can be attributed to the nature of the underlying geology of the study sites, shale for Touws and gneiss rock for Molototsi. This suggests that the pools are not losing water to the groundwater system. These findings differ from many studies that have indicated that groundwater sustains the pools (Bestland *et al.*, 2017; Lamontagne *et al.*, 2021). However, Walker *et al.* (2018) made the same finding in the Molototsi catchment using water levels and geochemical analyses. Hamilton *et al.* (2005) made similar findings for pools in Australia. This suggests that these pools lose water to the unsaturated zone and the atmosphere through evaporation.

The results imply that altering the flow regime will significantly affect the spatial distribution of pools and pool dynamics. These pools are not only important water sources for the surrounding communities but also provide habitat and maintain the aquatic life of the river (Bonada *et al.*, 2020). Further, improving food security for the surrounding communities (Sustainable Development Goal 2) as complete drying of pools may result in total loss of aquatic life, including fish (Marshall *et al.*, 2016). The result also showed that pools at the assessed study sites might not be sensitive to groundwater abstraction. All this indicates that water resource management should consider the effect that each practice has on pool distribution and dynamics.

## Conclusion

This study assessed the spatial and temporal distribution of pool and pool dynamics using remote sensing along non-perennial rivers in two contrasting catchments and the assessments were done at the catchment and pool scales. At the catchment scale, remote sensing mapped pools along the two-study areas with acceptable accuracy but failed to

detect pools of relatively small size (400 m<sup>2</sup>) in both catchments. This was the main factor in explaining the detected pools when compared to pools that were not detected. The pool in the sandy Molototsi river tends to migrate after flow events, whereas pools in the sandy-gravel Touws River remain in the exact location. Mapping of pools at the catchment scale is vital for the selection of sampling sites for ecological status sampling or livestock and wildlife watering. Overall, MNDWI performed better than the others in the mountainous Touws site, whereas NDWI performed better than other tested methods in the relatively flat Molototsi site. These methods estimated pool surface area with acceptable accuracy.

Using these remote sensing methods, the changes in pool sizes in the two catchments were determined. The pools in Touws showed a perennial pattern, whereas pools in the sandy Molototsi showed ephemeral behaviour lasting only for a few months after flows. The changes in the surface water area of the pools are related well to flow occurrence and rainfall. Groundwater levels did not respond to changes in the surface area of the pools or rainfall and flow events. This suggests that pools do not lose water to the groundwater system. Therefore, this indicates that direct rainfall into the pools, river flows, and evaporation are the three major factors controlling the occurrence and pool dynamics. Overall, the findings of this study provide the requisite baseline input data required for pool water balance analysis to establish how these fluxes control the changes in pools over time, including losses into the unsaturated zone.

## 5 WATER BALANCE OF POOLS

### 5.1 WATER LEVEL ASSESSMENT

The water balance analysis shows that the major gains in water level were due to river flow occurrences, and the minor gains were due to rainfall received over the pool (Figure 5.1). High losses always followed the episodes of high gains suggesting that water losses might be a function of water level. The depth to water of the shallow and deep boreholes shows no significant changes to pool water levels or the occurrence of flows. There is, however missing the water level data between 2020/02/07 to 2020/07/31 due to a stolen logger during the COVID-19 hard lockdown period.

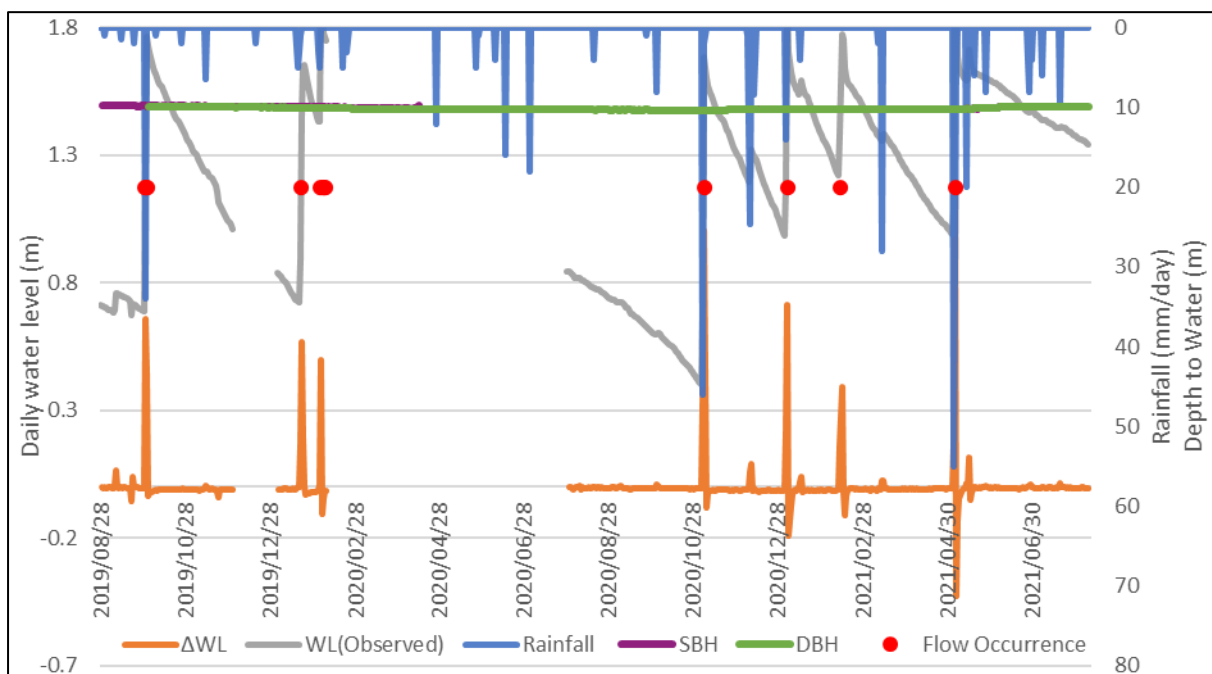


**Figure 5.1:** Changes in water levels of the pool with negative and positive values indicating losing and gaining pool respectively (orange line), actual water level (grey line), rainfall over the pool (blue line), and the flow occurrence (red dots). Depth to the water of the shallow (purple line) and deep borehole (green line).

#### 5.1.1 Assessment of the water losses from the pool

The assessment of the water level suggests that the pool loses approx. 0.2 m per month and 0.0066 m per day or 2.4 m per year using observed data from 2019 to 2021. The losses are high during the Southern hemisphere summer (~0.29 m/month) and low during the winter months (~0.09 m/month) (Figure 5.2). This indicates that on average when the pool

is full, it can last for ~258 days (8.5 months) without any inflows. This pool loses 0.7 m more per year (0.06 m/month) than the Penman estimated evaporation which may be water lost to the sub-surface area (Figure A2 in supplementary material). However, the analyses of the losses also revealed that water losses might have a relation to the size (water level) of the pool, i.e. the more water available in the pool, the more the water losses.

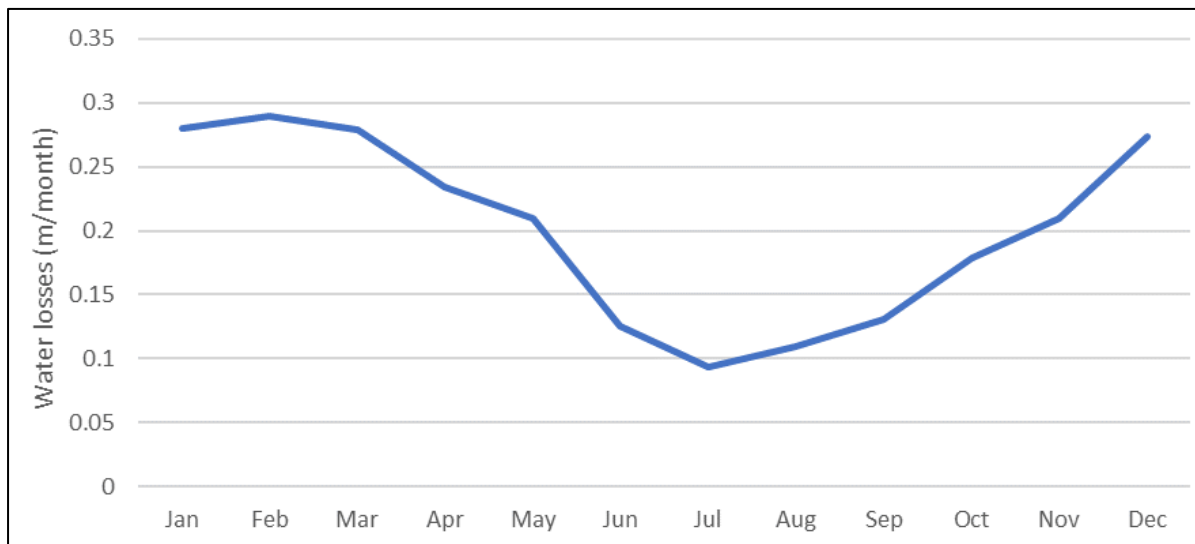


Figure 5.2: Total monthly water losses from the WW2 pool.

### 5.1.2 Probability of the pool drying out

Based on the observed losses, flow, and rainfall data from 1990 to 2020 were used to establish the chances of the pool drying out. There is only a 10% chance of finding the pool dry, as the pool was likely to have dried out eleven times in 30 years or potentially dried out for 1115 days out of 11322 days (30 years) (Table 5.1). This is based on no-flow and no-rain days exceeding 258 days. Rainfall reduces the number of potential pool dry days, for instance, 52 mm during the no-flow period can delay the drying of the pool by eight days. The pool's most prolonged period with no water was 411 days during the 2015-2017 drought, assuming it did not receive water from groundwater.

Table 5.1: Drying out of the pool using data from 1990-2020

No flow Period		No. of days the pool could be dry (excluding rainfall)	Rainfall (mm)	No. of days the pool could be dry (including Rainfall)
Start	End			
1991/01/29	1991/10/29	15.0	54.0	6.8
1994/03/14	1995/01/12	46.0	52.0	38.1
1996/01/15	1996/10/22	23.0	34.0	17.9
1997/10/11	1998/11/18	145.0	89.0	131.6
1998/12/26	1999/12/09	90.0	79.0	78.1
2000/03/14	2001/04/01	125.0	80.0	112.9
2002/02/05	2002/12/10	50.0	110.0	33.4
2005/10/12	2006/07/31	34.0	187.0	5.7
2010/01/03	2010/12/31	104.0	97.0	89.3
2015/12/14	2017/11/13	442.0	203.0	411.3
2017/11/14	2019/02/02	187.0	111.5	170.2
<b>Total</b>		<b>1283.0</b>	<b>1096.5</b>	<b>1115.3</b>
<b>Probability</b>		<b>0.113</b>		<b>0.099</b>

## 5.2 WATER BALANCE MODEL

Based on the understanding of the pool, the water balance approach was used to simulate the water levels of the pool. The water balance satisfactorily predicted the water levels (ME=-0.03 m; MAE=0.05 m; r =0.96) over the assessed period (2019/08/25 to 2021/08/10) (Figure 5.3). Besides the inputs (rainfall, evaporation), the model was supplied with a maximum water level of 1.7 m (which is also the cease-to-flow level) and the initial water level. Moreover, the model was able to predict the period where no observed data was available (February-July 2020). The model shows that when the pool has more water, the water is rapidly lost via flows downstream and seepage into the subsurface strata or aquifer, based on the model the seepage ranged from 0 to 0.005 m/day. Rainfall delays the drying of the pool. The pool is sensitive to flow occurrence. The assumption that every flow will fill the pool to capacity is correct and drives the model. After the flow has ceased, evaporation dominates the water losses. The model suggested that there is a threshold (~1.1 m) whereby

subsurface inflow begins to sustain the pool water level. At this point, evaporation becomes equal to, or more than the total water lost by the pool. This was observed from the initial model which did not take this into account resulting in the underestimation of water levels below ~1.1 m.

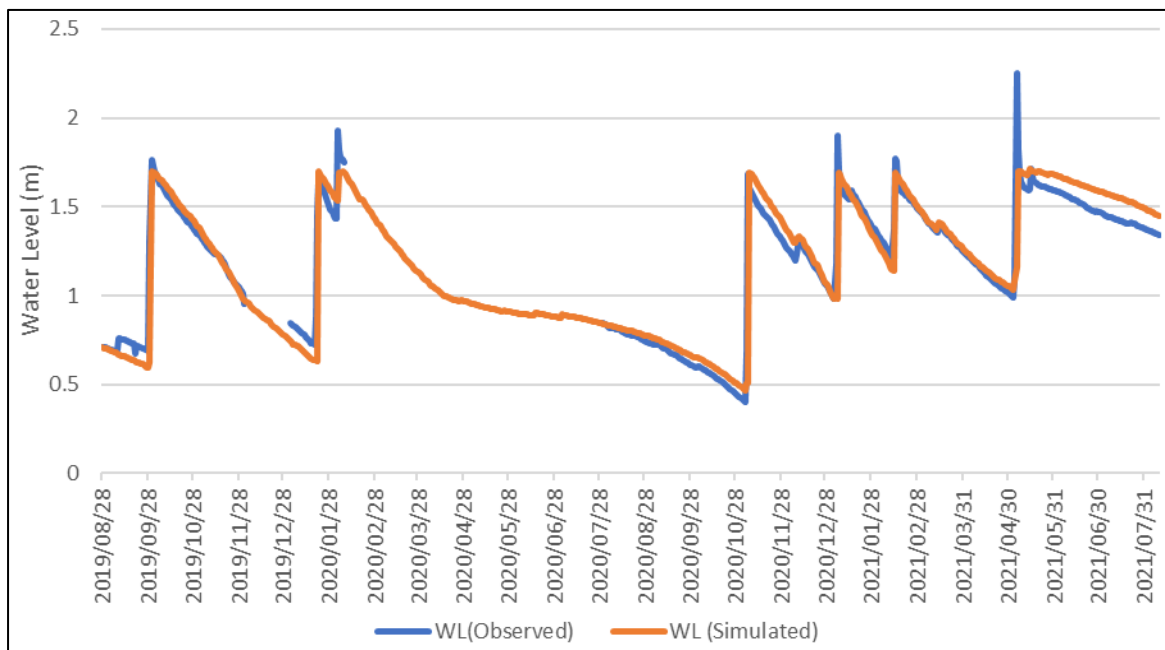


**Figure 5.3:** Water Balance model of water levels of the WW2 pool in Touws River. With the blue line indicating the observed water level and the orange line indicating the simulated water.

### Transferability of the water balance to the surrounding pools

To assess the transferability of the water balance model derived for the WW2 pool, two pools were used; one, 700 meters upstream of Wolverfontein 2 and another 450 m downstream were used. The simulated water levels of the WW1 pool were in good agreement with the observed water level ( $r=0.96$ ;  $ME=-0.02$  m;  $MAE=0.04$  m) (Figure 5.4). The only changes made from the original water balance model from the WW2 pool was the maximum water level which was adjusted through trial and error to be 0.95 m for the WW1 pool and the observed initial water level. However, the model overestimated the pool's losses between December 2020 and November 2021, resulting in the lowest predicted level of 0.2 m. For the TWB pool that is 450 m downstream of the WW2 pool, the model did not perform as well as the WW1 pool ( $r=0.86$ ;  $ME=0.02$  m;  $MAE=0.06$  m), suggesting that the pool significantly varies from the focus pool (WW2). Seepage into the pool was observed during a field visit. The constant water level between June and August

2021 of the pool suggests that the pool receives substantial subsurface inflows to maintain such water levels.

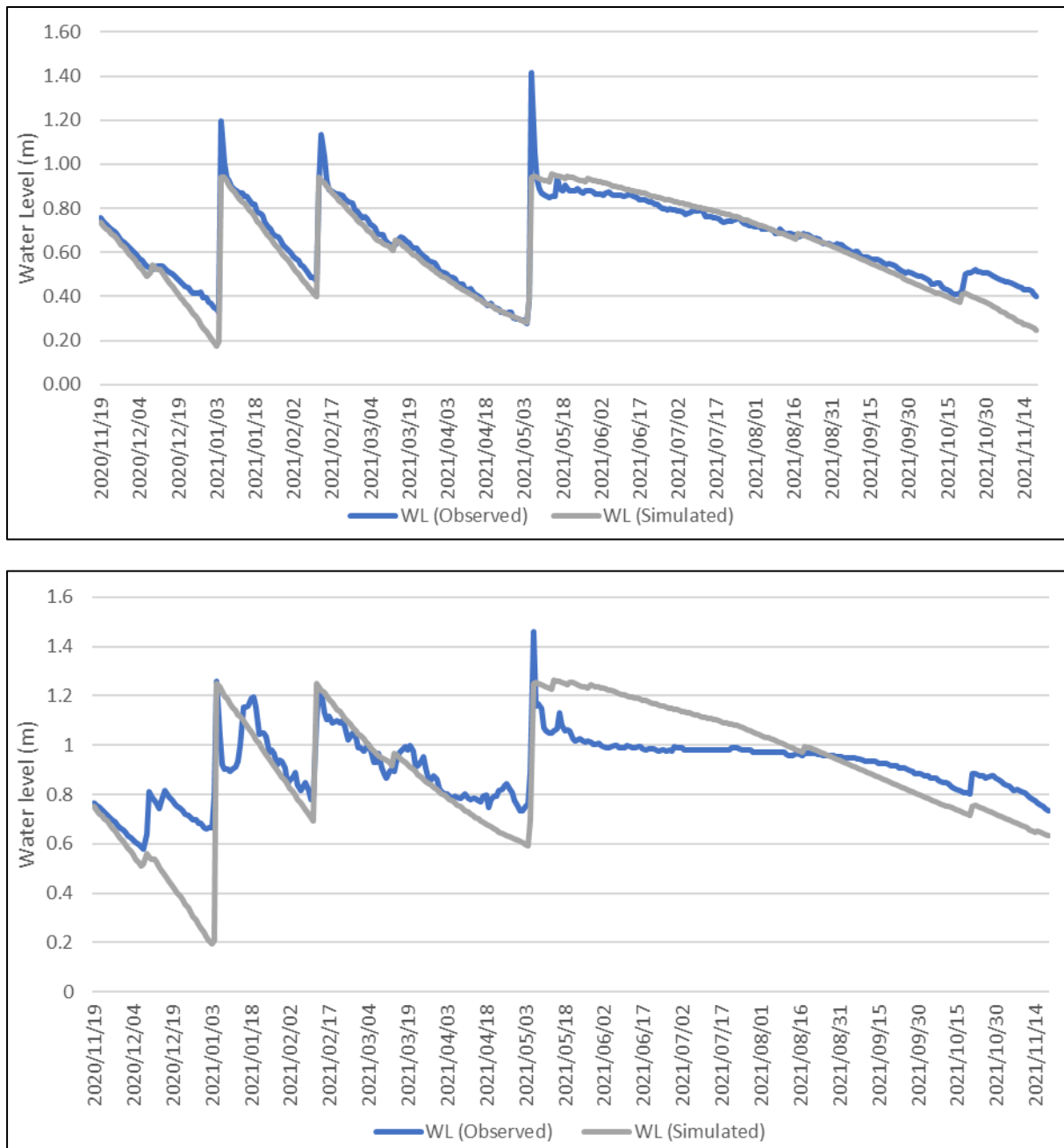


**Figure 5.4:** Observed (blue line) and simulated (grey line) water level for WW 1 pool (top) and TWB pool (bottom).

The paired  $t$ -test ( $t=8.3$ ) showed that at the 5% significance level, there is no statistically significant difference between the observed daily mean water level (0.64 m) and simulated mean (0.62 m) for the WW1 pool. There was, however, a significant difference ( $t=1.9$ )

between the modelled mean water level (0.89 m) from the observed mean (0.91 m) of the TWB pool.

### 5.3 REMOTE SENSING WATER BALANCE ANALYSIS

#### Comparison of the remote sensing and observed models' inputs

In terms of comparing the inputs, CHIRPS rainfall estimates compared well with the observed rainfall data ( $r=0.6$ ). However, it has errors during some periods, such as July to Aug 2020 (Figure 5.5). Although, remotely sensed evaporation rates from MODIS 16 PET are closely related to observed evaporation derived using the Penman equation ( $r=0.98$ ). However, they overestimated the months with lower evaporation (April to Sept) (Figure 5.6). A general assessment of the climatic water balance shows that the remotely sensed climatic water balance is strongly associated with the observed climatic water balance ( $r=0.87$ ) (Figure 5.7). This suggests that a monthly-based water balance can have errors caused by rainfall and evaporation, but these are likely to be small. The negative climate water balance indicates that the catchment is potentially in a water deficit.

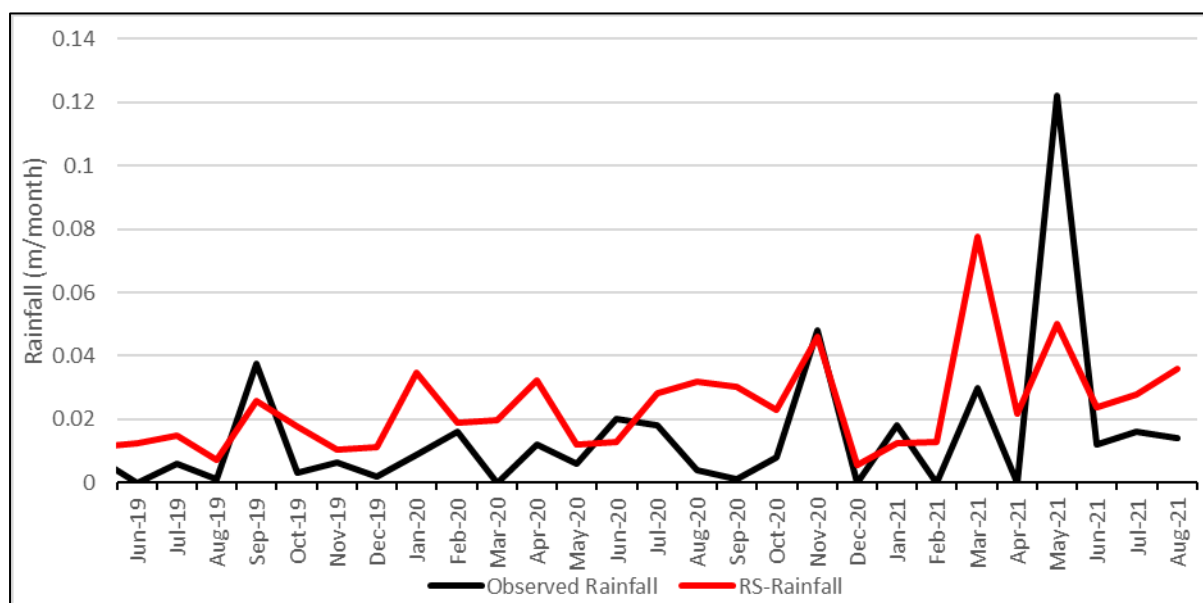


Figure 5.5: Comparison of observed (black line) and estimated rainfall by CHIRPS (red line).

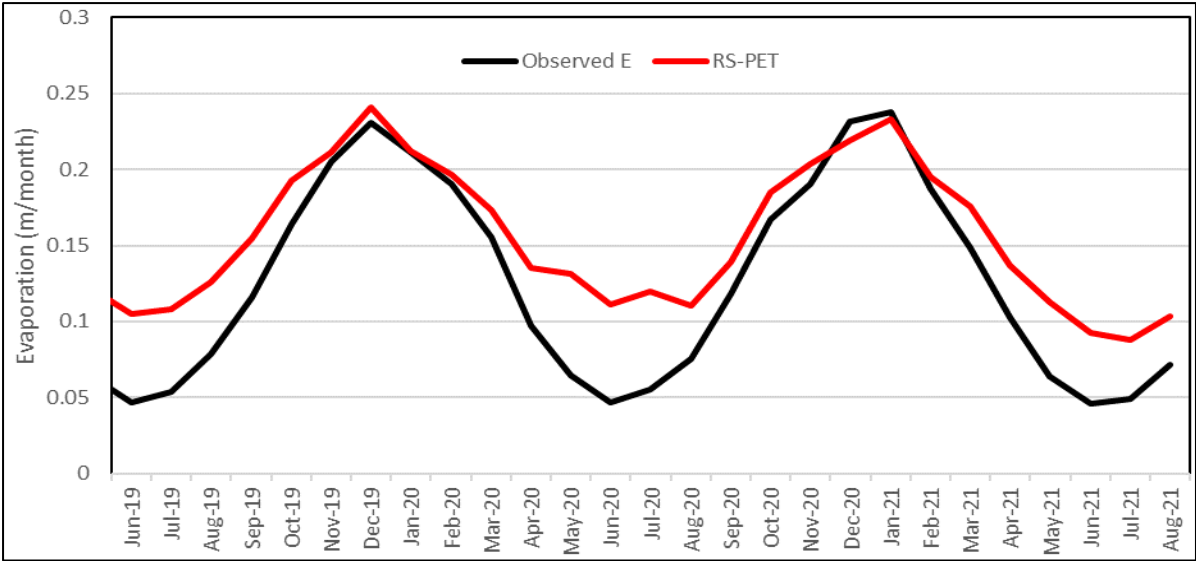


Figure 5.6: Comparison of observed evaporation (black line) and estimated potential evaporation by MODIS 16 (red line).

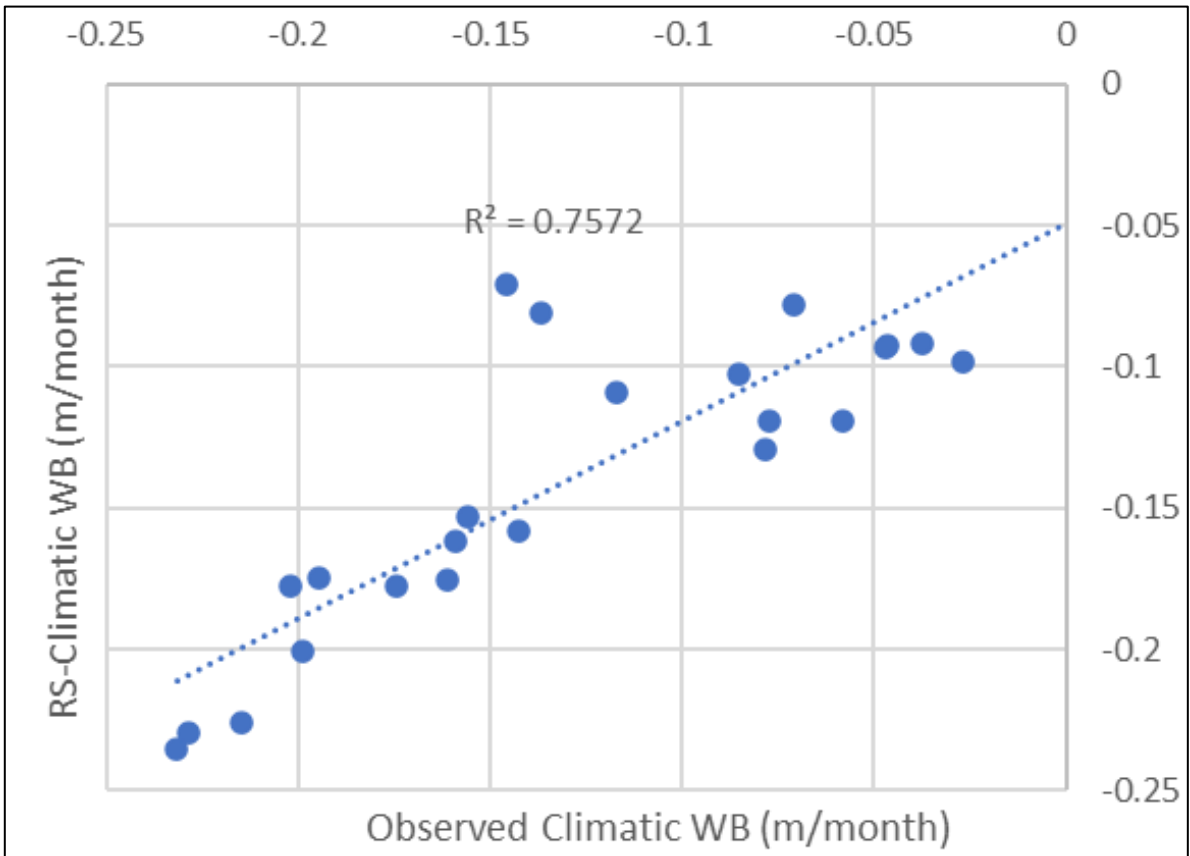
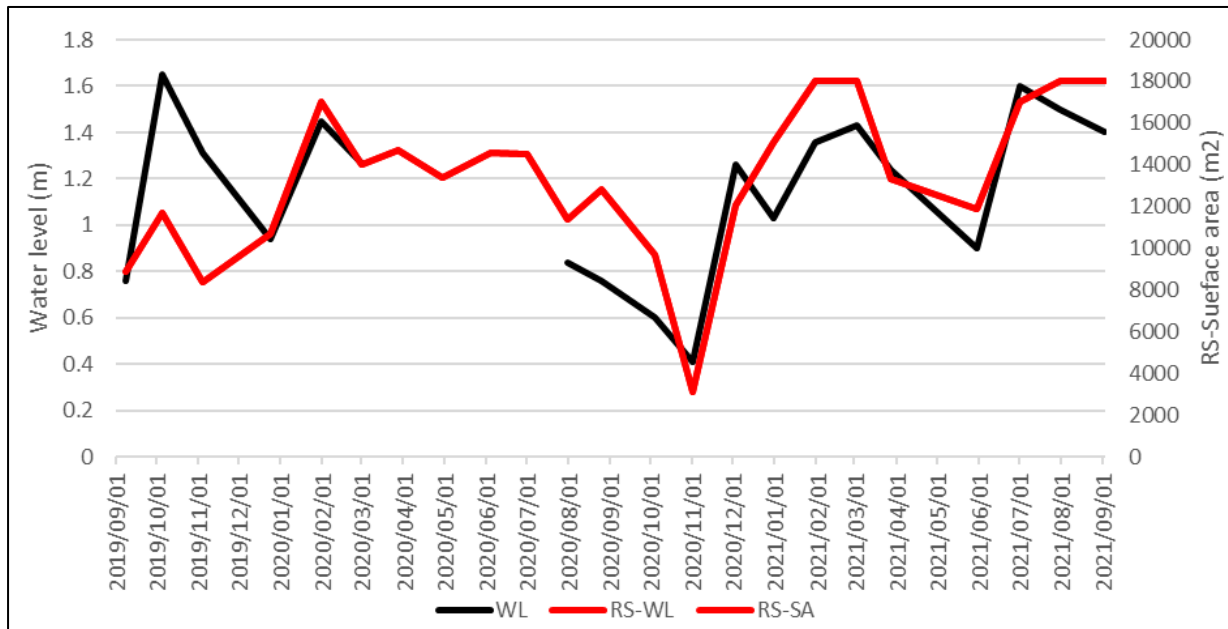


Figure 5.7: Correlation between observed and estimated climate water balance (rainfall-potential evaporation).

The comparison between the observed water level and the remotely sensed surface area of the pool has a good agreement ( $r=0.72$ ) (Figure 5.8). The discrepancies seem to be more minor when the pool is almost full (Water level > 1.2 m). Overall, the remote sensing estimated surface water of the pool is promising.



**Figure 5.8:** Comparison between observed (black line) and estimated water level (primary axis) based on remote sensing surface area (secondary y-axis) (red line).

Therefore, freely accessible remote sensing data were incorporated into water balance, particularly CHIRPS and MODIS16 PET data. The initial and maximum water level and flow occurrence were the only inputs used. This also assumes that no information about water losses to subsurface/groundwater. The results show an underestimation of the water losses as expected (Figure 5.9) as losses into the sub-surface are not incorporated.

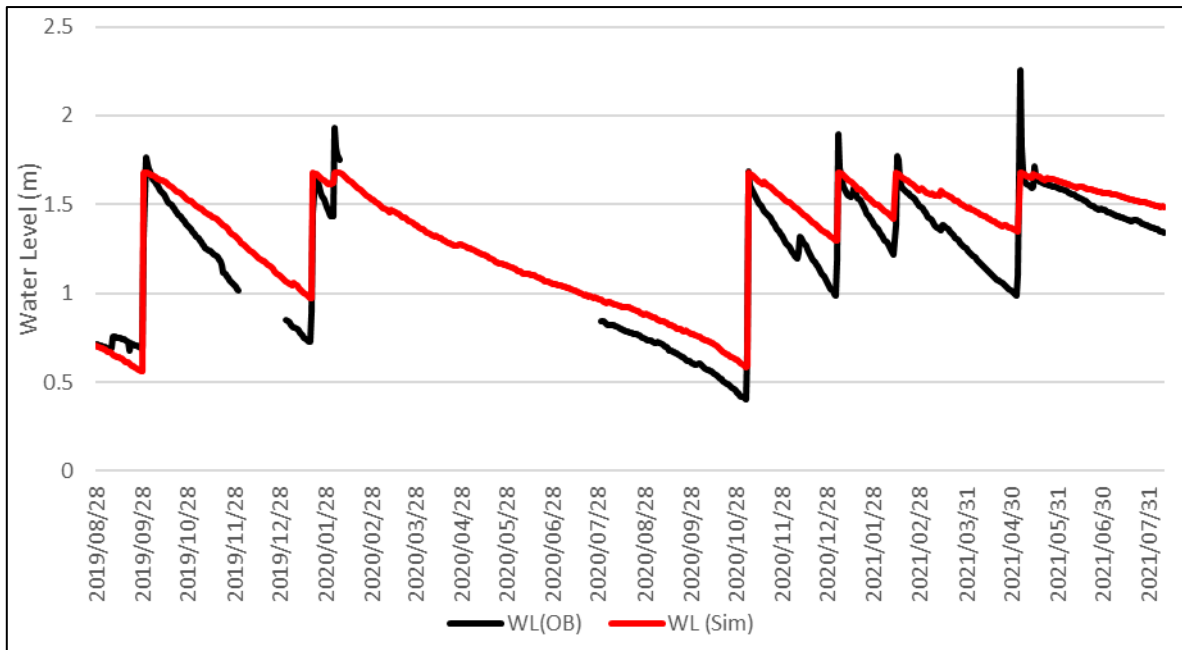
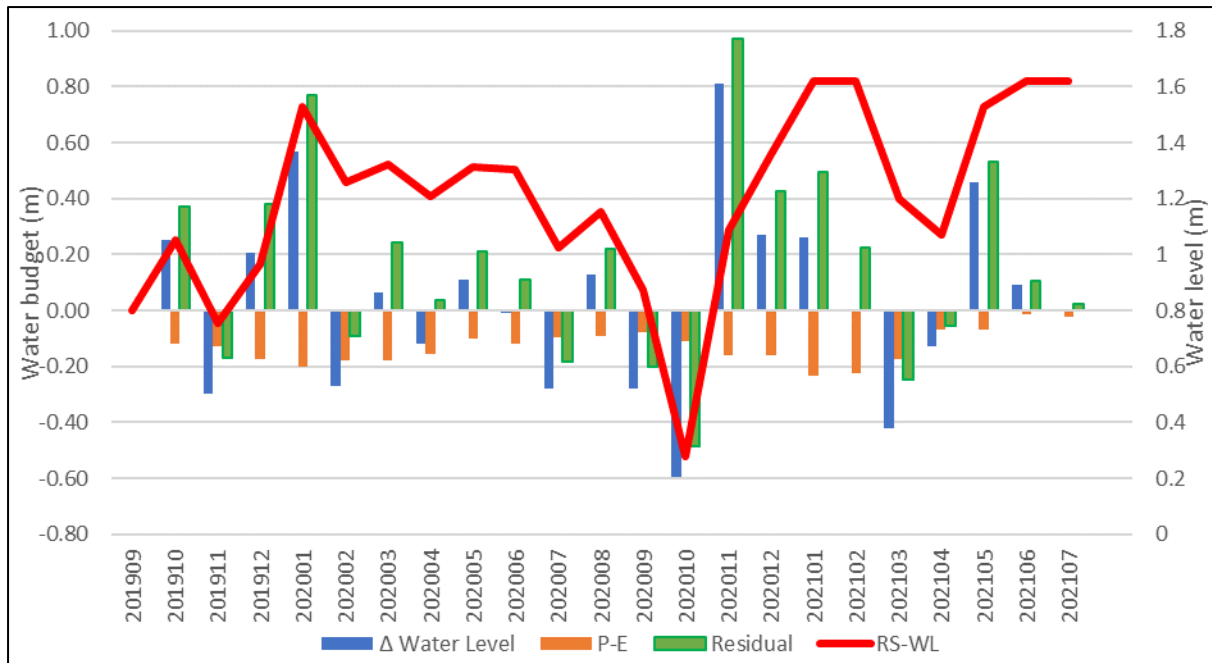


Figure 5.9: Observed water level (black line) and simulated water levels based on remote-sensed estimated climatic variables (rainfall and evaporation) (red line).

The surface area of the pool obtained from remote sensing was converted to water level (equation 19). The remote sensing-based estimation showed an increase in water level in response to flow occurrence. The remote sensing-based water balance suggests that 65% of the water is lost through evaporation, therefore 35% is lost to the subsurface (negative residual), which is higher than the outcomes from the in-situ-based model (Figure 5.10).



**Figure 5.10:** Remotely sensed water balance of the pool with the negative and positive values denoting losing and gaining pool respectively (blue bar), estimated water level (red line) and the difference between evaporation and rainfall over the pool (orange bar) and the residual of water level and the difference between precipitation and evaporation (green bars).

## 5.4 DISCUSSION AND CONCLUSION

### 5.4.1 Discussion

The study focused on improving the understanding of pool dynamics along non-perennial rivers by assessing the water fluxes that influence pool dynamics using the water balance approach. The results showed that one flow event can sustain the pool for 258 days without any inflows, although the probability of such a prolonged no-flow is low (10%). This suggests that the focus WW2 pool is semi-permanent to permanent. Pools in South Australia have similar persistency, i.e. 286 days for the pool with a maximum water level of greater than 1.6 m (Marshall *et al.*, 2016). The water balance model also supports that the pool is sensitive to flow occurrence, as indicated by Maswanganye *et al.*, (2022). The persistency of the pool might change over time, as evaporation increases and rainfall declines over the region due to climate change (Department of Environmental Affairs, 2018). These findings also suggest that if there is dam construction upstream, reducing the frequency of river flows, the pools will be impacted and could lead to drying out of the pools, which further has implications for the biodiversity found in these pools (Bonada *et al.*, 2020; Larned *et al.*, 2010). Therefore,

this information should be considered when proposing development such as dam construction.

The water balance models indicate that there might be groundwater inflow into the pools, although this might be seasonal as similarly observed by Bestland *et al.* (2017), in this case, this was observed when the pool reached a certain level, as stated that the study catchment has no clear wet and dry season. Maswanganye *et al.* (2022) inferred that groundwater is not feeding the pool based on that there were no groundwater level fluctuations relating to surface flow and rainfall observed. The water balance revealed that water losses into the subsurface from the pool are insignificant to cause groundwater level fluctuations. The pool's substrate and the underlying geology also suggest that it is limited and has no interaction (low conductivity) (Hwang *et al.*, 2017; Mohuba *et al.*, 2020). The interaction might also depend on the gradient between the pool and the water table, as illustrated in Figure 5.11. This observation is further supported by the elevation plot using DGPS measurements which shows that groundwater usually fluctuates at around 1.1 m of the pools (Figure 5.12). Bourke *et al.* (2020) referred to these kinds of pools as through-flow pools.

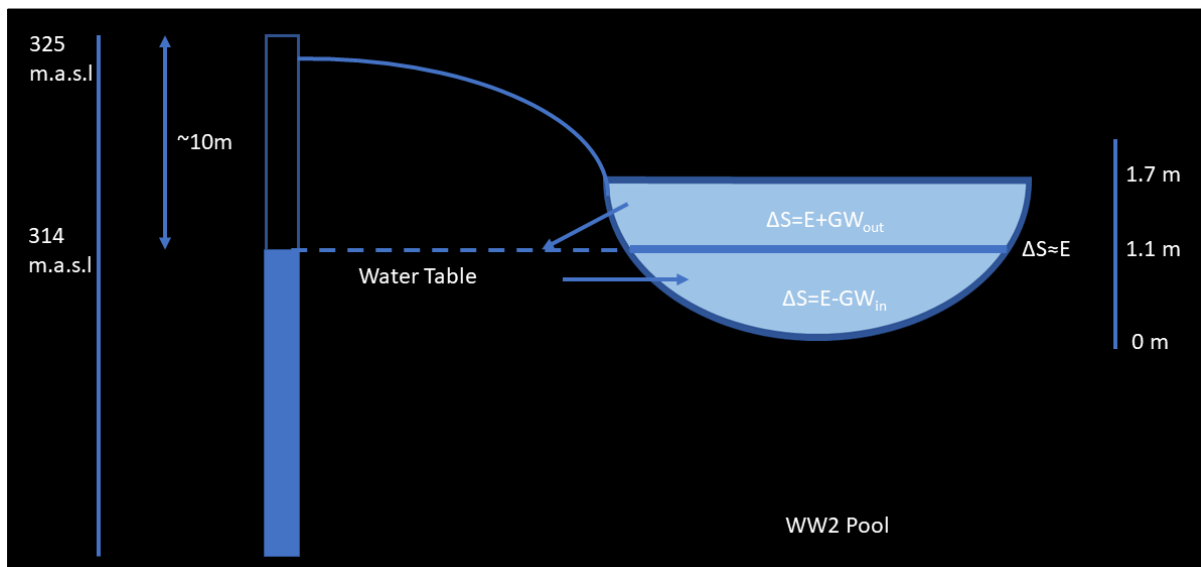
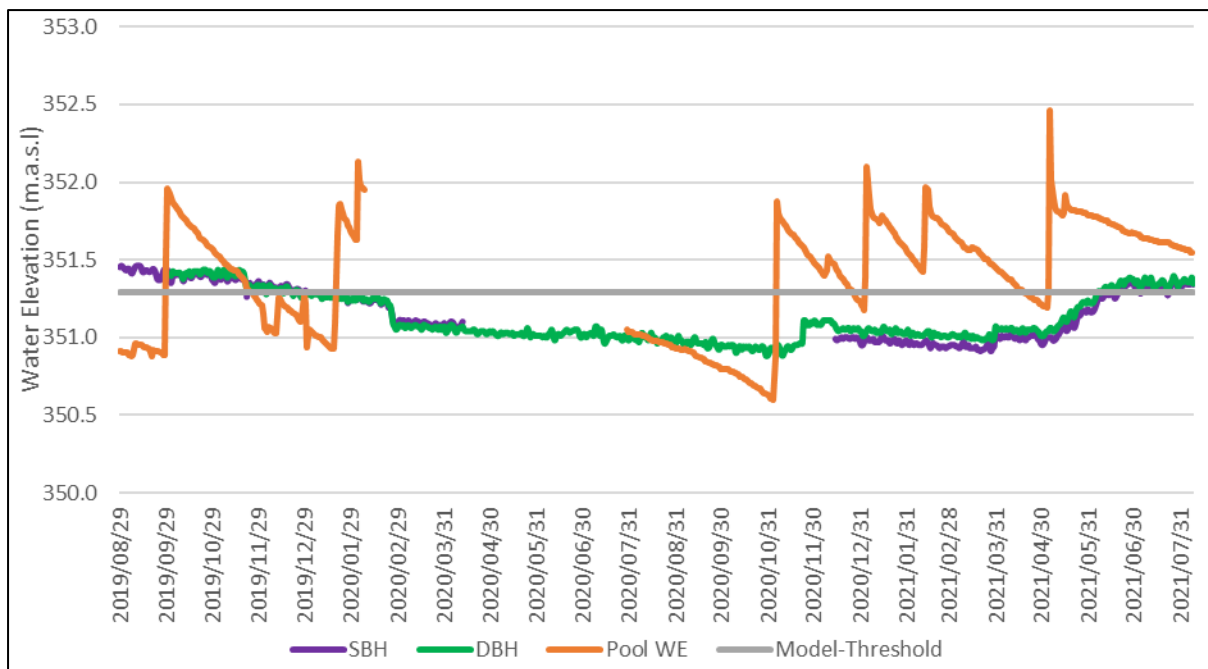


Figure 5.11: Conceptual Model of the pool based on Water Balance simulation.



**Figure 5.12:** Water elevation of shallow (purple line) and deep (green line) boreholes compared to an observed water elevation of the pool (orange line) and threshold whereby groundwater could flow into the pool as estimated using the model (grey line).

Although the water balance models performed well using just flow occurrence, having information about discharge into and out of the pool could have provided more insight. For instance, the relationship between discharge and pool water level, and how this then affects water losses. Furthermore, to determine whether the pool water losses from the upstream are detected downstream (interaction between the pools) as some studies have suggested that pools can remain hydrological connected through shallow groundwater paths while disconnected on the surface (Larned *et al.*, 2010).

The water balance model displayed robustness and transferability to the WW1 pool albeit with minor adjustments to maximum and initial water levels. However, it did not perform as well when evaluated at the TWB pool. This might be due to the pool having a strong subsurface flow impact that influences the dynamics of the pool. It is also possible that the TWB pool may differ in properties such as the presence of algae and shade over the water which might significantly reduce evaporation (Trimmel *et al.*, 2018). Furthermore, (Seaman *et al.*, 2016) indicated that neighbouring pools along the same reach can significantly differ. WW1 pool (upstream) is shown to have the same pattern as the WW2 pool, will, however, dry out before WW2 because it is smaller in size. TWB pool (downstream) showed a very

distinct pattern in terms of losses, capable of sustaining its size or water level for longer periods, suggesting that this could be a permanent pool.

Based on the results, remote sensing detects the pools and provides a general overview of pool dynamics as suggested by Maswanganye *et al.* (2022) as it was able to detect major changes correctly but does not provide detailed information or understanding of pool dynamics at the water balance level. This might be due to errors emanating from each of the model input variables. Furthermore, errors may also be caused by the resolution of remote sensing data as compared to the size and temporal dynamics of the pool. When the water balance approach is applied to larger surface bodies such as large dams and lakes, these errors might be negligible (Chen *et al.*, 2022; Dues *et al.*, 2018). The water balance can also provide better insight when applied on a long-term basis. However, to improve the remote sensing-based water balance model, there is a need to acquire information on flow occurrence. This could be done by detecting flows from satellite images or can be predicted through rainfall (runoff-rainfall model). Furthermore, the groundwater information that is required to predict pool water losses to subsurface stores is still a mystery for the remote sensing field. The remote sensing-based water budget suggests 35% water losses to groundwater which is three times more than observed. This could be predicted using the climatic variable(s), for instance, in this study groundwater losses could be expressed as 11% of evaporation, this estimation should consider the substrate and underlying geology of the area. Predicting the  $GW_{in}$  flow will still be a challenge as it was shown that it could be a function of the groundwater table. The GRACE showed to be useful in larger water bodies (Deus *et al.*, 2013). However, the incorporation of remotely sensing-based climatic variables showed to be limited by the unknown groundwater-pool interaction. This suggests that for pools not influenced by groundwater processes, remote sensing can use to understand pool dynamics

Overall, the results provided a better understanding of the pool dynamics and imply that the water balance approach can be useful to understand pools along non-perennial rivers. The information derived from the water balance should be incorporated into the water resource management of NPRs and catchments. Water resource managers can establish water available in the pools by knowing the last day of flow.

#### 5.4.2 Conclusion

There are limited studies on the hydrology of pools along non-perennial rivers. Using pools along the Touws River in the Karoo region of South Africa, this study assessed pool

dynamics using the water balance approach. The study established that Wolverfontein 2 pool is a semi-permanent pool with little chance of completely drying out. The water balance of pools was established and modelled with limited data. The simulated water levels showed satisfactory performance. The model was transferable to the neighbouring pools though it required adjusted maximum water and initial water levels. The water balance approach applied to the pool provided more insight into the pool dynamics.

The models suggest that there is groundwater-pool interaction at the assessed site. However, the magnitude of the losses is minor when compared to losses in the atmosphere via evaporation. The pool has a point whereby the rate of losses is less than evaporation, indicating potential gain from groundwater. These gains and rainfall in the pools delay the out-drying of the pools. We assume errors are due to uncertainty related to a full understanding of pool-groundwater interactions. The use of remotely sensed climatic variables with maximum water level can provide temporal dynamics for pools with no groundwater influence when flow occurrence is known. Because of the size of the pool, remote sensing can provide an overview of the general behaviour pool but cannot provide the detailed information that *in situ* observation provided. However, with all the rapid advancements in the remote sensing field, remote sensing will close the gap soon. This study successfully used the water balance approach to understand the pool dynamics. The information derived from the water balance models is significant in managing pools and pool dynamics in semi-arid environments.

## 6 DETECTION OF HYDROLOGICAL PHASES

### 6.1 DETECTION OF THE HYDROLOGICAL PHASES IN THE TOUWS AND MOLOTOTSI RIVER

Remote sensing methods were able to detect and distinguish the hydrological phases of the selected NPRs, the accuracy varied with sites. In the Touws River, only pools and flow phases were detected and observed, the river did not dry up (Figure 6.1A). In Touws River, the presence of pools was better detected (User's and Producer's Accuracy= 99%) compared to flow (UA and PA=86%). High accuracies were also obtained in the Molototsi River (OA=90%), however, the dry phase had the lowest producer accuracy (78%), and the flow phases were better detected (Figure 6.1B). The Sentinel-2 data had 70% flow detection power (eq. 1) in Molototsi River, suggesting that there is a 30% chance that a flow event can be missed due to cloud cover. The detection power was 65% for the Touws River. Overall, pools were the dominant phase for both rivers, the Touws Rivers pool did not dry out during the study period. Because of the two phases observed, the Touws River hydrological phases were detected better than the Molototsi River. Furthermore, the Molototsi River has a few pools phase that was confused with the dry phases (Figure 6.2B). Only on one occasion was flow occurrence misclassified as a pool.

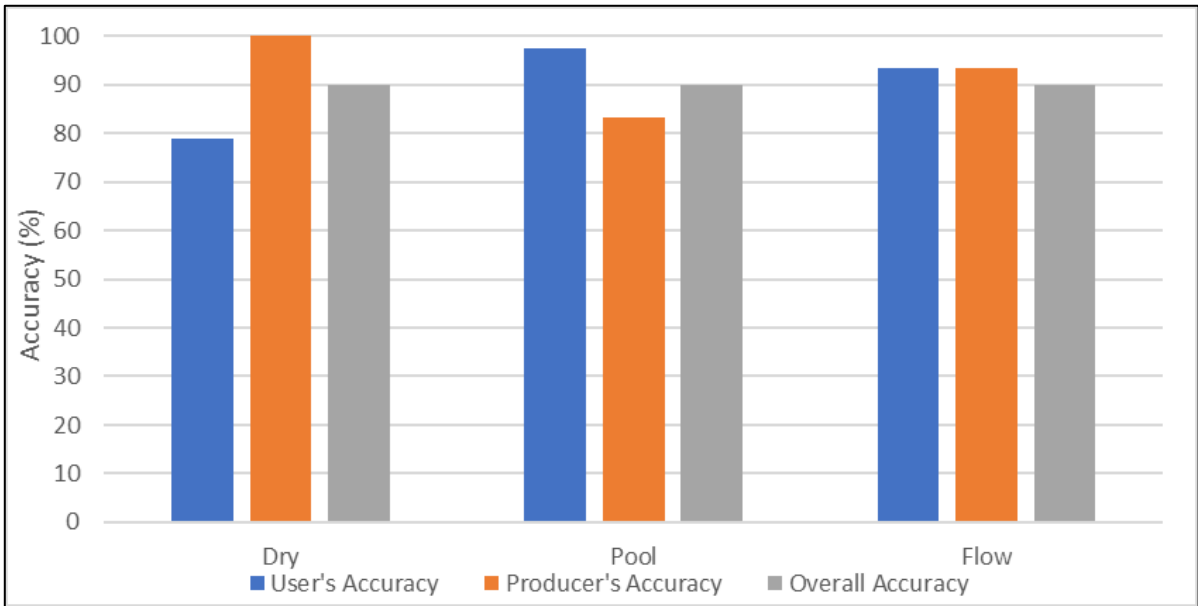
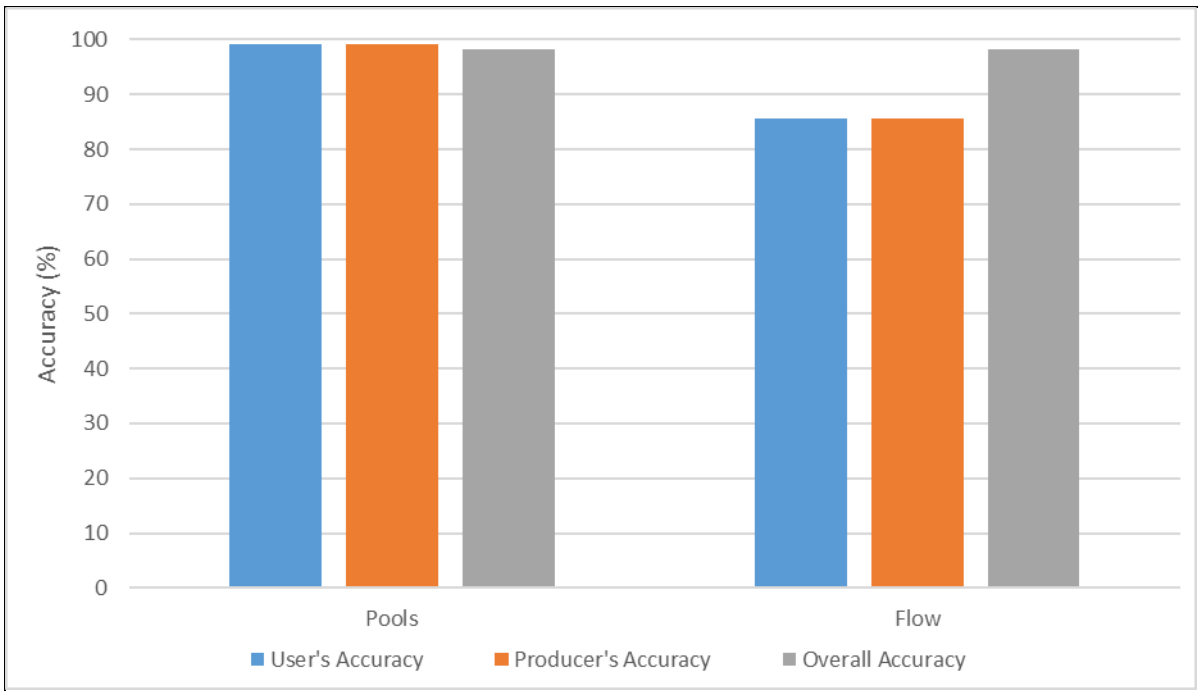


**Figure 6.1:** Accuracy of the Remote Sensing in distinguishing between hydrological phases in the Touws (A) and Molototsi River (B). The Touws River only had two phases whereas the Molototsi River had none.

## 6.2 RELATIONSHIP BETWEEN FLOW DETECTION AND FLOW EVENT DURATION AND THE USE OF SENTINEL-1 TO IMPROVE FLOW DETECTION.

Sentinel-1 was able to detect two of the three events missed by Sentinel-2 in the Molototsi River, improving the flow phase detection by 20% (Table 6.1). However, it was not able to detect any of the events missed in Touws River. It even failed to detect some of the flow events detected by Sentinel-2. Sentinel-1B faced challenges in 2021 resulting in the images being unavailable. The short-duration flow events tend to be difficult to detect using remote sensing as 83% of the missed events had a duration of fewer than five days (Table 1), which is problematic as most NPRs have a short flow duration.

Table 6.1: Remote sensing's (RS) ability to detect flow events with various duration

Touws River			
Duration (days)	Observed events	RS-detected events	Missed events
<5	6	2	4
6-10	4	4	0
11-15	1	1	0
Molototsi River			
<5	5	3(+1)	2
6-10	3	2(+1)	1
11-15	2	2	0

*N.B.: +1 indicates additional events detected using Sentinel-1*

## 6.3 TEMPORAL DYNAMICS OF THE PHASES

Non-perennial rivers are known to be highly dynamic and difficult to predict. Touws River hydrological phases are less dynamic but showed no seasonal pattern, hence unpredicted. Although Molototsi River is more dynamic in terms of changes between the phases, it is however seasonal. Flow usually occurs during southern hemisphere summer (Dec to Feb), this is then followed by pools occurring from autumn into winter (March to August), and then dry riverbed tends to be dominant from August to November (Figure 6.2B). The general cycle is usually dry to flow to pools. Comparing the two catchments, Molototsi River flows are more frequent and tend to last longer.

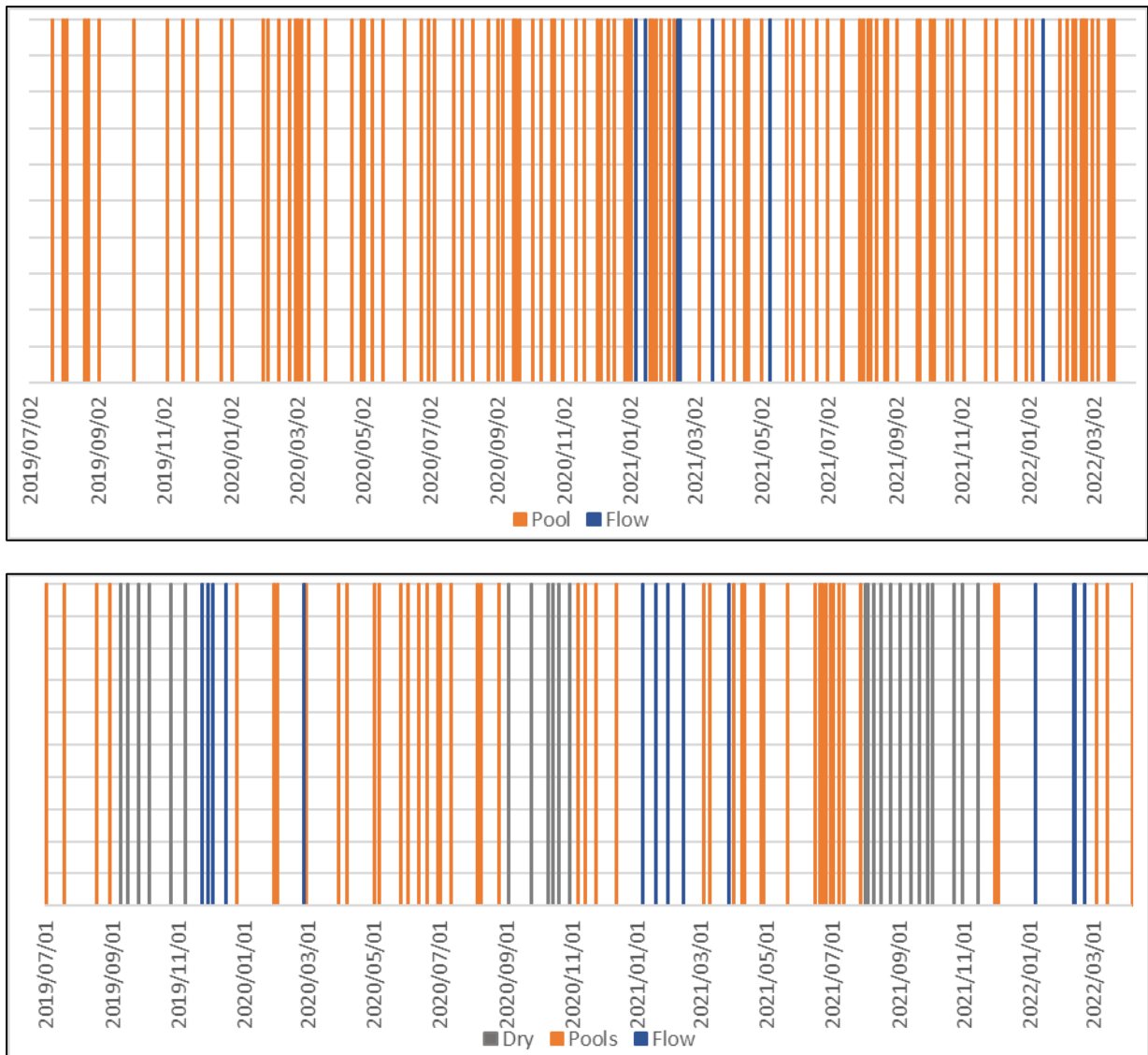


Figure 6.2: The temporal changes of hydrological phases in the Touws (A) and Molototsi River (B), detected through remote sensing.

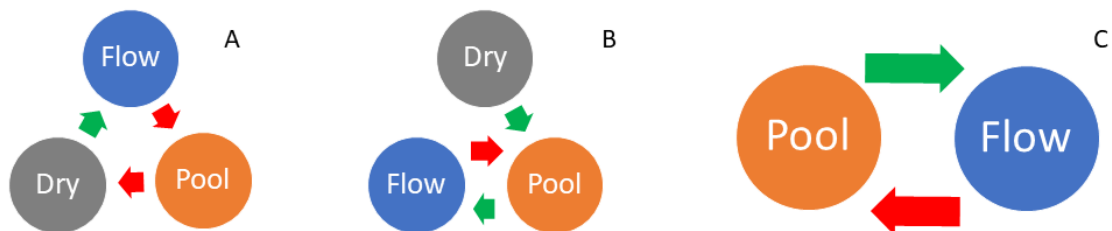


Figure 7: Summary of hydrological phases pattern observed in this study, A and B were observed in Molototsi and C was observed in Touws River. The green arrows denote water added to the river, and the red arrows indicate water loss by the river.

## 6.4 FLOW CONTRIBUTING AREA IN THE TOUWS AND MOLOTOTSI RIVER

The spatial distribution of rainfall that results in flows in the Touws River suggests that the Southwestern part of the catchment (Quaternary catchment J12J) tends to receive more rainfall (Figure 8A). This further suggests that this area may be generating most of the runoff observed in the river. However, there are cases whereby rainfall was received elsewhere (shown using a red frame in Figure 8A). The rainfall distribution suggests that there are also flow events that may have occurred mid to lower parts of the catchment but did not occur upstream of the river. The highest 5-days antecedent rainfall (i.e. total rainfall preceding the flow event) observed was ~120 mm and the lowest was 20 mm.

In the Molototsi River, rainfall leading to the majority of the flow events tends to occur in the upper catchment (B81G) (Figure 8B). There were events whereby rainfall occurs in mid-catchment (shown using a red frame in Figure 8B). The locals suggest that the flows originating from the upper catchment (Modjadjiskloof) area tend to last for longer compared to other parts of the catchment. The highest antecedent rainfall observed for the Molototsi catchment was ~96 mm and the lowest was 24 mm. However, receiving the highest rainfall sometimes does not result in any runoff being generated and/or observed, the physical characteristics (soil type, slope, and land use and cover) of the catchment have a significant role to play in this regard.

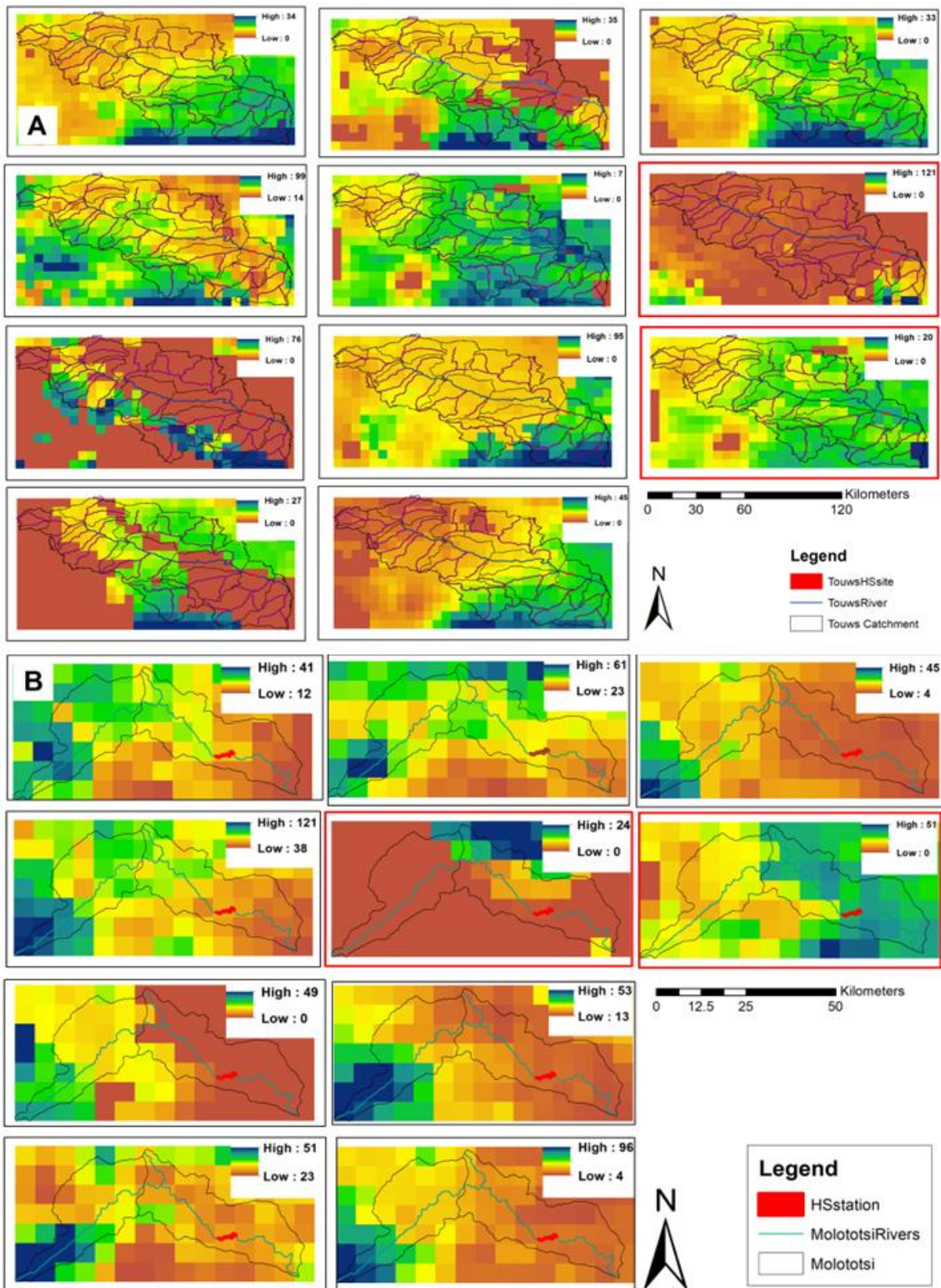


Figure 8: Spatial distribution of the antecedent rainfall for flow events that occurred between August 2019 to March 2022 in the Touws (A) and Molototsi River (B).

### *Curve number method*

To consider the physical characteristics of the catchment, the SCS curve number (CN) was used to determine contribution areas. Due to the small variation in soil types and land cover in the Touws catchment, the curve numbers showed small variation, indicating that runoff produced in the catchment is mainly controlled by the spatial distribution of rainfall. The area where most of the antecedent rainfall occurs (Figure 8A) is also one of the areas with a high probability of producing runoff (CN>61) (Figure 9A). The upper parts of Molototsi Catchment have higher curve numbers (>78), implying that it is likely to produce more runoff than the lower parts (B81G) (Figure 9B). The area also tends to receive more rainfall. Comparing the two catchments, the curve number method suggests that the Molototsi catchment has a greater probability of producing runoff (Figure 10), and generally receives more antecedent rainfall. The estimated initial abstraction derived through the curve number method is similar to the estimated antecedent rainfall (remotely sensed estimated) for the Molototsi Catchment, which indicates that some parts of the catchment can potentially start to generate runoff from receiving as little as 10-20 mm of rainfall (Figure 10). Whereas the Touws catchment can potentially generate runoff from 20-30 mm of rain.

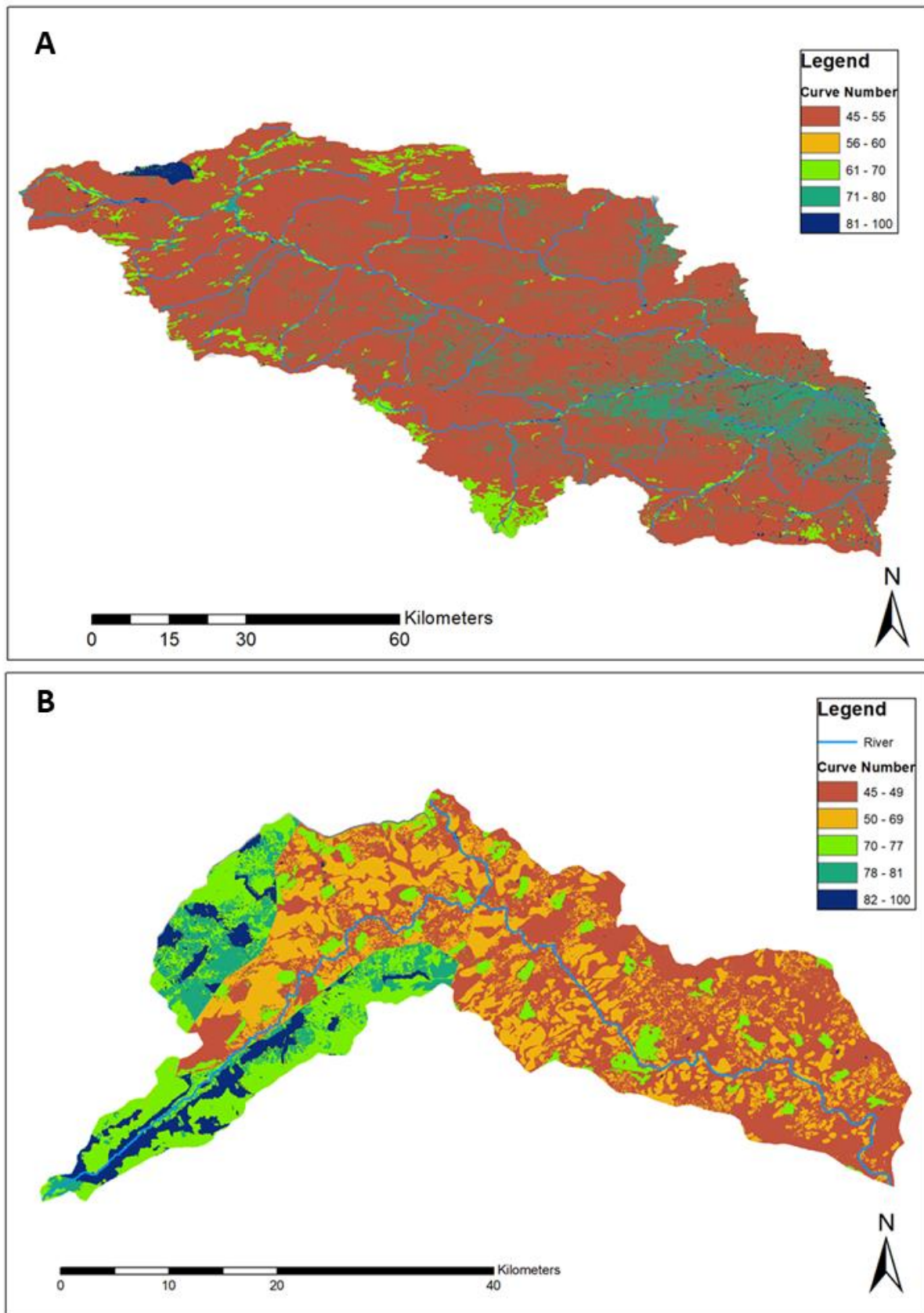


Figure 9: Runoff curve numbers of the Touws (A) and Molototsi (B) Catchment using AMC II.

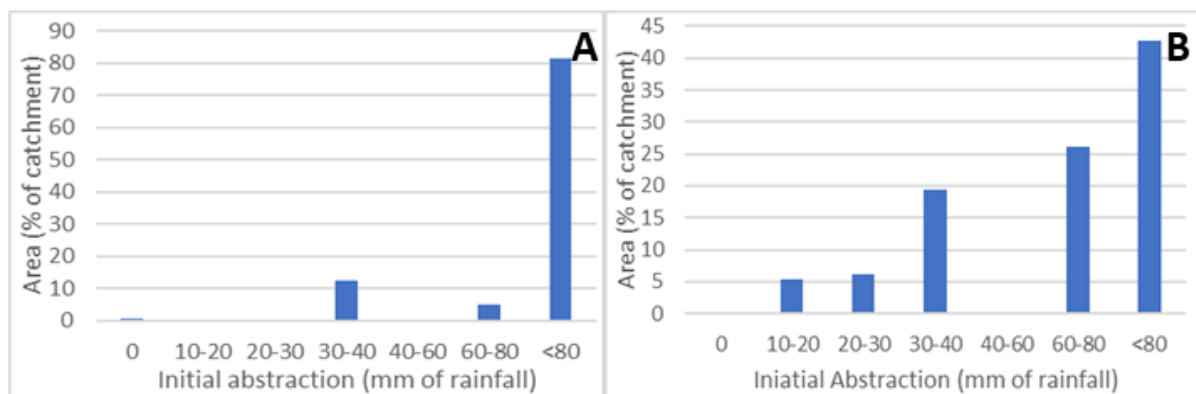


Figure 10: Initial abstraction of rainfall before runoff as a proportion of the Touws (A) and Molototsi catchment area (B).

## 6.5 DISCUSSION AND CONCLUSION

Non-perennial rivers are highly dynamic, switching between different hydrological phases. Remote sensing was used to detect these phases and showed to have the ability to distinguish between the hydrological phases. Although, the detection of the transition between the phases especially from pools to dry seems to be a slight challenge for remote sensing. This might be caused that the pools becoming very small to be detected at satellite spatial resolution as Maswanganye et al. (2022) suggested that it is a challenge to detect pools of less than 400 m<sup>2</sup>. The remote sensing performance was better in Touws River than in Molototsi River this might be because

- i) the river only had two phases
- ii) the pools in the Touws River tend to be bigger as observed by Maswanganye et al. (2022), allowing for easy detection.

This suggests the method used might not be applicable in rivers with a small width (<40 m). Molototsi River phases have shown to be more dynamic in changes the phases. The findings of this study in terms of the persistence of the pools in both catchments are in line with the results made by Maswanganye et al. (2022) which suggested that the pools are permanent to semi-permanent in the Touws River and ephemeral in the Molototsi River.

The flows in the Molototsi River tend to be more persistent, allowing more time to capture cloud-free images than the Touws River. The missed flow event by Sentinel-2 was of shorter duration (<5 days), this suggests that flow of short duration has a greater chance to be missed. This study used Sentinel-1 to overcome these issues. Although Sentinel-1 had poor detection of pools (Maswanganye et al., 2022), Sentinel-1 was able to detect two of three flow events missed due to cloudy images in the Molototsi River, however, it was

unsuccessful in the Touws River. Seaton & Dube (2021) suggested that this is a result of the flat and aridity landscapes creating similar backscatter to water, resulting in difficulty in the separation of water and the surrounding areas. Using Sentinel-2 and Sentinel-1 and including other remote sensing data from various satellites can improve the temporal resolution, hence giving it the potential to estimate the duration of the flow events.

The analysis of major contributing areas of flows for the Touws River suggests that the site or reach used in this study did not capture the hydrological states of the upper stream well as much of the runoff generated in the mid-catchment, therefore, there is a need to use multiply sites when determining the hydrological state to provide a good representation of the river. This can be located in between the major confluences of the main river. This can be easily done through remote sensing but might be timely and laborious for direct observation. The minimum antecedent rainfall was estimated to be 20 and 24 mm in the Touws and Molototsi catchments, respectively. However, the spatial coverage of the antecedent rainfall is also important. The Touws catchment is drier compared to the Molototsi catchment, as it receives less rainfall. The runoff curve numbers further suggest that the Molototsi catchment has a better probability of generating runoff than the Touws catchment.

## 7 DISCHARGE ESTIMATION

### 7.1 THE COMPARISON OF THE SPECTRAL SIGNATURE OF POOLS AND FLOWING WATER IN NON-PERENNIAL RIVERS

Before applying the same method to detect pools and flows, it is necessary to establish if pools and flowing water have the same spectral signature in Sentinel-2 images. The hill shadow and the water in the pool (Wolverfontein-2) had a similar spectral signature but it was different compared to flowing water (Figure 7.1). This suggests that it might be easier to distinguish between flowing water and hill shadows than a pool from a shadow.

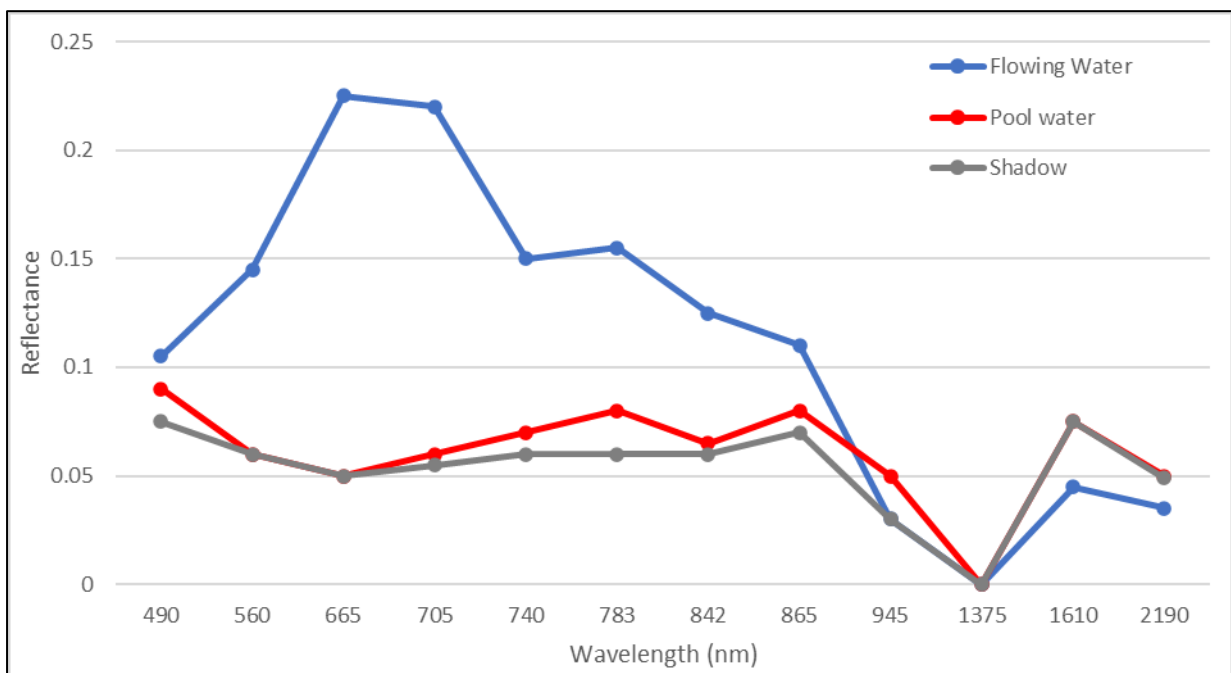


**Figure 7.1** Spectral signature of the flowing river (blue line), pool and a hill shadow of Sentinel-2 in Touws River.

The spectral signature was extracted from the four points in figure 7.2. The results show that there is a difference between flowing water and stagnant water (pools), especially in the visible region of the spectrum (490 to 865nm) (Figure 7.2).



Figure 7.2 Four points that were used for reflectance analysis on Google Earth

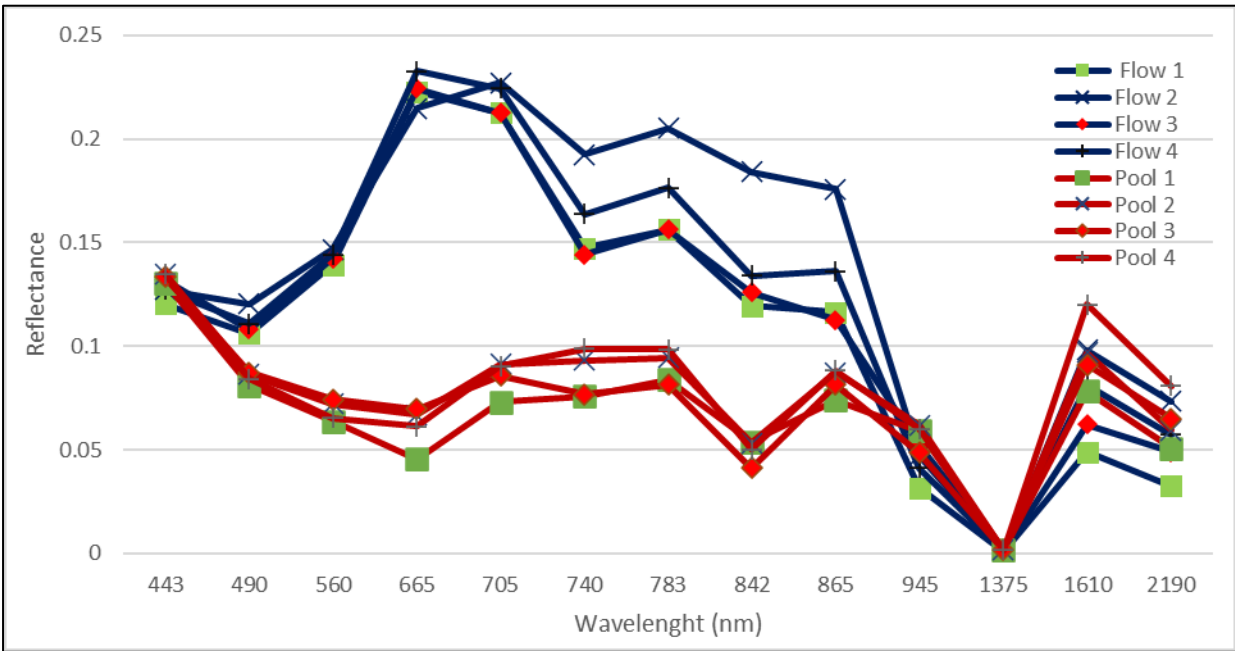


Figure 7.3 Comparison of the spectral signature of flowing water (2019/02/05) and stagnant water or pools (2019/03/24) at 4 points along the Touws River using Sentinel-2 data.

Furthermore, field observations support this: flowing water carries sediments hence it appears brown, whereas in stagnant water the sediments settle at the bottom and the water

appears blue to green (Figure 7.4 and Figure 7.5). These images were taken using the same device.



Figure 7.4 Molototsi river when (a) flowing, and (b) when stagnant in a form of pools



Figure 7.5 Touws River when (a) flowing, (b) a day after flow (b), and (c) after a month flow.

## 7.2 ESTABLISHING THE RATING CURVES

### 7.2.1 Heuningnes

With Sentinel-2, it was challenging to determine flow in the Heuningnes catchment as the river has small widths (~15 m), which is occupied by one pixel of the Sentinel-2 image. It was not feasible to determine the changes in both the width and surface area of the flow. Images with better resolution (SPOT) imagery were requested to overcome this challenge. However, the images that SANSA could provide were not concurrent with events and were not enough to conduct this kind of analysis.

The catchment has a relatively flat slope which results in waterlogging, this means that even without flow, there is the presence of water. There was a drought between 2016 and 2018 with little to no flow, but there was water in the channels (Figure 7.6).

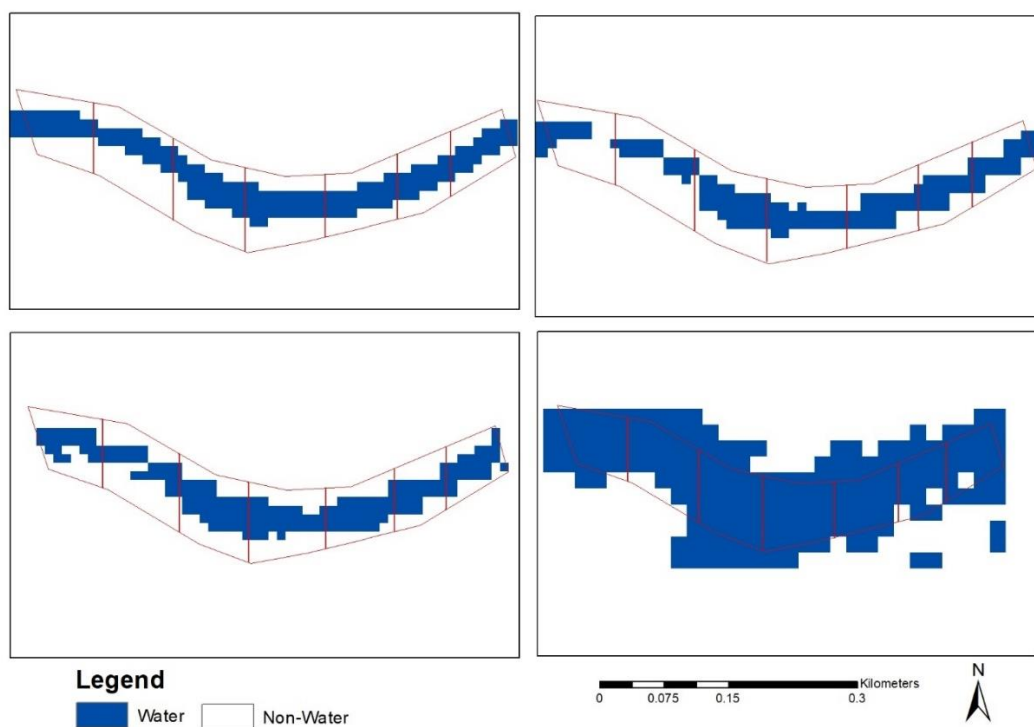


Figure 7.6 Detected water area in the channel during a dry period with no flow in Nuwejaars river using NDVI (top left), MNDWI (top left), MNDWI with a threshold (bottom left) and NDWI (bottom right).

The river channel is narrow and relatively deep, therefore there are little changes in width and surface area which may not be detected using remote sensing at the current spatial resolution.

Challenges from exploring possible data sets

1. Have been few events since the launch of Sentinel-2
2. No cloud-free images for Molototsi during flow events and four events which are not enough to establish a rating curve and validate it.

### 7.2.2 Touws River

Touws River had four flow events since 2015 when Sentinel-2 was launched. This meant that the area-discharge rating curve could not be established with confidence. Therefore, Landsat 8 was used to establish the rating curve, width, and water-surface area (Table 7.1).

Table 7.1: Images used for Touws River flow estimation.

Event	Satellite Image name	Observed Daily Flow (m <sup>3</sup> /s)	Estimated Width (m)	Surface Area (m <sup>2</sup> )
2013/10/25 to 2013/12/13	LC08_L1TP_173084_20131102_2017042_9_01_T1	16.0	36	30600
	LC08_L1TP_174083_20131125_2017042_8_01_T1	1.4	13.3	5625
2014/01/07 to 2014/02/20	LC08_L1TP_173084_20140121_2018052_6_01_T1	2.9	15	18900
2015/06/04 to 2015/08/17	LC08_L1TP_174083_20150608_201704_08_01_T1	4.5	28.2	29250

Although removing the outliers provides a better relationship between width and flow, the outliers indicate the possibility of overestimation associated with the method. The outlier may be due to sensor-related or classification-related issues.

### 7.2.3 Estimation of flow

The correlation between the width and discharge, and surface area and discharge were used to determine which method to use (area-rating or width-rating curve). In this case, the average width and discharge were better than an area-discharge relationship, hence width-

discharge was used (Figure 7.7). Correlation analysis was used to decide on the type of equation that will describe data better. The exponential curve was used as it had a better correlation ( $R^2=0.89$ ) than the linear curve (Figure 7.8).

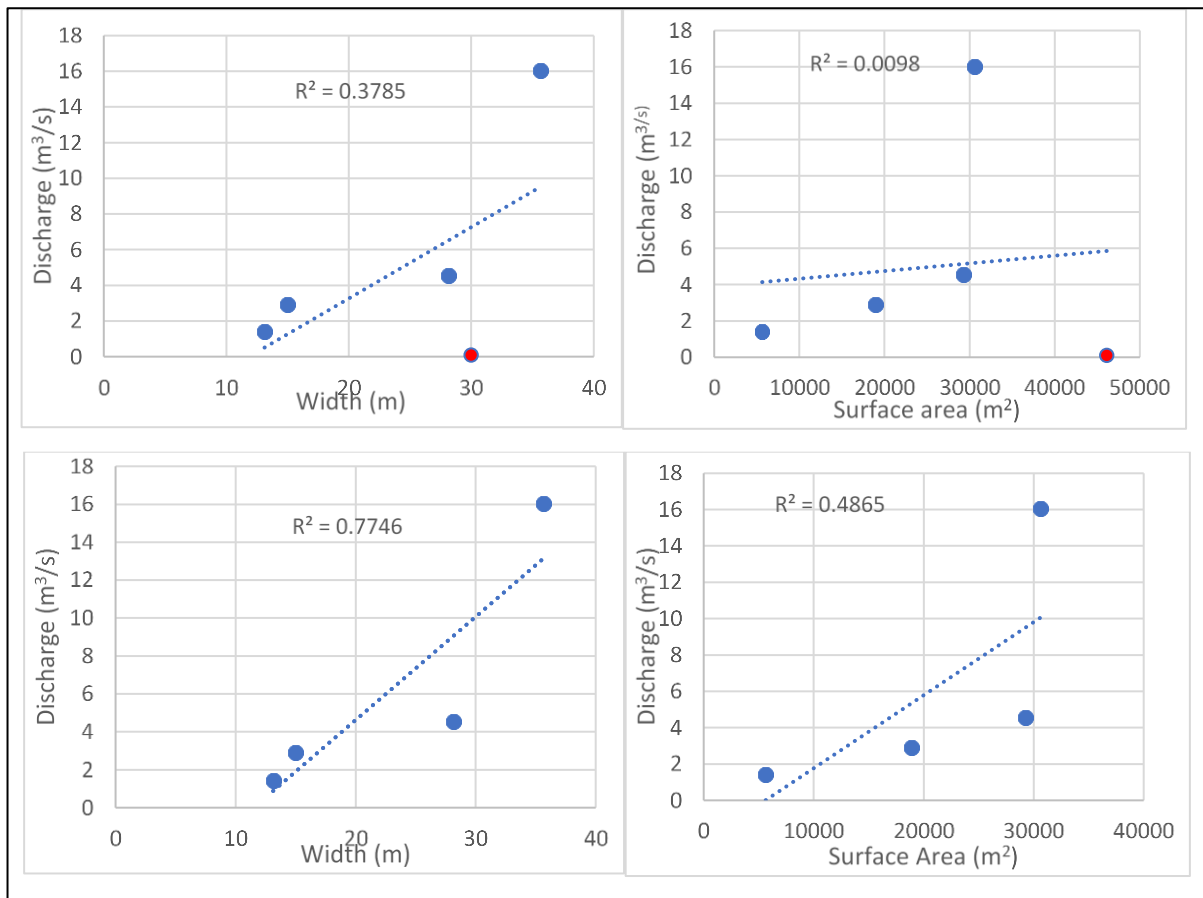


**Figure 7.7** The linear relationship between observed river discharge and remote sensed derived width (left) and surface area (right) in the Touws River, with the outlier (top) indicated as a red dot and without the outlier (bottom).

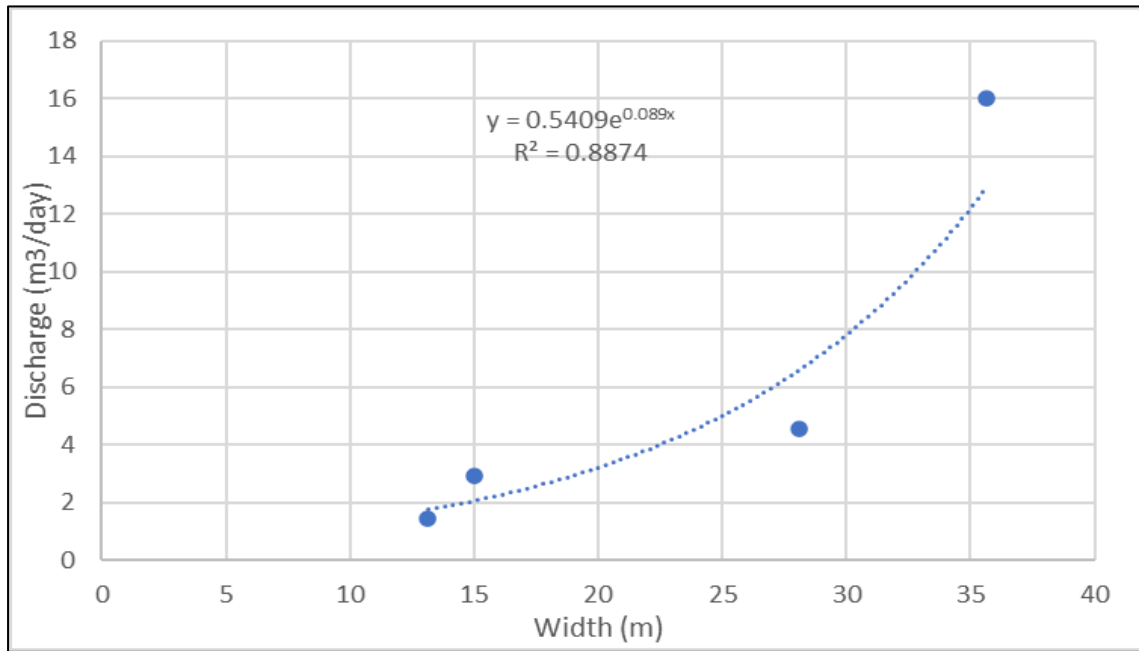


**Figure 7.8** The exponential relationship between observed river discharge and remote sensed derived width.

### 7.3 EVALUATION OF THE REMOTE SENSING DISCHARGE ESTIMATE

The rating curve needs to be improved by adding more data points, especially between 6 and 16 m<sup>3</sup>/s of discharge. Only four events occurred after the training events; three of the events were of very low flows. Using the above-developed rating curve (Figure 7.8), the RS method overestimated the flows as compared to the observed flows for all five events, mean error and mean absolute error of 1.25 m<sup>3</sup>/s (Figure 7.9). It appears that the rating can be adjusted to improve the estimates which yielded better results, a mean error of -0.162 and a mean absolute error of 0.172 m<sup>3</sup>/s. However, there are cases like 2021/01/16, where differences between observed and estimated cannot significantly be reduced by adjusting the equation.

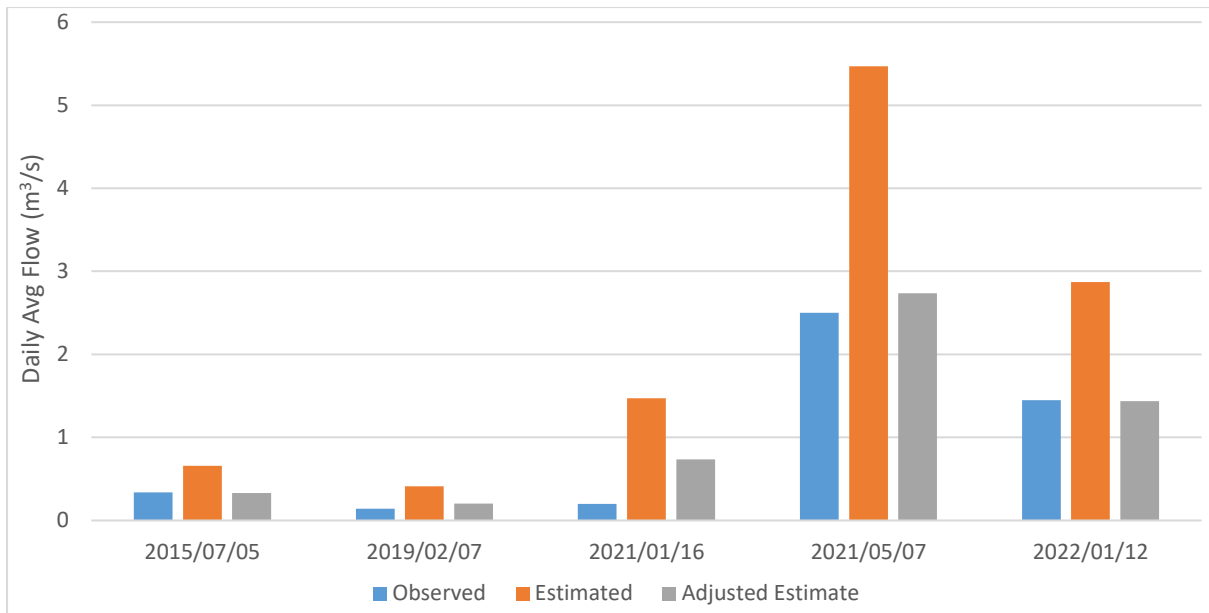


**Figure 7.9** Comparison of observed and rating curve-based estimated flows in Touws River.

The empirical equation used by Kebede et al. (2022) yielded unrealistic results, overestimating all events by at least 100 folds. The one proposed by this study of using Google Earth to estimate depth from width performed reasonably well (ME=-0.22 m<sup>3</sup>/s; MAE=0.32 m<sup>3</sup>/s) (Figure 7.10).

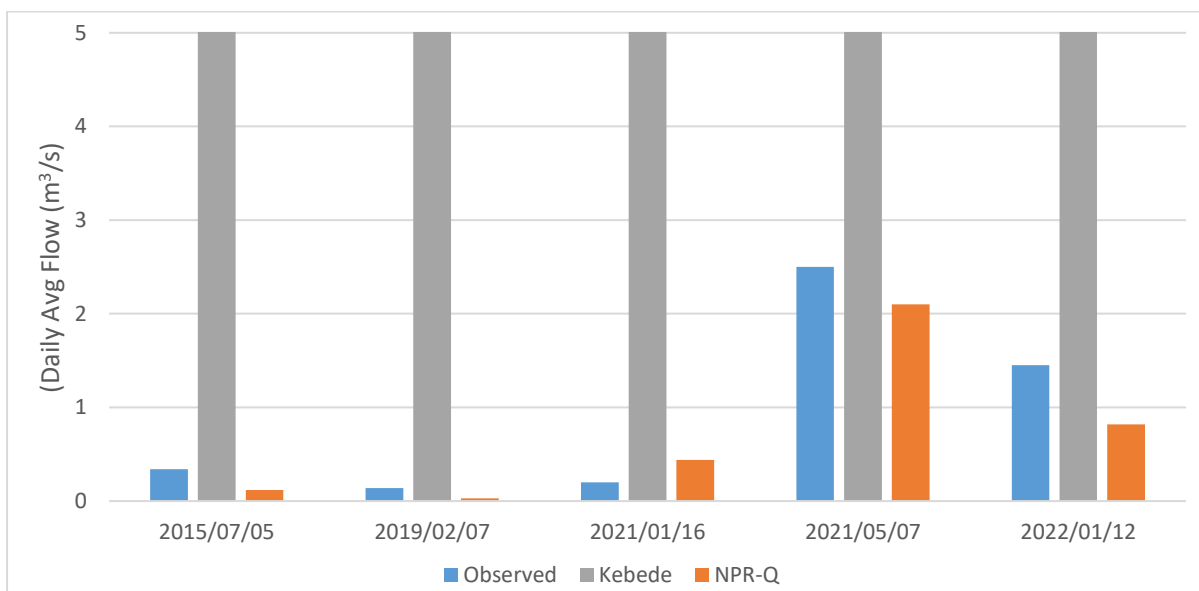


**Figure 7.10** Comparison of observed and empirical equation-based estimates. Methods used by Kebede et al. (2020) (grey bar) and the one proposed in this study (orange bar).

## 7.4 DISCUSSION AND CONCLUSION

The estimation of flow remote sensing relies on the information that can be obtained from RS data, width, and surface area in this case. The flow methods are still in the exploratory stages. However, the preliminary results demonstrated that it would be difficult to determine flow using remote sensing in areas with narrow streams and waterlogging because RS relies on changes in surface area and width of the flow. However, it also demonstrates the possibility of getting a useful estimate when the conditions are ideal for remote sensing (wide channel).

The accuracy of the estimates using the width-discharge method may be affected by the number of observations used to derive the rating curve, which can be easier obtained in perennial rivers but difficult to obtain in many non-perennial rivers as the flow can cease for years. This was the case with the Touws rivers. This is further worsened by the temporal resolution of satellite imagery (15 days for Landsat, 5 days for Sentinel-2), which in some cases misses the entire flow event. Furthermore, for the Touws River, the width-discharge rating curve was better suited compared to area-discharge methods, these findings are different from those of Kebede et al., (2020) but similar to the approach proposed by Gleason and Wang (2015).

In terms of the empirical equations, the one proposed by this study performed better and had acceptable accuracy considering that it was solely remote sensing based and that flow estimated is of small magnitudes, which are generally difficult to estimate. The method used by Kebede et al. (2020) was very poor this might be caused by the high width-depth ratio derived from perennial river, which tends to be deeper, whereas many NPRs tends to flow over the channel, not in the channel, hence often wide and not deep. The Touws River is a typical example of these wide but shallow channels.

Sometimes the image is available but cannot be used due to clouds. The use of SAR data was proposed as a solution to the issue of cloud cover, however, it was not successful when used in the Touws River, here and in the last section (6), as it yielded poor separation between water and other features.

Surface Water and Ocean Topography (SWOT), the first "water satellite" that combines both width and water depth measurements on one platform, was thought to be a solution for monitoring surface water and improving remote sensing discharge estimates. However, it is limited for use in non-perennial rivers as it has a spatial resolution of 50 m, in South Africa, only a few rivers, such as the Orange River, may fully benefit from SWOT. Perhaps combining water depth from SWOT with 10 cm height accuracy and higher resolution

imagery from the other platforms (e.g. Sentinel-2) can yield a positive outcome. We recommend further testing of the methodologies.

## 8 DEVELOPMENT OF A PREDICTIVE TOOL

### 8.1 INTRODUCTION

This chapter reports on the development and implementation of a predictive tool for water storage, abstraction, and length of use. This work package aimed to calculate the volume and water capacity of a riverbed in Limpopo and give the users a method to supply the data. Achieving this requires measurement information and geospatial data of the area containing the water. The chapter, therefore, presents a summary of the methodology used in this development and the proposed webpage interface. It concludes with an outline of work that could be carried out in the future to fully operationalise this tool.

### 8.2 METHODOLOGY

#### 8.2.1 Data requirements and data used

The area of interest used for this development is in a section of the Molototsi river located in Limpopo, South Africa. This perennial river contains subsurface water that is abstracted by the local communities. The abstraction rate, rainfall, and depth of the water level in the riverbed are measured on daily basis and will supply the user input to the water capacity calculation.

Further geospatial information required for the calculation is stored in a database and can only be modified by someone with administrative access to the application.



Figure 8.1. The Molototsi river area of interest is coloured yellow.

## 8.2.2 Calculation

For the users to make the best use of the available stored water, two calculations are required. The first is to determine how much water is stored in the riverbed and the second is to indicate whether the current rate of water abstraction is sustainable

### 8.2.2.1 Water Capacity

To determine the water capacity of the river some spatial information is required. The shape of the river section is available as well as the approximate depth of the aquifer. Given this information, we conceptually have a 3-dimensional representation of the total storage area. Since this is a relatively small section of the Molototsi river, a homogeneous aquifer can be assumed and therefore has a constant permeability.

Making use of the water level measured from the surface, it is assumed the water level is the same at any point along the river section. The area at the water level is interpolated and the volume between this area and the bottom of the aquifer is calculated.

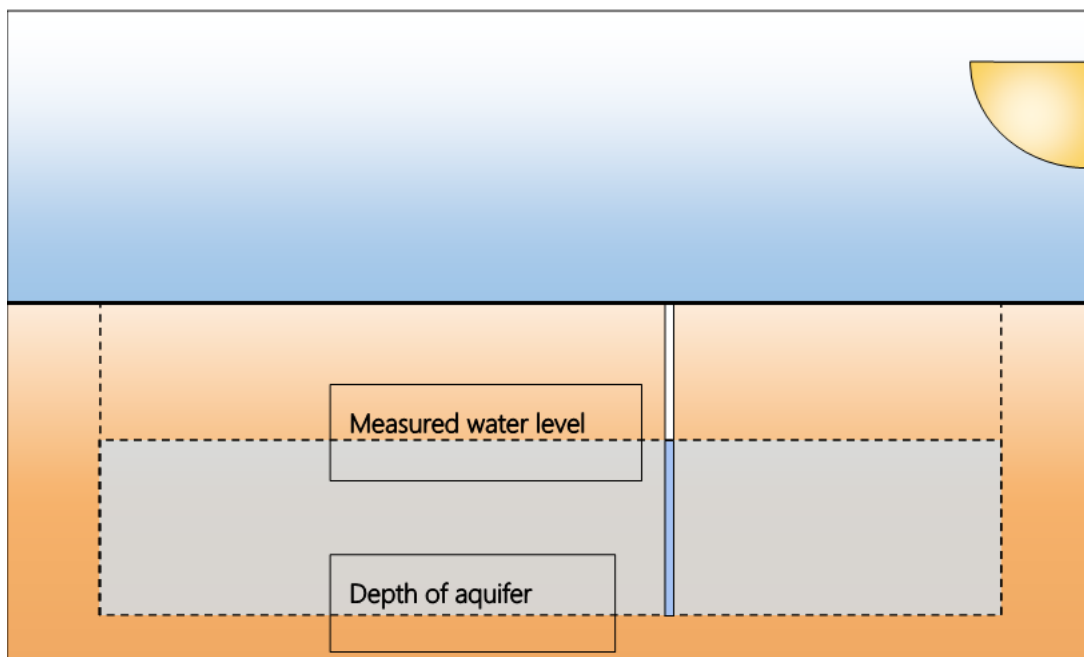


Figure 8.2. Diagrammatic representation of the section of the Molototsi river being considered.

### 8.2.2.2 Water Abstraction Rate

To assist the user to determine if the current abstraction rate is sustainable, the water balance equation for this aquifer is calculated. While this might seem like an overly complicated way of calculating the aquifer capacity, the same method can be used to

calculate the capacity of a much larger area and take into account a more complex geology profile.

$$\Delta S = \text{Run in} + \text{Rain} - \text{Run out} - \text{Evaporation} - \text{Seepage} - \text{Abstraction}$$

$$\Delta S = \text{Final Storage} - \text{Initial Storage}$$

The only input required from the user is the measured rainfall and abstraction rate and the time in hours since the last measurement. The values for the “run in”, “run out”, evaporation and seepage rate are predetermined and do not require modification by the users.

Along with the change in the capacity that the equation provides, an estimate for the remaining pump hours is calculated. Although this is only an estimation it could provide the user with useful information to adjust the abstraction rate to ensure the best use of the water stored.

### 8.3 WEBSITE INTERFACE

The website viewed here is in its most basic form and can be adapted to fit any template and style of the host website. It was created using the latest python Django framework, which is a continuously developed open-source web platform. The aim was to develop an interface that is easy to use for any user.

Two sections of the web application need to be noted. An administration page allows the administrator to specify and modify the geospatial parameters required for the calculations as well as view all the measurements and calculations saved in the database. The other section allows the user to enter the measurements and initiate the calculations.

### 8.4 WEB APPLICATION

Once the URL is entered into a browser, the user is met with a list of locations, Figure 3. The application has been developed in a way that allows for more locations to be added. It must be noted that this requires some work on the backend to prepare the necessary files containing the spatial information of the area of interest.

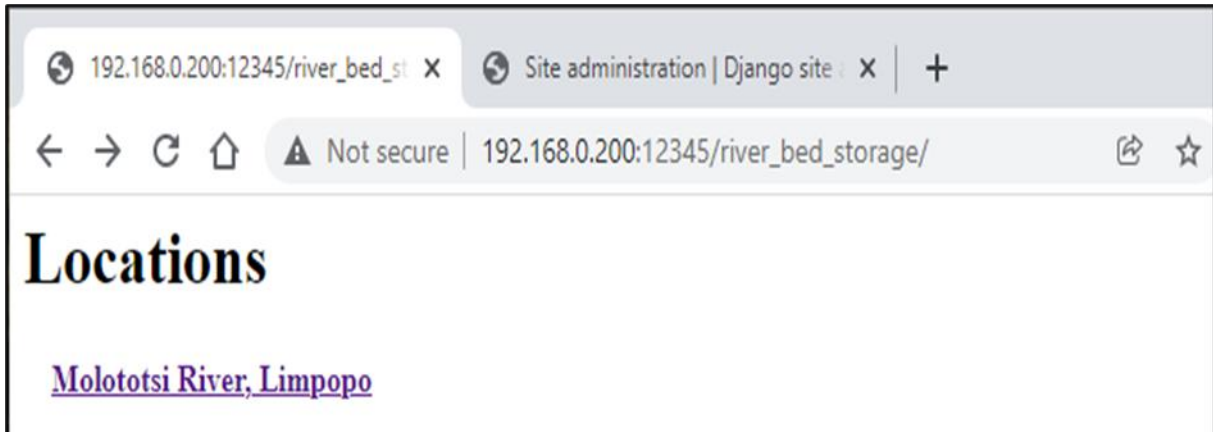


Figure 8.3. Web application landing page

Selecting the location, the user is met with a page containing links where the Rainfall, Abstraction and Water Level measurements can be added, Figure 8.4. Once the necessary measurement data has been supplied, Figure 8.5, the calculations can be initiated. Finally, underneath the links is a table containing the last calculations made.

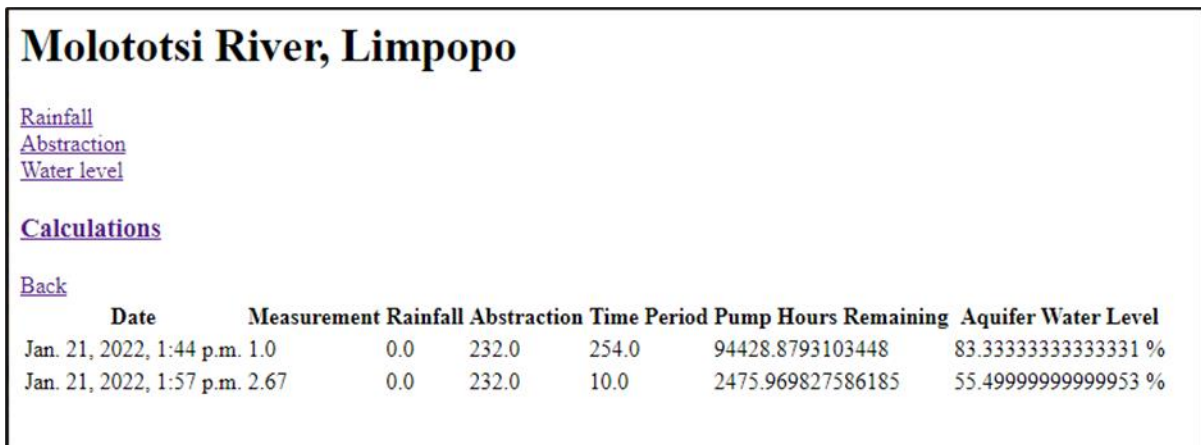


Figure 8.4. The webpage contains the links to where the data can be entered for the selected location.

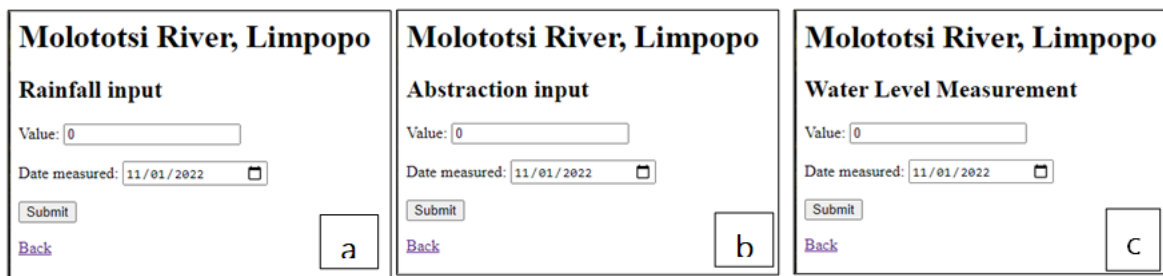


Figure 8.5. The webpages where Rainfall (a), Abstraction (b) and Water Level data (c) is entered.

Once data is entered for the rainfall, Abstraction rate and water level measurement, a calculation can be made. Going to the Calculation page, Figure 8.6, allows the user to select the measurements to use for the calculation. Since the measurements might not be made at the same time, the input boxes default to the latest entry in the database. There might be some other useful information about the measurements used or any other observation that can be supplied in the Comment box. The only input required by the user is the time in hours over which the calculation needs to take place. It defaults to the difference between the current date and time and the date and time of the last abstraction measurement. Once these values are selected and entered, the Submit button is pressed. After a few seconds, a Results page is displayed.

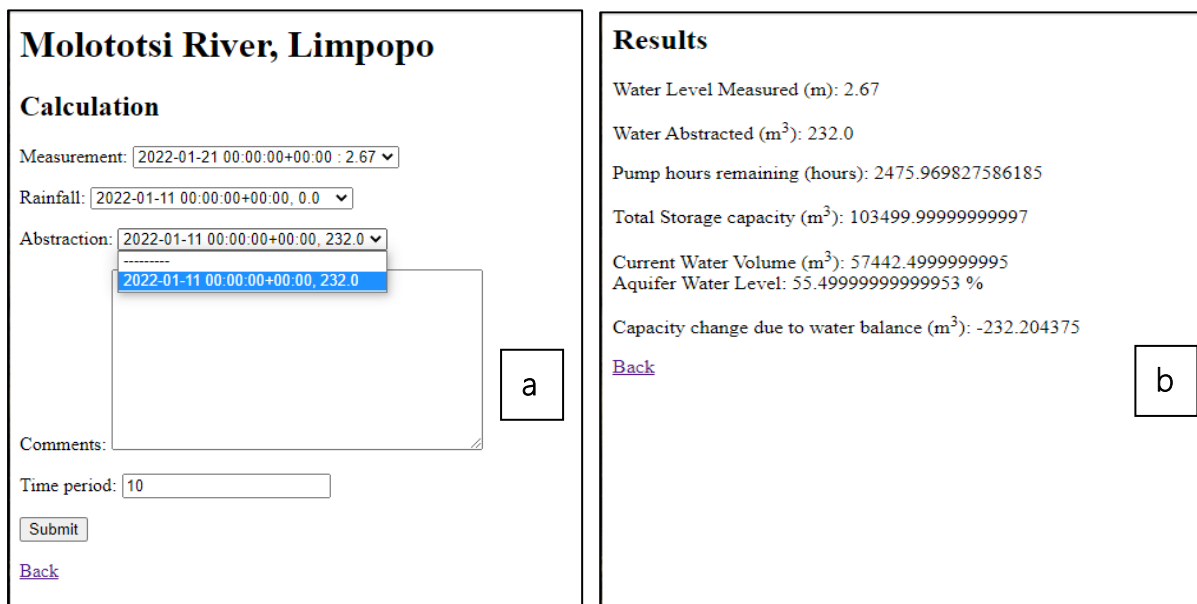


Figure 8.6. The Calculation (a) and Results (b) webpage.

The following information is displayed on the Results page.

Water Level Measured (m)	This is supplied by the user
Water Abstracted (m <sup>3</sup> )	This is supplied by the user
Pump hours remaining (hours)	This is the remaining pump hours remaining in the aquifer. This calculation is based on the <i>current water volume</i> and the <i>current abstraction</i> rate over the last <i>time</i> supplied by the user.
Total Storage Capacity (m <sup>3</sup> )	This is calculated based on spatial information available for the aquifer.
Current Water Volume (m <sup>3</sup> )	This is calculated based on the known depth of the aquifer and the <i>water level</i> measurement supplied by the user.
Aquifer Water Level (%)	
Capacity changes due to water balance (m <sup>3</sup> )	The water balance equation is populated by the <i>abstraction</i> and <i>rainfall</i> measurements supplied by the user and the other environmental information stored in the Parameters table which we will address in the next section.

## 8.5 THE ADMINISTRATION SITE

The admin page requires a login to access the information stored in the database, Figure 8.7. An initial administrator username and password will be supplied to the client but can be changed at a later stage.

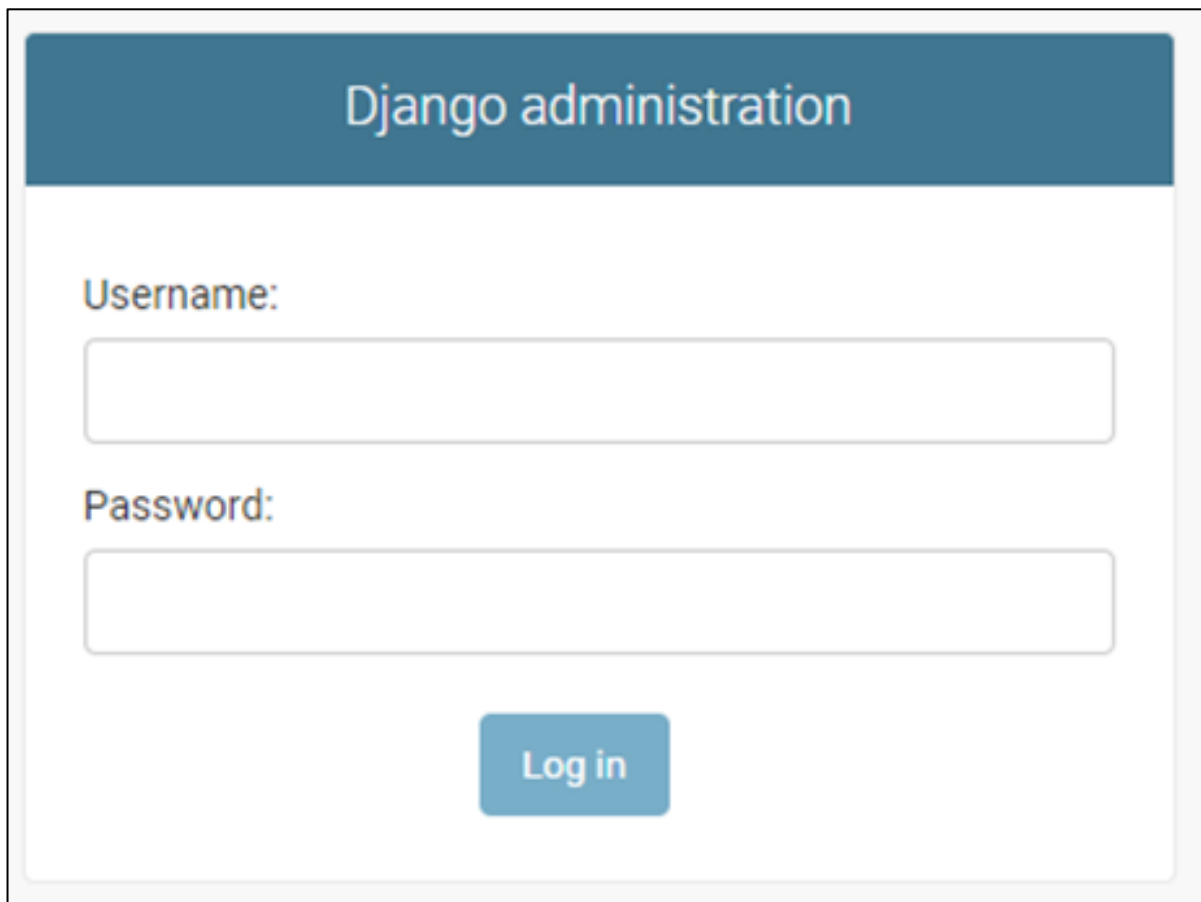


**Figure 8.7.** The login page for the admin site

Once logged in the administrator is met with the landing page which contains two sections, Figure 8.8. The *Authentication and Authorization* section allows the administrator to create new users and/or user groups if required. The second section, *Riverbed storage*, is used to manage the database tables which the web application requires for the water capacity calculations.

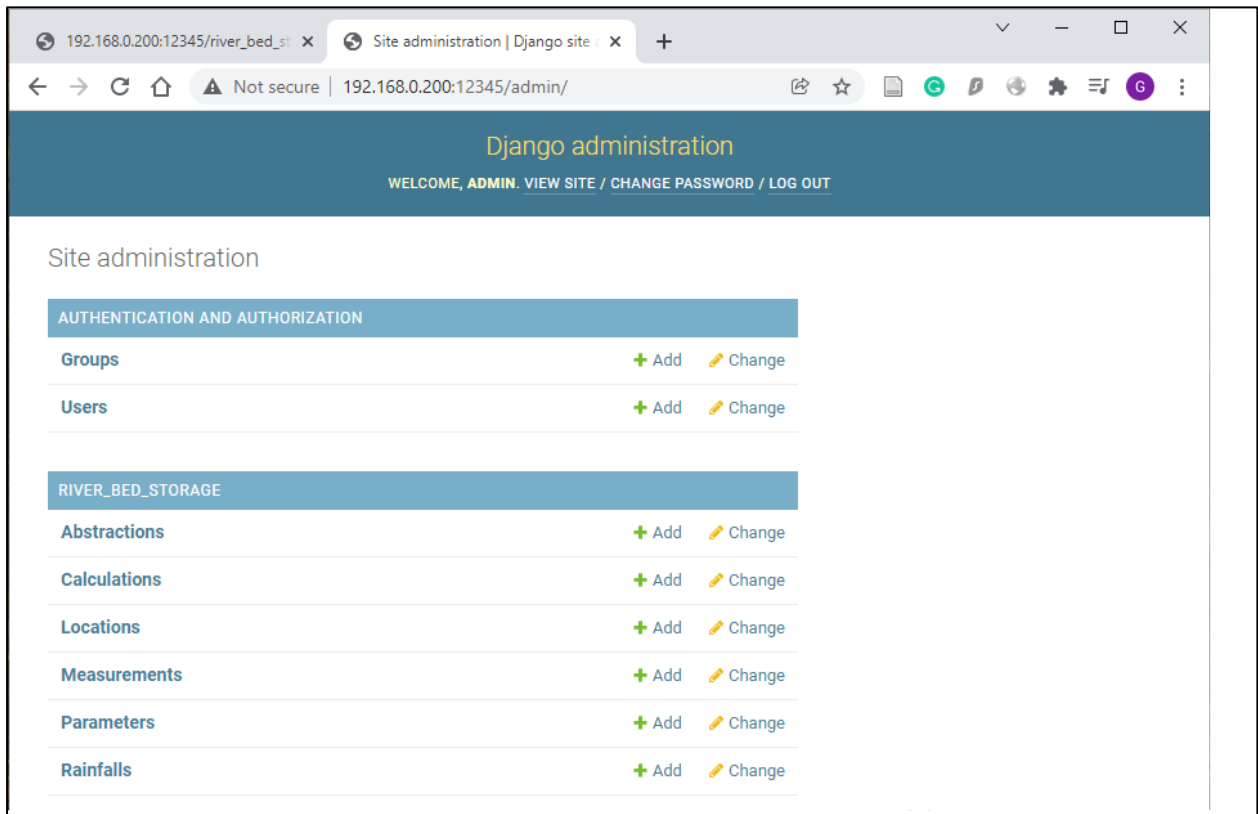


Figure 8.8. The landing page for the administration site.

It is currently set up so that anyone with a login can add locations and the associated environmental variables. The Abstraction, Measurement and Rainfall tables contain information entered by the user through the web application as explained in the previous section.

The location information can be modified as seen in Figure 8.9. This iteration of the application focuses on one location in Limpopo. Besides the physical shape of the volume that stores the water (which is managed by the backend of the application and is inaccessible by the administrator or users), it requires the permeability of the aquifer. This is stored in the *coef* field. In this case, it is only a single field since the aquifer is considered homogenous.

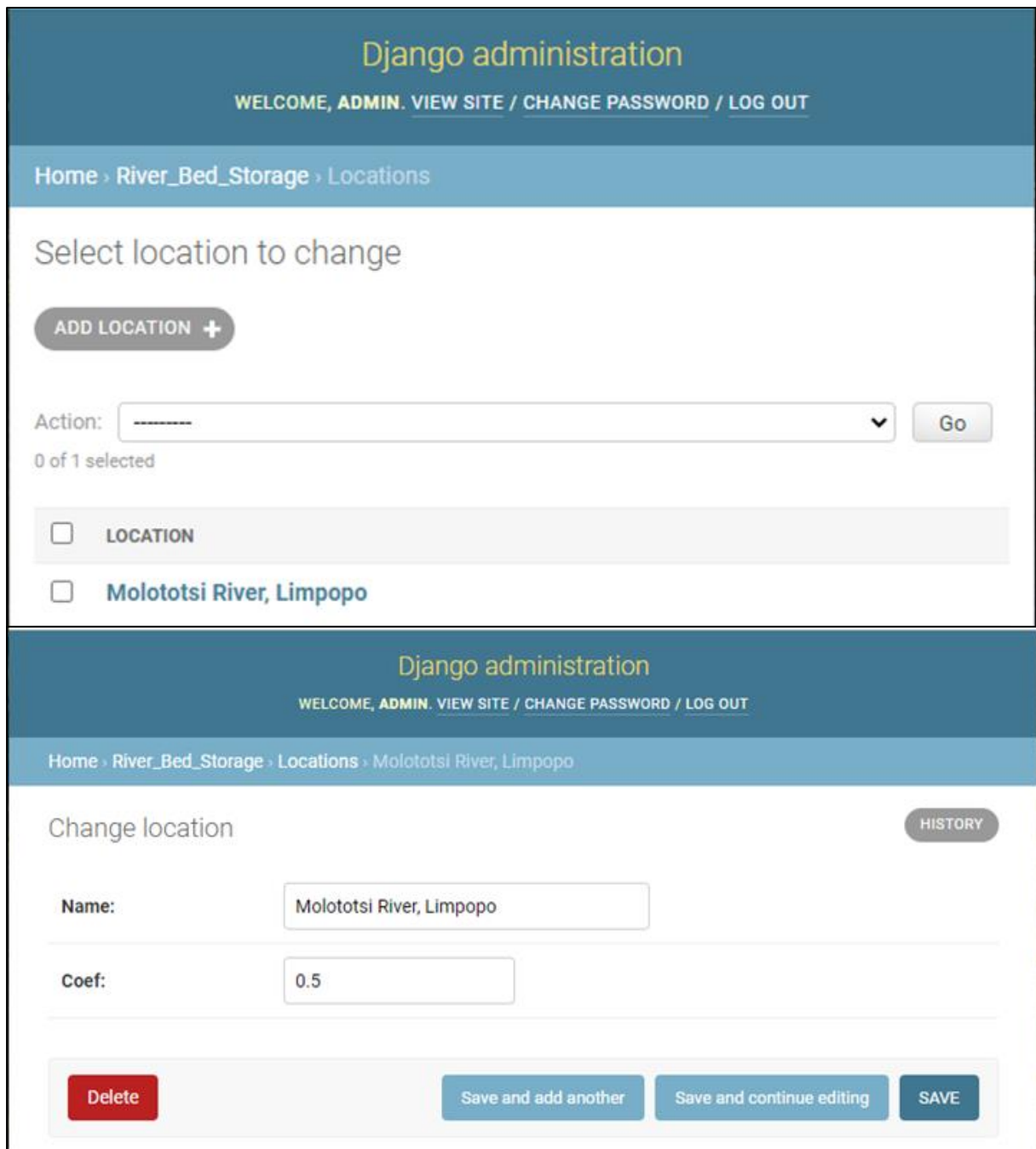


Figure 8.9. Modifying location information including the permeability coefficient

More information is required when calculating the water balance equation for the aquifer and is stored in the *Parameter* table, Figure 8.10.

Table 8.1. The information required to calculate the water balance of the aquifer is stored in the *Parameter* table.

Field	Units	
Location	-	Selected from available locations
Evaporation rate	m <sup>3</sup> /day	Supplied by the administrator.
Run in rate	m <sup>3</sup> /day	
Run out rate	m <sup>3</sup> /day	
Seepage rate	m <sup>3</sup> /day	
Vol avail	m <sup>3</sup>	

The screenshot shows the Django administration interface for modifying parameters. The header includes 'Django administration' and 'WELCOME, ADMIN. VIEW SITE / CHANGE PASSWORD / LOG OUT'. The breadcrumb trail is 'Home > River\_Bed\_Storage > Parameters > Molototsi River, Limpopo: 0.5, 0.02, 0.01, 0.0005, 244950.0'. The main content area is titled 'Change parameter' and contains a 'HISTORY' button. The form fields are:
 

- Location: Molototsi River, Limpopo (dropdown menu)
- Evaporation rate: 0.5
- Run in rate: 0.02
- Run out rate: 0.01
- Seepage rate: 0.0005
- Vol avail: 244950.0

 At the bottom, there are four buttons: 'Delete' (red), 'Save and add another' (blue), 'Save and continue editing' (blue), and 'SAVE' (blue).

Figure 8.10. Modifying the parameters required for the water balance equation.

## 9 CONCLUSIONS

This is the final report on the study of spatial and temporal dynamics flows and pools along non-perennial rivers.

In terms of assessing the spatial and temporal distribution of pool and pool dynamics using remote sensing along non-perennial rivers, the assessments were done at the catchment and pool scales. At the catchment scale, remote sensing mapped pools along the two-study sites (Touws and Molototsi) with acceptable accuracy but failed to detect pools of smaller size in both catchments. The mapping of pools at the catchment scale is vital for identifying the location of pools for selecting sampling sites for ecological status or livestock and wildlife watering. Overall, MNDWI performed better than the other assessed methods in the mountainous Touws site, whereas NDWI performed better than other tested methods in the relatively flat Molototsi site. These methods estimated pool surface area with acceptable accuracy.

Using these remote sensing methods, the changes in pool sizes at different phases (full to dry) in the two catchments were determined. The pools in Touws River showed a perennial pattern, whereas pools in the sandy Molototsi showed ephemeral behaviour lasting only for a few months after flows. The changes in the surface water area of the pools are related to flow occurrence and rainfall. The water balance of the pools in Touws River reveals that the pool does receive water from the sub-surface. However, river flow occurrence remains the major contributor to the pools.

The results showed that hydrological phases (dry, pools or flowing) could be determined using the remote sensing method with good accuracy. However, the results also showed that the acquisition of cloud-free images is one of the biggest challenges for remote sensing during the period of short-duration flows. Some of the events missed by Sentinel-2 were detected using Sentinel-1. The trap camera also proved to be a useful way of determining the hydrological phase of the river. The flow-contributing areas were identified using freely available data, these areas should strategically be protected to maintain the hydrological phases. The analyses further showed that the study catchments start the generation of runoff after receiving about 20 mm of rainfall. However, the Molototsi River have a better probability of generating runoff as compared to the Touws River. The approach that was used in this study can be adopted in other catchments to extract such useful information. Water resource and catchment management should consider monitoring and assessing hydrological states as well as identifying flow-contributing areas to make informed decisions.

The exploration of estimating the flow of NPRs revealed that estimation in an area with narrow streams and waterlogging can be very challenging. However, the results for the Touws River are promising. Exploring the best ways to obtain flow using remote sensing is still growing science; this includes exploring newly launched satellites with better resolution imagery and using a different method to obtain the relationships between observed and remote sensing-derived information.

Overall, the study showed various ways that hydrological information of non-perennial rivers can be extracted from freely available remote sensing data while improving the understanding of spatial and temporal dynamics of flows and pools along non-perennial rivers in semi-arid and arid areas. The insights provided by this study are useful for better management of NPRs and their host catchments. The methods used in this study can be used by water resource managers for planning and decision-making.

For the water tool, it is admitted that this is the initial development of the tool and that there is more work to be included for eventual operationalisation. These include:

**Website:** Currently, the web application is in its most basic form but can be easily adapted to fit the hosting site's template and style. Once it is used to enter data and do the calculations, user feedback will lead to modifications that will improve usability. Another benefit of having the data stored centrally is the possibility of creating dashboards and automatically generating monthly or annual reports

**Data Entry:** Although a website was the quickest way to create an online platform for users to access, it relies heavily on an internet connection. Another way to supply the measured data is via messaging services like WhatsApp and Telegram or even SMS. These messaging services have an API that can receive the measured data and reply with the results from the calculations. Although a website has the potential of providing a detailed analysis of water usage, a simpler way of data entry might improve the user experience.

## 10 REFERENCES

- Acharya, T.D., Subedi, A., Lee, D.H., 2019. Evaluation of Machine Learning Algorithms for Surface Water Extraction in a Landsat 8 Scene of Nepal. *Sensors*, 19(12), 2769
- Bangira, T., Alfieri, S.M., Menenti, M., van Niekerk, A., 2019. Comparing thresholding with machine learning classifiers for mapping complex water. *Remote Sens.* 11. <https://doi.org/10.3390/rs11111351>
- Bonada, N., Cañedo-Argüelles, M., Gallart, F., von Schiller, D., Fortuño, P., Latron, J., Llorens, P., Múrria, C., Soria, M., Vinyoles, D., Cid, N., 2020. Conservation and management of isolated pools in temporary rivers. *Water (Switzerland)* 12, 1-24. <https://doi.org/10.3390/w12102870>
- Brovelli, M.A., Molinari, M.E., Hussein, E., Chen, J., Li, R., 2015. The first comprehensive accuracy assessment of global and 30 at a national level: Methodology and results. *Remote Sens.* 7, 4191-4212. <https://doi.org/10.3390/rs70404191>
- Busker, T., de Roo, A., Gelati, E., Schwatke, C., Adamovic, M., Bisselink, B., Pekel, J.-F., Cottam, A., 2018. A global lake and reservoir volume analysis using a surface water dataset and satellite altimetry. *Hydrol. Earth Syst. Sci. Discuss.* d, 1-32. <https://doi.org/10.5194/hess-2018-21>
- Chen, Q., Liu, W., Huang, C., 2022. Long-Term 10 m Resolution Water Dynamics of Qinghai Lake and the Driving Factors. *Water* 14, 671. <https://doi.org/10.3390/w14040671>
- Deus, D., Gloaguen, R., Krause, P., 2013. Water balance modeling in a semi-arid environment with limited in situ data using remote sensing in lake Manyara, east African rift, Tanzania. *Remote Sens.* 5, 1651-1680. <https://doi.org/10.3390/rs5041651>
- Gajbhiye, S., 2015. Estimation of Surface Runoff Using Remote Sensing and Geographical Information System. *Int. J. u- e-Service, Sci. Technol.* 8, 113-122. <https://doi.org/10.14257/ijunesst.2015.8.4.12>
- Gleason, C.J., Smith, L.C., 2014. Toward global mapping of river discharge using satellite images and at-many-stations hydraulic geometry. *Proc. Natl. Acad. Sci.* 111, 4788-4791. <https://doi.org/10.1073/pnas.1317606111>

- Gleason, C.J., Wang, J., 2015. Theoretical basis for at-many-stations hydraulic geometry. *Geophys. Res. Lett.* 42, 7107-7114. <https://doi.org/10.1002/2015GL064935>
- Grenfell, M.C., Grenfell, S.E., Mazvimavi, D., 2021. Morphodynamic modelling of dryland non-perennial riverscapes, with implications for environmental water allocation. *Prog. Phys. Geogr.* <https://doi.org/10.1177/0309133321996639>
- Helsel, D.R., Hirsch, R.M., Ryberg, K.R., Archfield, S.A., Gilroy, E.J., 2020. *Statistical Methods in Water Resources Techniques and Methods 4 – A3*. USGS Tech. Methods.
- Hirpa, F.A., Hopson, T.M., De Groeve, T., Brakenridge, G.R., Gebremichael, M., Restrepo, P.J., 2013. Upstream satellite remote sensing for river discharge forecasting: Application to major rivers in South Asia. *Remote Sens. Environ.* 131, 140-151. <https://doi.org/10.1016/j.rse.2012.11.013>
- Hussey, S.W., 2007. *Water from Sand rivers. Guidelines for abstraction*. Water, Engineering and Development Centre (WEDC), Loughborough University of Technology, UK, 194 pp.
- Hwang, H.T., Jeon, S.W., Suleiman, A.A., Lee, K.K., 2017. Comparison of saturated hydraulic conductivity estimated by three different methods. *Water (Switzerland)* 9, 1-15. <https://doi.org/10.3390/w9120942>
- Jovanovic, N, Bugan, R.D.H., Lebea, T., Aysi, K., Kena, M., Mushadu, W., Du Preez, D., Walker, D., and Whitehead, R., 2018. Riparian shallow groundwater utilization for small-holder irrigation in the Mopani District (Limpopo Province). Water Research Commission Report k5/2426, Pretoria, South Africa.
- Kebede, M.G., Wang, L., Li, X., Hu, Z., 2020. Remote sensing-based river discharge estimation for a small river flowing over the high mountain regions of the Tibetan Plateau. *Int. J. Remote Sens.* 41, 3322-3345. <https://doi.org/10.1080/01431161.2019.1701213>
- Larned, S.T., Datry, T., Arscott, D.B., Tockner, K., 2010. Emerging concepts in temporary-river ecology. *Freshw. Biol.* 55, 717-738. <https://doi.org/10.1111/j.1365-2427.2009.02322.x>
- [Love, D.](#), [van der Zaag, P.](#), [Uhlenbrook, S.](#), [Owen, R.J.S.](#), A water balance modelling approach to optimising the use of water resources in ephemeral sand rivers. *River Research and Applications* 27(8), 908-925.

- Maswanganye, S.E., 2018. A COMPARISON OF REMOTELY-SENSED PRECIPITATION ESTIMATES WITH OBSERVED DATA FROM RAIN GAUGES IN THE WESTERN CAPE, SOUTH AFRICA . by 121.
- Mbanguka, R.P., Lyon, S.W., Holmgren, K., Lopez, M.G., Jarsjö, J., 2016. Water balance and level change of lake Babati, Tanzania: Sensitivity to hydroclimatic forcings. *Water (Switzerland)* 8. <https://doi.org/10.3390/w8120572>
- McFeeters, S.K., 1996. The use of the Normalized Difference Water Index (NDWI) in the delineation of open water features. *Int. J. Remote Sens.* 17, 1425-1432. <https://doi.org/10.1080/01431169608948714>
- Mohuba, S.C., Abiye, T.A., Demlie, M.B., Modiba, M.J., 2020. Hydrogeological Characterization of the Thyspunt Area, Eastern Cape Province, South Africa. *hydrology* 7. <https://doi.org/https://doi.org/10.3390/hydrology7030049>
- Penman, H.L., 1948. Natural evaporation from open water, bare and grass. *Proc. R. Soc. Lond. Ser. A.*
- Pham-Duc, B., Prigent, C., Aires, F., 2017. Surface water monitoring within Cambodia and the Vietnamese Mekong Delta over a year, with Sentinel-1 SAR observations. *Water (Switzerland)* 9, 1-21. <https://doi.org/10.3390/w9060366>
- Pipitone, C., Maltese, A., Dardanelli, G., Brutto, M. Lo, Loggia, G. La, 2018. Monitoring water surface and level of a reservoir using different remote sensing approaches and comparison with dam displacements evaluated via GNSS. *Remote Sens.* 10, 1-24. <https://doi.org/10.3390/rs10010071>
- Rumora, L., Miler, M., Medak, D., 2019. Contemporary comparative assessment of atmospheric correction influence on radiometric indices between Sentinel-2A and Landsat 8 imagery. *Geocarto Int.* 0, 1-15. <https://doi.org/10.1080/10106049.2019.1590465>
- Samboko, H.T., Abas, I., Luxemburg, W.M.J., Savenije, H.H.G., Makurira, H., Banda, K., Winsemius, H.C., 2020. Evaluation and improvement of remote sensing-based methods for river flow management. *Phys. Chem. Earth* 117, 102839. <https://doi.org/10.1016/j.pce.2020.102839>

- Sawunyama, T., Senzanje, A., Mhizha, A., 2006. Estimation of small reservoir storage capacities in Limpopo River Basin using geographical information systems (GIS) and remotely sensed surface areas: Case of Mzingwane catchment. *Phys. Chem. Earth* 31, 935-943. <https://doi.org/10.1016/j.pce.2006.08.008>
- Seaman, M., Watson, M., Avenant, M., King, J., Joubert, A., Barker, C., Esterhuysen, S., Graham, D., Kemp, M., Le Roux, P., Prucha, B., Redelinghuys, N., Rossouw, L., Rowntree, K., Sokolic, F., Van Rensburg, L., Van Der Waal, B., Van Tol, J., Vos, T., 2016. DRIFT-ARID: A method for assessing environmental water requirements (EWRs) for non-perennial rivers. *Water SA* 42, 356-367. <https://doi.org/10.4314/wsa.v42i3.01>
- Seaton, D., Dube, T., Mazvimavi, D., 2020. Use of multi-temporal satellite data for monitoring pool surface areas occurring in non-perennial rivers in semi-arid environments of the Western Cape, South Africa. *ISPRS J. Photogramm. Remote Sens.* 167, 375-384. <https://doi.org/10.1016/j.isprsjprs.2020.07.018>
- Sichangi, A., Wang, L., Hu, Z., 2018. Estimation of River Discharge Solely from Remote-Sensing Derived Data: An Initial Study Over the Yangtze River. *Remote Sens.* 10, 1385. <https://doi.org/10.3390/rs10091385>
- Sichangi, A.W., Wang, L., Yang, K., Chen, D., Wang, Z., Li, X., Zhou, J., Liu, W., Kuria, D., 2016. Estimating continental river basin discharges using multiple remote sensing data sets. *Remote Sens. Environ.* 179, 36-53. <https://doi.org/10.1016/j.rse.2016.03.019>
- Smith, L.C., Pavelsky, T.M., 2008. Estimation of river discharge, propagation speed, and hydraulic geometry from space: Lena River, Siberia. *Water Resour. Res.* 44, 1-11. <https://doi.org/10.1029/2007WR006133>
- Tena, T.M., Mudenda, F., Nguvulu, A., Mwaanga, P., Gathenya, J.M., 2021. Analysis of River Tributaries' Streamflow Contribution Using WEAP Model: A Case of the Ngwerere and Kanakatampa Tributaries to the Chongwe River in Zambia. *J. Water Resour. Prot.* 13, 309-323. <https://doi.org/10.4236/jwarp.2021.134019>
- Trimmel, H., Weihs, P., Leidinger, D., Formayer, H., Kalny, G., Melcher, A., 2018. Can riparian vegetation shade mitigate the expected rise in stream temperatures due to climate change during heat waves in a human-impacted pre-alpine river? 437-461.
- Yihdego, Y., Webb, J.A., 2018. Comparison of evaporation rate on open water bodies: Energy balance estimate versus measured pan. *J. Water Clim. Chang.* 9, 101-111. <https://doi.org/10.2166/wcc.2017.139>